AD-A169 612 RADON OPTICAL PROCESSING IN RADON SPACE(U) ARIZONA UNIV 1/2
TUCSON OPTICAL SCIENCES CENTER H H BARRETT 15 JUN 86
AFOSR-84-0188

UNCLASSIFIED F/G 9/3 NL

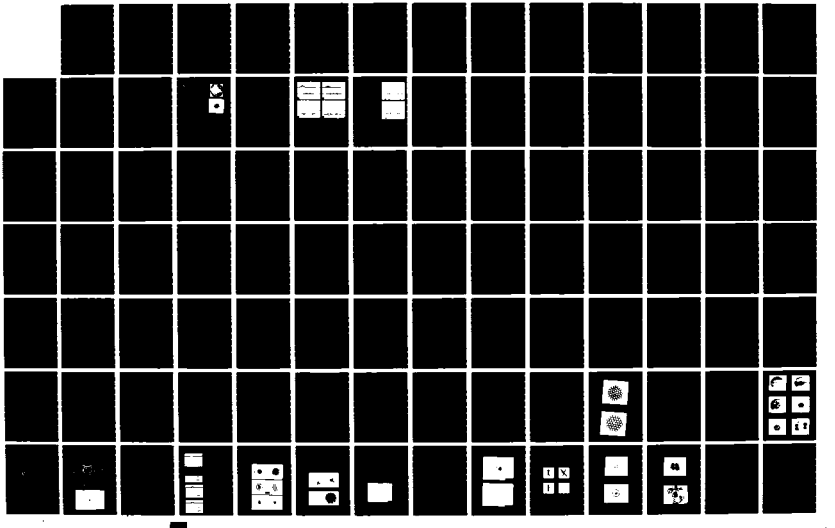

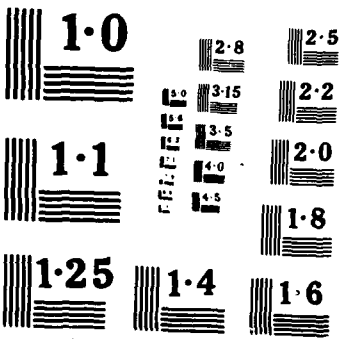
1·0
1·1
1·25
1·4
1·6
1·8
2·0
2·2
2·5
2·8
3·15
3·5
4·0
4·5

AD-A169 612

OPTICAL PROCESSING IN RADON SPACE

Harrison H. Barrett
Optical Sciences Center
University of Arizona
Tucson, Arizona 85721

June 15, 1986

Final Report for Period July 1984 - January 1986

Approved for public release;
distribution unlimited

Prepared for

Air Force Office of Scientific Research
Bolling Air Force Base
Washington, D.C. 20332

DTIC FILE COPY

OPTICAL PROCESSING IN RADON SPACE

Harrison H. Barrett
Optical Sciences Center
University of Arizona
Tucson, Arizona 85721

June 15, 1986

Final Report for Period July 1984 - January 1986

Approved for public release;
distribution unlimited

Prepared for

Air Force Office of Scientific Research
Bolling Air Force Base
Washington, D.C. 20332

UNCLASSIFIED

SECURITY CLASSIFICATION OF THIS PAGE

REPORT DOCUMENTATION PAGE

1a. REPORT SECURITY CLASSIFICATION Unclassified	1b. RESTRICTIVE MARKINGS
2a. SECURITY CLASSIFICATION AUTHORITY	3. DISTRIBUTION/AVAILABILITY OF REPORT Approved for public release; distribution unlimited.
2b. DECLASSIFICATION/DOWNGRADING SCHEDULE	
4. PERFORMING ORGANIZATION REPORT NUMBER(S)	5. MONITORING ORGANIZATION REPORT NUMBER(S)
6a. NAME OF PERFORMING ORGANIZATION Optical Sciences Center 6b. OFFICE SYMBOL (If applicable)	7a. NAME OF MONITORING ORGANIZATION
6c. ADDRESS (City, State and ZIP Code) University of Arizona Tucson, Arizona 85721	7b. ADDRESS (City, State and ZIP Code)
8a. NAME OF FUNDING/SPONSORING ORGANIZATION AFOSR 8b. OFFICE SYMBOL (If applicable)	9. PROCUREMENT INSTRUMENT IDENTIFICATION NUMBER AFOSR 84-0188
8c. ADDRESS (City, State and ZIP Code) Bolling Air Force Base Washington, DC 20332	10. SOURCE OF FUNDING NOS. PROGRAM ELEMENT NO. / PROJECT NO. / TASK NO. / WORK UNIT NO.
11. TITLE (Include Security Classification) Optical Processing in Radon Space (U)	
12. PERSONAL AUTHOR(S) Harrison H. Barrett	
13a. TYPE OF REPORT Final 13b. TIME COVERED FROM 84Jul TO 86Jan	14. DATE OF REPORT (Yr., Mo., Day) 86June15 15. PAGE COUNT 7 + appendix
16. SUPPLEMENTARY NOTATION	

17 COSATI CODES		
FIELD	GROUP	SUB. GR.

18. SUBJECT TERMS (Continue on reverse if necessary and identify by block number)
Optical processing
Radon space

19. ABSTRACT (Continue on reverse if necessary and identify by block number)

This is the final report of technical progress of a three-year program to investigate application of the Radon transform to signal processing. The stated goals of the program were:

(1) Theoretical investigation of the role of the Radon transform in signal processing, including enumeration of the operations achievable in Radon space.

(2) Construction of a practical system for 2-D spectral analysis and image filtering.

(3) Proof-of-principle experiments for other processing operations, such as bandwidth compression and calculation of the Wigner distribution function.

(4) Determination of the feasibility of Radon-space processing of 3-D data, emphasizing not only system architecture but also storage media capable of saving and rapidly retrieving the requisite data arrays.

In the theoretical investigations we have discovered several 2-D signal-processing operations susceptible to solution in Radon space. These include the Hartley transform, certain joint coordinate-frequency representations (e.g., the Wigner distribution function and Woodward ambiguity

20. DISTRIBUTION/AVAILABILITY OF ABSTRACT UNCLASSIFIED/UNLIMITED ☒ SAME AS RPT. ☐ DTIC USERS ☐	21. ABSTRACT SECURITY CLASSIFICATION Unclassified
22a. NAME OF RESPONSIBLE INDIVIDUAL Harrison H. Barrett	22b. TELEPHONE NUMBER (Include Area Code) (602) 621-4425 22c. OFFICE SYMBOL

DD FORM 1473, 83 APR EDITION OF 1 JAN 73 IS OBSOLETE.

Unclassified

SECURITY CLASSIFICATION OF THIS PAGE

19. Abstract (Continued)

function), certain algorithms for spectrum estimation (e.g., the periodogram and the Yule-Walker autoregressive model), and the cepstrum. Most of these Radon-space operations have been demonstrated in computer simulations and some have been performed by means of analog hardware in the hybrid Radon-space signal-processing system. This system can perform a family of processing operations at about five frames per second, limited by the image-rotation rate. Processing is performed by surface acoustic wave (SAW) filters, and the 2-D processed signal is displayed on a CRT. Studies of the feasibility of processing 3-D data in Radon space concentrated primarily on analysis of prospective materials for wavelength-multiplexed mass-data storage.

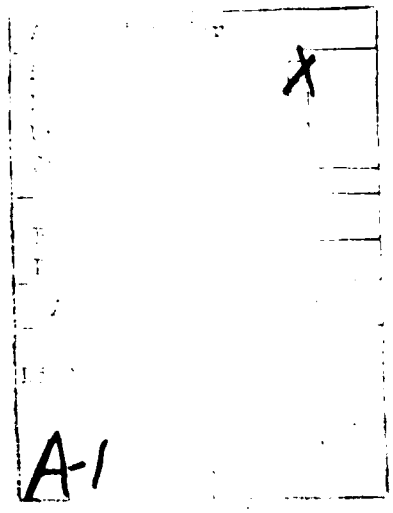

CONTENTS

INTRODUCTION 1

THEORETICAL INVESTIGATION OF THE RADON TRANSFORM APPLIED TO SIGNAL PROCESSING 2

CONSTRUCTION OF A PRACTICAL SYSTEM FOR 2-D SPECTRAL ANALYSIS AND IMAGE FILTERING 4

PROOF-OF-PRINCIPLE EXPERIMENTS FOR OTHER PROCESSING OPERATIONS 5

FEASIBILITY OF USING THE RADON TRANSFORM FOR 3-D DATA PROCESSING 6

PUBLICATIONS RESULTING FROM AFOSR SUPPORT IN THE COURSE OF THE PROGRAM 6

PAPERS PRESENTED AT TECHNICAL MEETINGS DURING THE COURSE OF THE PROGRAM 7

REFERENCES 7

APPENDIX 8

INTRODUCTION

Optical methods for signal processing have long been touted as playing an important role in the future: they will enable complex operations to be performed on large arrays of data at a very rapid rate. This prediction is based on the inherent capability of optical systems to operate on two-dimensional (2-D) data planes and on the ability of spherical lenses to perform the Fourier transform. However, the promise of optical methods to rapidly perform signal-processing tasks remains unfulfilled, with certain notable exceptions (e.g., processing synthetic aperture radar and stellar speckle interferometry data). There are several reasons for this, but the most salient are the limitations of available 2-D input/output devices (spatial light modulators and detector arrays), the fact that the optical phase of the processed signal cannot be directly detected, and the sensitivity of coherent optical systems to mechanical disturbances and speckle noise.

In contrast to the situation for 2-D optical hardware, signal processor technology for temporal (1-D) signals is quite advanced in capability and flexibility, and thus presents the interesting prospect of applying these 1-D devices to 2-D signal processing if a suitable dimensional transformation can be employed. In effect, this would allow the rapid parallel processing capability to be "traded off" for more precise, flexible, and noise-immune 1-D serial processing in a hybrid system. Several dimensional transformations are available for deriving 1-D signals from 2-D data and reconstructing processed 2-D outputs, the most familiar being the television raster. But another algorithm, the Radon transform, has some very nice mathematical properties that make it an excellent candidate for application to signal processing. These properties were derived by an Austrian mathematician, Johann Radon, early in this century, and the transform bearing his name has become well-known in recent years as the mathematical basis for medical computed tomography. In the Radon transform, 1-D signals are derived from 2-D input data by "projection," i.e., integration along sets of parallel lines. The 2-D

signal can be regenerated by "smearing" and summing appropriately filtered 1-D projections back over the 2-D space. The mathematical properties of the transform enable 2-D signal-processing operations based on the Fourier transform and/or convolution operations to be performed by means of 1-D operations on the projections. Such operations include: generation of complex Fourier transform, Hartley transform, Wigner distribution function, general 2-D filtering and correlation, bandwidth compression, spectrum analysis, and cepstrum analysis.

THEORETICAL INVESTIGATION OF THE RADON TRANSFORM APPLIED TO SIGNAL PROCESSING

In his original development of the mathematical theory of the transform, Johann Radon proved two theorems that have been the basis for application of the Radon transform to signal processing: the central-slice (or projection-slice) theorem and the filter theorem. They demonstrate that 2-D Fourier transforms and convolutions can be performed by 1-D operations on the projection data. To illustrate mathematically, a projection of a 2-D function $f(\mathbf{r})$ is commonly defined by a linear space-variant integral transformation:

$$R_2[f(\mathbf{r})] \equiv \lambda_f(p,\phi) = \int_{-\infty}^{\infty}\int_{-\infty}^{\infty} d^2r\ f(\mathbf{r})\ \delta(p - \mathbf{r}\cdot\hat{\mathbf{n}}), \tag{1}$$

where R_2 denotes the Radon transform operator. As is customary, we denote scalar variables and vectors by normal-face and bold-face characters, respectively. The projection λ_f is a function of two variables: the radial spatial dimension p and the azimuth angle ϕ. However, all of the operations we consider operate on p alone, and therefore we can consider the projections λ_f to be 1-D functions of p parameterized by the azimuth angle ϕ. The central-slice theorem states that the Fourier transform of the 2-D function $f(\mathbf{r})$ is obtained by performing 1-D Fourier transforms of each projection

and displaying the outputs at the proper radial azimuths:

$$\mathcal{F}_2\,[f(r)]\big|_{\rho=\nu} = \mathcal{F}_1\,[\lambda_f(p,\phi)] \equiv \Lambda_f(\nu,\phi). \tag{2}$$

The geometry of the Radon transform and the central-slice theorem are shown in Figure 1 of Ref. 1. The filter theorem demonstrates that the 1-D convolution of the projections of two functions at the same azimuth is identical to the projection of the 2-D convolution, i.e.,

$$R_2[f(r) \;**\; g(r)] = R_2[f(r)] * R_2[g(r)], \tag{3}$$

where * and ** denote 1-D and 2-D convolution respectively. It is easy to see that the same result holds for correlation operations as well. The processed 2-D function may be reconstructed using any of several algorithms to perform the inverse Radon transform.[2]

Our analysis of 2-D operations susceptible to solution in Radon space has primarily exploited these two theorems. We have investigated those useful signal-processing operations that can be decomposed into a sequence of Fourier transforms, convolutions, and other achievable 1-D and 2-D operations such as addition, pointwise multiplication, and taking logarithms. Such operations include Fourier analysis (computation of both the power spectrum and complex transform), the Hartley transform, image filtering and correlation, bandwidth compression, generation of the Woodward ambiguity function and the Wigner distribution function, some spectrum estimation algorithms (periodograms, Blackman-Tukey analysis, and Yule-Walker autoregressive models), and the cepstrum. Work by other authors has established[3] that the Radon transform can be useful for pattern recognition through calculation of image moments and the Hough transform.

CONSTRUCTION OF A PRACTICAL SYSTEM FOR 2-D SPECTRAL ANALYSIS AND IMAGE FILTERING

The hybrid system constructed to perform signal processing in Radon space consists of an optical scanner (to generate the Radon transform data), 1-D signal processors, and a computer-controlled CRT display. The optical Radon transformer uses a laser source, a Bragg-cell scanner, and anamorphic optics to project a line-of-light onto a 2-D reflective or transmissive object. By collecting the light reflected or transmitted by the object onto a detector, a signal proportional to the line integral of the reflectance or transmittance is generated. The line-of-light is scanned parallel to itself by the Bragg cell to produce a temporal signal proportional to the line-integral projection for one azimuth angle. After one projection is generated, the azimuth angle is changed by an image-rotating prism. Thus, the Radon projections are generated as a sequence of temporal electronic signals. For obvious reasons, the optical Radon transformer is called a flying-line scanner, and is shown schematically in Figure 2 of Ref. 1. Though we had originally planned to demonstrate Radon transformation at video rates (30 frames/s), we are limited by the rotation rate of the stepper motor for the image rotator to about 5 frames/s. This is by no means a fundamental limit for signal processing in Radon space--optical systems have been built to rotate images at 75 frames/s with excellent stability and image quality.

After derivation of the projection data, signal processing can be performed by 1-D electronic or hybrid devices. For the demonstration of 2-D spectrum analysis and Fourier transformation, we implemented the chirp transform algorithm with surface acoustic wave dispersive filters to produce the 1-D transform of the temporal input data within 30 μs. The time-bandwidth product of the Fourier transformer is only 50, but again this is by no means a fundamental limitation. Filtering of the 1-D signals was performed by applying the projection signal to one port of a monolithic SAW convolver.

A fast ECL function generator was constructed to store the filter function to be applied to the other port of the SAW convolver.

To construct the 2-D Fourier transform signal, the 1-D processed signal was displayed in the proper polar format on a computer-controlled CRT. The results obtained with the system are available in Ref. 4, which is available in the Appendix.

It had been our intention to design and construct a custom SAW filter to perform the filtering operation for image reconstruction from projections. However, the capabilities of the available photolithographic facilities were not adequate for the task, and instead we utilized the SAW convolver for the filtering operation. The ECL function generator was built to store the filter function. Recognizable reconstructions were derived of input scenes at approximately 5 frames/s, but were not of useful quality for two reasons. The signal-to-noise ratio of the output from the SAW convolver was not adequate, and the original image rotator used to perform the inverse Radon transform exhibited too much runout. The results obtained are to be published shortly.

PROOF-OF-PRINCIPLE EXPERIMENTS FOR OTHER PROCESSING OPERATIONS

Both computer simulations and demonstrations in hardware were performed for a number of the 2-D processing operations listed above, including Fourier spectrum analysis, complex Fourier transformation, the Hartley transform, data compression, generation of the Wigner distribution function, power spectrum estimation[5] (periodograms, the Blackman-Tukey algorithm, and the Yule-Walker autoregressive model), and the cepstrum. Most of these results have been reported either in the open literature[1,2,4,6,7,8] or by presentation at technical meetings. Papers dealing with the remaining operations are in preparation.

FEASIBILITY OF USING THE RADON TRANSFORM FOR 3-D DATA PROCESSING

An architecture for a 3-D image processor was developed prior to the commencement of the contract period, and so the work in this program concentrated on investigation of materials for rapid storage and retrieval of the data arrays. The proposed technique utilizes wavelength-multiplexed storage in alkali-halide crystals. A theoretical examination of data-storage mechanisms in the crystals was made to describe the conditions for a linear relationship between exposure intensity (or exposure time) and hole depth. The two data-storage mechanisms are photochemical holeburning (PHB) and nonphotochemical holeburning (NPHB). It was discovered that PHB materials do exhibit the necessary linear relationship, but NPHB materials do not. The results were reported in Ref. 9.

PUBLICATIONS RESULTING FROM AFOSR SUPPORT IN THE COURSE OF THE PROGRAM

Smith, W.E. and H.H. Barrett, "Radon transform and bandwidth compression," Opt. Lett. **8**, 395 (1983).

Easton, R.L. Jr., H.H. Barrett, and A.J. Ticknor, "Using SAW filters to process two-dimensional data via the Radon transform," Proc. IEEE Ultrasonics Symposium, p. 185 (1983).

Easton, R.L. Jr., A.J. Ticknor, and H.H. Barrett, "Application of the Radon transform to optical production of the Wigner distribution function," Opt. Eng. **23**, 738 (1984).

Ticknor, A.J., R.L. Easton, Jr., and H.H. Barrett, "A Two-dimensional Radon-Fourier transformer," Opt. Eng. **24**, 082 (1985).

Easton, R.L. Jr., A.J. Ticknor, and H.H. Barrett, "Two-dimensional complex Fourier transform via the Radon transform," Appl. Opt. **24**, 3817 (1985).

Atcheson, P.D., "An investigation of analog optical storage through photochemical holeburning," Ph.D. dissertation, University of Arizona (1985).

PAPERS PRESENTED AT TECHNICAL MEETINGS

DURING THE COURSE OF THE PROGRAM

Easton, R.L. Jr., H.H. Barrett, and A.J. Ticknor, "Using SAW filters to process two-dimensional data via the Radon transform," at the IEEE Ultrasonics Symposium, Atlanta, 1983.

Ticknor, A.J., R.L. Easton, Jr., and H.H. Barrett, "High-speed processing of 2-D data via the Radon transform," at the Annual meeting of the Optical Society of America, San Diego, 1984.

Easton, R.L., Jr., A.J. Ticknor, and H.H. Barrett, "Processing of 2-D data via the Radon transform II: Applications," at the Annual meeting of the Optical Society of America, San Diego, 1984.

Easton, R.L., Jr., "Two-dimensional signal processing in Radon space," at the Annual meeting of the Optical Society of America, Washington, 1985.

REFERENCES

References 1, 2, 4, 6-8 are included in the Appendix for the reader's convenience.

1. Easton, R.L. Jr., A.J. Ticknor, and H.H. Barrett, "Application of the Radon transform to optical production of the Wigner distribution function," *Opt. Eng.* **23**, 738 (1984).

2. Easton, R.L. Jr., and H.H. Barrett, "Tomographic transformations in optical signal processing," in *Optical Signal Processing*, J. Horner, ed. (Academic Press, New York, to be published).

3. Gindi, G.R. and A.F. Gmitro, "Optical feature extraction via the Radon transform," Opt. Eng. **23**, 499 (1984).

4. Easton, R.L. Jr., A.J. Ticknor, and H.H. Barrett, "Two-dimensional complex Fourier transform via the Radon transform," Appl. Opt. **24**, 3817 (1985).

5. Cadzow, J.A., "Spectral estimation: an overdetermined rational model approach," Proc. IEEE **70**, 907 (1982).

6. Easton, R.L. Jr., H.H. Barrett, and A.J. Ticknor, "Using SAW filters to process two-dimensional data via the Radon transform," Proc. IEEE Ultrasonics Symposium, p. 185 (1983).

7. Ticknor, A.J., R.L. Easton, Jr., and H.H. Barrett, "A two-dimensional Radon-Fourier transformer," Opt. Eng. **24**, 082 (1985).

8. Smith, W.E. and H.H. Barrett, "Radon transform and bandwidth compression," Opt. Lett. **8**, 395 (1983).

9. Atcheson, P.D., "An investigation of analog optical storage through photochemical holeburning," Ph.D. dissertation, University of Arizona (1985).

Application of the Radon transform to optical production of the Wigner distribution function

Roger L. Easton, Jr.
Anthony J. Ticknor
Harrison H. Barrett
Optical Sciences Center
University of Arizona
Tucson, Arizona 85721

Abstract. The Wigner distribution function (WDF), a simultaneous coordinate and frequency representation of a signal, has properties useful in pattern recognition. Because the WDF is computationally demanding, its use is not usually appropriate in digital processing. Optical schemes have been developed to compute the WDF for one-dimensional (1-D) signals, often using acousto-optic signal transducers. Some recent work has demonstrated the computation of two-dimensional (2-D) slices of the four-dimensional (4-D) WDF of a 2-D input transparency. In this latter case, the required 2-D Fourier transformation is performed by coherent optics. We demonstrate that computation of the WDF of real 2-D signals is susceptible to Radon transform solution. The 2-D operation is reduced to a series of 1-D operations on the line-integral projections. The required projection data are produced optically, and the Fourier transformation is performed by efficient 1-D processors (surface acoustic wave filters) by means of the chirp-transform algorithm. The resultant output gives 1-D slices through the 4-D WDF nearly in real time, and the computation is not restricted to coherently illuminated transparencies. This approach may be useful in distinguishing patterns with known texture direction. The optical setup is easily modified to produce the cross-Wigner distribution function, a special case of the complex, or windowed, spectrogram.

Keywords: optical pattern recognition; optical data processing; Wigner distribution function; Radon transform; surface acoustic wave signal processing.

Optical Engineering 23(6), 738-744 (November/December 1984).

CONTENTS

1. Introduction
2. Radon transform
3. Flying line scanner
4. Surface acoustic wave chirp Fourier transform
5. Radon implementation of the 4-D Wigner distribution function
6. Computation of the cross-Wigner distribution function and its relation to the sliding-window spectrum
7. Conclusions
8. Acknowledgments
9. References

1. INTRODUCTION

The Wigner distribution function (WDF) was introduced in 1932 as a phase space representation in quantum mechanics.[1] Because it describes a signal simultaneously in Fourier reciprocal variables, it has potential applications in the recognition of nonstationary patterns.[2,3] The WDF of a 1-D input function of f(x) is a 2-D function and is commonly defined as

$$W_f(x_0,u) = \int_{-\infty}^{\infty} f\left(x_0 + \frac{x'}{2}\right) f^*\left(x_0 - \frac{x'}{2}\right) e^{-2\pi i u x'} dx'$$

$$= {}_{x'}\mathcal{F}_u\left[f\left(x_0 + \frac{x'}{2}\right) f^*\left(x_0 - \frac{x'}{2}\right)\right], \quad (1)$$

where the operator ${}_{x'}\mathcal{F}_u$ represents a 1-D Fourier transformation of coordinate x' to frequency u. In the 2-D case, the WDF is four-dimensional and is defined as

$$W_f(\mathbf{r}_0,\mathbf{u}) = \int_{-\infty}^{\infty}\int_{-\infty}^{\infty} f\left(\mathbf{r}_0 + \frac{\mathbf{r}'}{2}\right) f^*\left(\mathbf{r}_0 - \frac{\mathbf{r}'}{2}\right) \times e^{-2\pi i \mathbf{u}\cdot\mathbf{r}'} d^2\mathbf{r}', \quad (2)$$

where $\mathbf{r}_0$ and $\mathbf{r}'$ are 2-D coordinate vectors and $\mathbf{u}$ is a 2-D spatial frequency vector. If $W_f(x_0,u)$ is evaluated at zero frequency and a change of variables is performed, the WDF becomes an autoconvolution. Thus, the WDF may be interpreted as a generalized autoconvolution at nonzero frequency.[4]

Several authors[5-7] have reviewed the properties of the WDF, including some aspects that make it suitable for implementation by optical processing. Most importantly, the WDF of any real or complex function is real (though not always positive), since it is the

Invited Paper PR-107 received March 2, 1984; revised manuscript received March 28, 1984; accepted for publication June 24, 1984; received by Managing Editor Sept. 4, 1984.
© 1984 Society of Photo-Optical Instrumentation Engineers.

Fourier transform of $f[x_0 + (x'/2)]f^*[x_0 - (x'/2)]$, which is Hermitian with respect to x'. In addition, the region of support of $W_f(x_0,u)$ is identical to that of f(x) in both the coordinate and frequency domains.

In computing the WDF, the major bottleneck is the Fourier transformation. In the case of a 1-D (2-D) input signal, a full 1-D (2-D) Fourier transform must be performed for each value of the 1-D (2-D) coordinate. Were this to be done digitally in the case of a 1-D discrete signal of n samples, it would require n multiplications to produce the product function. A total of $n\log_2 n$ multiplications is needed to compute the subsequent fast Fourier transform, giving a total of $n + n\log_2 n$ multiplications per point. This sequence must be evaluated at each sample in the sequence [corresponding to each value of x in Eq. (1)], giving a total of $n[n + n\log_2 n] \simeq n^2\log_2 n$ multiplications to compute a 1-D discrete WDF. For a 2-D $n \times n$ array, similar reasoning demonstrates that a total of $n^2[n^2 + n^2\log_2 n^2] \simeq 2n^4\log_2 n$ multiplications is required. The motivation to find optical processing algorithms is quite apparent, especially in the application of feature detection or recognition, due to the large quantity of output data.

Several schemes have been developed to generate the 2-D WDF of 1-D signals.[7-9] Recent work by Bamler and Glünder[10] has demonstrated computation of 2-D slices of the 4-D WDF of a real-valued 2-D input transparency. The product function was produced optically by an autocollimating telescope, and the Fourier transformation was performed by a lens. By scanning over the coordinates of the input transparency, all 2-D slices of the complete 4-D WDF can be found.

Computation of Fourier transforms is also susceptible to solution by the Radon transform.[11-14] Data of dimension m, where $m \geq 2$, are reduced to 1-D by integration over $m - 1$ dimensions. A 1-D Fourier transform of the projection data yields one line through the origin of the m-D Fourier transform. Varying the projection angle allows building up the complete Fourier transform. This procedure is easily adapted to computation of the WDF and offers advantages in certain applications.

2. RADON TRANSFORM

The Radon transform has received much attention in the scientific community since the invention of x-ray computed tomography (CT) in the 1960s. It has been used in the fields of astronomy, geology, and nuclear magnetic reasonance.[11] Recently, it has been adapted to feature extraction in optical data processing.[15] In 1917 Johann Radon published[16] the mathematics of the transform, in which he proved that a 2-D mathematical function can be reconstructed from the complete set of its line-integral projections. The basic mathematical analysis of the Radon transform is straightforward and has been considered by several authors,[11,12] so we shall only touch briefly on the main points relevant to 2-D Fourier analysis.

The 1-D line-integral projection $\lambda(p,\phi)$ of a 2-D function $f(\mathbf{r})$ along azimuth direction ϕ (relative to the x-axis) is defined as

$$\lambda(p,\phi) = \int_{-\infty}^{\infty}\int_{-\infty}^{\infty} d^2r f(\mathbf{r})\delta(p - \mathbf{r}\cdot\hat{n}) \, . \tag{3}$$

The projection λ may be regarded as a 1-D function of p, parametrized by ϕ. The 1-D delta function in the integrand reduces the area integral to a line integral along a line normal to $\hat{n}$ and at a distance p from the origin (Fig. 1). The set $[\lambda(p,\phi)]$ for all azimuth angles ϕ constitutes the Radon transform of $f(\mathbf{r})$. As will be demonstrated, the WDF of a 2-D function $f(\mathbf{x})$ may be computed by performing operations on the line-integral projections of an easily derived 2-D function, reducing the 2-D computation of the Fourier transforms for each value of the coordinate vector $\mathbf{x}$ to a series of 1-D operations. This can be seen if a 1-D Fourier transform of a line-integral projection is performed:

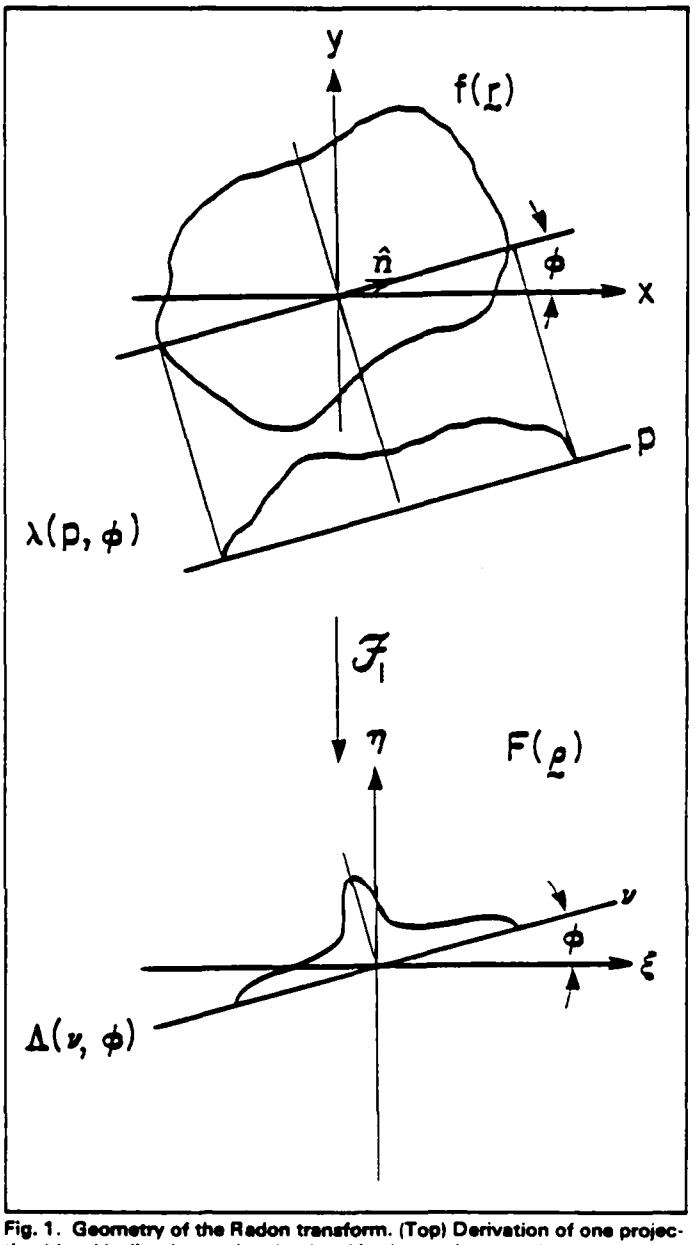

Fig. 1. Geometry of the Radon transform. (Top) Derivation of one projection $\lambda(p,\phi)$ by line-integral projection. Line integrals are evaluated along the azimuth direction $[\phi + (\pi/2)]$ to yield the projection along azimuth direction (ϕ). The unit vector $\hat{n}$ defines the azimuth (ϕ). (Bottom) Central-slice theorem: the 1-D Fourier transform of a line-integral projection yields one line through the 2-D Fourier transform of the original 2-D function.

$$\mathcal{F}_{p\to\nu}[\lambda(p,\phi)] = \Lambda(\nu,\phi)]$$

$$= \int_{-\infty}^{\infty} dp\, e^{-2\pi i\nu p} \int_{-\infty}^{\infty}\int_{-\infty}^{\infty} d^2r\, f(\mathbf{r})\delta(p - \mathbf{r}\cdot\hat{n})$$

$$= \int_{-\infty}^{\infty}\int_{-\infty}^{\infty} d^2r\, f(\mathbf{r})e^{-2\pi i\hat{n}\nu\cdot\mathbf{r}}$$

$$= F(\rho)_{\rho = \hat{n}\nu} \, . \tag{4}$$

where lowercase letters denote functions in coordinate space and uppercase letters denote the Fourier transforms, and ρ is the 2-D spatial frequency vector. This result shows that the 1-D Fourier transform of the line-integral projection $\lambda(p,\phi)$ of the 2-D function $f(r)$ yields one line through the origin of the 2-D Fourier transform of $f(r)$ (Fig. 1). This is the central-slice or projection-slice theorem. The advantage of using the Radon transform approach to 2-D Fourier transformation results from the ability to do the Fourier transformation in one dimension once the projections are available. There are several efficient 1-D processors available to perform the Fourier transformation, including acousto-optic cells, charge-coupled device (CCD) transversal filters, and surface acoustic wave (SAW) dispersive delay lines. The system constructed uses SAW delay lines in the chirp-transform algorithm, as will be discussed shortly.

3. FLYING LINE SCANNER

To use the Radon transform to compute Fourier transforms, it is first necessary to produce the line-integral projection of the 2-D function. This is easily done optically using a device we call a flying line scanner (Fig. 2.), which projects a line of light onto the input transparency. The azimuth of the line of light can be selected by an image rotator, e.g., a dove prism. The light transmitted through the transparency is proportional to the line integral of the intensity transmission along that line. An acousto-optic scanner allows the line of light to be swept perpendicular to itself [i.e., varying p in $\lambda(p,\phi)$, Eq. (3)]. The light transmitted is collected by the photomultiplier tube (PMT), whose output current in time is proportional to $\lambda(p,\phi)$. Rotation of the dove prism varies the angle ϕ and allows the entire set $[\lambda(p,\phi)]$ to be collected.

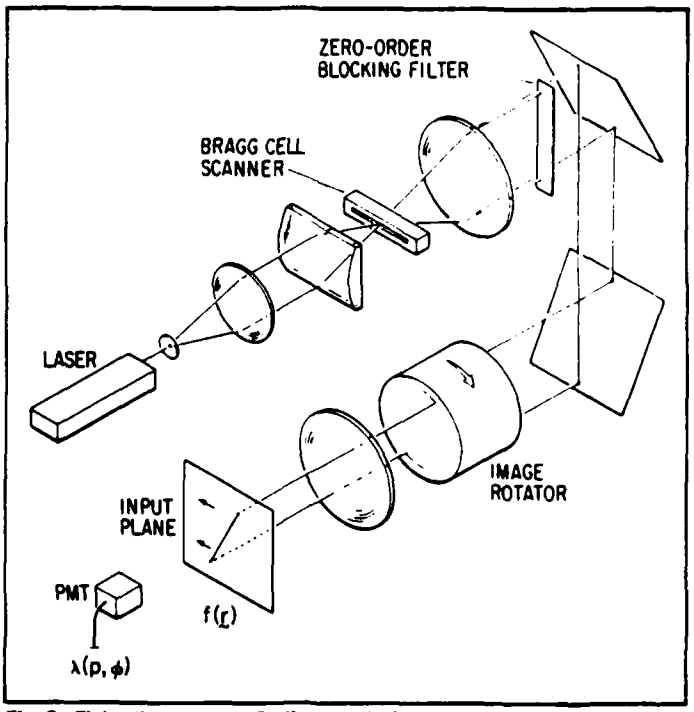

Fig. 2. Flying line scanner. Collimated He-Ne laser light is focused onto the Bragg cell by a cylindrical lens. The zero-order diffraction is blocked by the filter, and the first-order beam passes through to the image rotator. The relay optics images the line of light onto the transparency $f(\vec{r})$. Application of a linear FM signal to the Bragg cell scans the line of light across the transparency. The transmitted light is collected by the photomultiplier tube. For a particular azimuth angle ϕ selected by the image rotator, the PMT output signal in time is proportional to the line-integral projection $\lambda(p,\phi)$.

4. SAW CHIRP FOURIER TRANSFORM

The SAW filter is an acoustoelectric device that can be designed to have one of a wide variety of impulse responses. It consists of a piezoelectric crystal substrate upon which is deposited a pair of conductive interdigital transducers (Fig. 3). A rf signal applied to one transducer produces a rf field between the fingers of the transducer. This field distorts the crystal piezoelectrically, and these displacements travel along the crystal surface at the sound velocity. When the acoustic wave reaches the second transducer, an electric field is piezoelectrically induced in the conductor. The resulting electric signal is the convolution of the input signal and the filter's impulse response. By appropriate design of the interdigital transducers, the desired response may be obtained.[17]

To perform Fourier transformation, three filters with linear FM impulse responses are required for the chirp-transform algorithm. The impulse response of a linear FM filter is

$$h(t) = e^{i(\omega_0 \pm \alpha t)t} = e^{i\omega_0 t} e^{\pm i\alpha t^2}, \tag{5}$$

where ω_0 is the frequency at $t = 0$ and α is the "chirp rate."

If we ignore the constant frequency ω_0, a signal $f_i(t)$ applied to a filter of impulse response $h(t) = e^{+i\alpha t^2}$ will produce an output signal $f_0(t)$:

$$f_o(t) = f_i(t) * e^{i\alpha t^2}$$

$$= \int_{-\infty}^{\infty} d\tau\, f_i(\tau)\, e^{i\alpha(t-\tau)^2}, \tag{6}$$

where * denotes convolution. Expanding the exponential factor, we obtain

$$f_o(t) = e^{i\alpha t^2} \int_{-\infty}^{\infty} d\tau \left[f_i(\tau)\, e^{i\alpha\tau^2} \right] e^{-2i\alpha\tau t}. \tag{7}$$

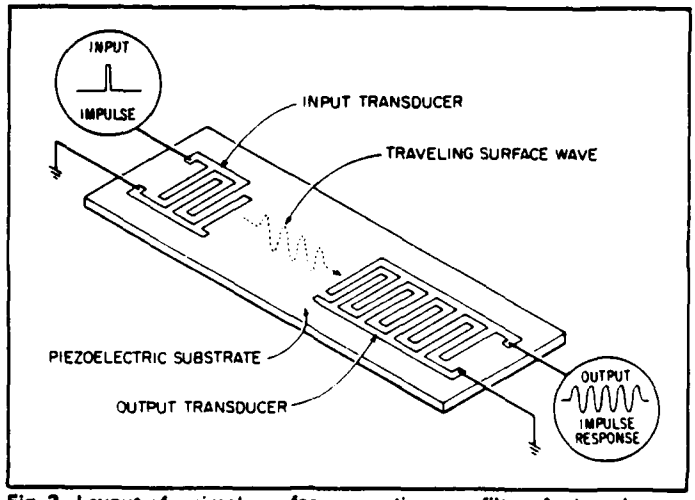

Fig. 3. Layout of a simple surface acoustic wave filter. An impulse applied to one transducer produces a traveling acoustic wave on the surface of the piezoelectric substrate. The frequency of the wave is determined by the spacing of the fingers in the interdigital transducer and the amplitude by the amount of finger overlap. The acoustic wave is sampled by the output transducer. The overall filter impulse response is the convolution of the responses of the two transducers. For linear chirp filters, the response to an impulsive input is a signal varying linearly in frequency over time.

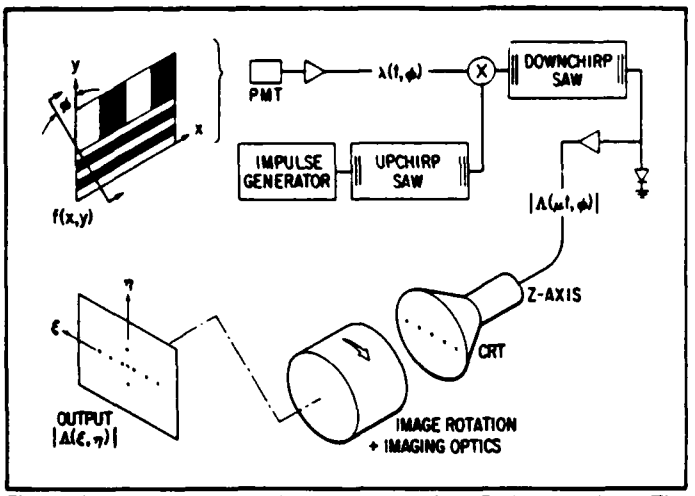

Fig. 4. Fourier spectrum analysis by means of the Radon transform. The line of light produced by the flying line scanner (Fig. 2) passes through the input transparency $f(x,y) = f(\bar{r})$. The light collected by the PMT produces a time signal proportional to the line-integral projection $\lambda(t,\phi)$. This signal is multiplied by an upchirp $[h(t) = e^{+i\alpha t^2}]$ and convolved with a downchirp $[h(t) = e^{-i\alpha t^2}]$. The output is demodulated, giving a signal proportional to the magnitude of the 1-D Fourier transform of $\lambda(t,\phi)$. This is displayed on a CRT and integrated on the output plane (photographic film) to give the 2-D Fourier power spectrum.

Identifying t as $\pi\nu/\alpha$ produces the equation

$$f_o(t) = f_o\left(\frac{\pi}{\alpha}\nu\right) = e^{i\alpha t^2}\int_{-\infty}^{\infty}\left[f_i(\tau)\,e^{i\alpha\tau^2}\right]e^{-2\pi i\nu\tau}\,d\tau$$

$$= e^{i\alpha t^2}\,\underset{\tau\to\nu}{\mathcal{F}}\left[f_i(t)\,e^{i\alpha t^2}\right]. \qquad (8)$$

The Fourier transform is thus obtained in three steps:

(1) $f_i(t)$ is multiplied by $e^{-i\alpha t^2}$ (premultiplication).
(2) This product is convolved with a filter of impulse response $e^{i\alpha t^2}$.
(3) The resultant is multiplied by $e^{-i\alpha t^2}$ (postmultiplication).

If only the modulus is required, the postmultiplication can be deleted. Of course, in actuality, the filters have finite time windows of width T, which affect the limits on the integrals in Eqs. (6) through (8), and overall have the effect of convolving the result with a sinc(t/T) function. In practice, the premultiply and postmultiply chirps are produced by applying an impulse input at the appropriate time to SAW filters whose impulse response is the appropriate chirp.

A Fourier transformer with this algorithm was constructed using dispersive filters from Andersen Labs (models DS-120-10-20-251A and -251B). The time dispersion of both models is 20 μs, and the bandwidth is 10 MHz. The chirp slopes of the two models are of opposite sign. The time-bandwidth product of the system (and hence the number of resolvable spots in the transform) is only 50, but with more sophisticated filters the time-bandwidth product could be boosted to 2000 or more, if required.

A 2-D Fourier spectrum analyzer was constructed using the flying line scanner to produce the projection and the SAW filters to take the transform (Fig. 4.). The transformed signal is demodulated and applied to the z-axis of a CRT. For each projection, this gives one line through the 2-D Fourier transform. For each new azimuth, a new line is written on the CRT and displayed on the output plane at the proper orientation by the image-rotating dove prism. Results of the Fourier analysis of a test pattern are shown in Fig. 5. Taking the line-integral projection data requires 10 μs, and the transform data are read out less than 20 μs later, so it is feasible to perform the full 2-D spectrum analysis at video rates if the image rotation rate is 900 rpm, requiring a prism rotation rate of 450 rpm.

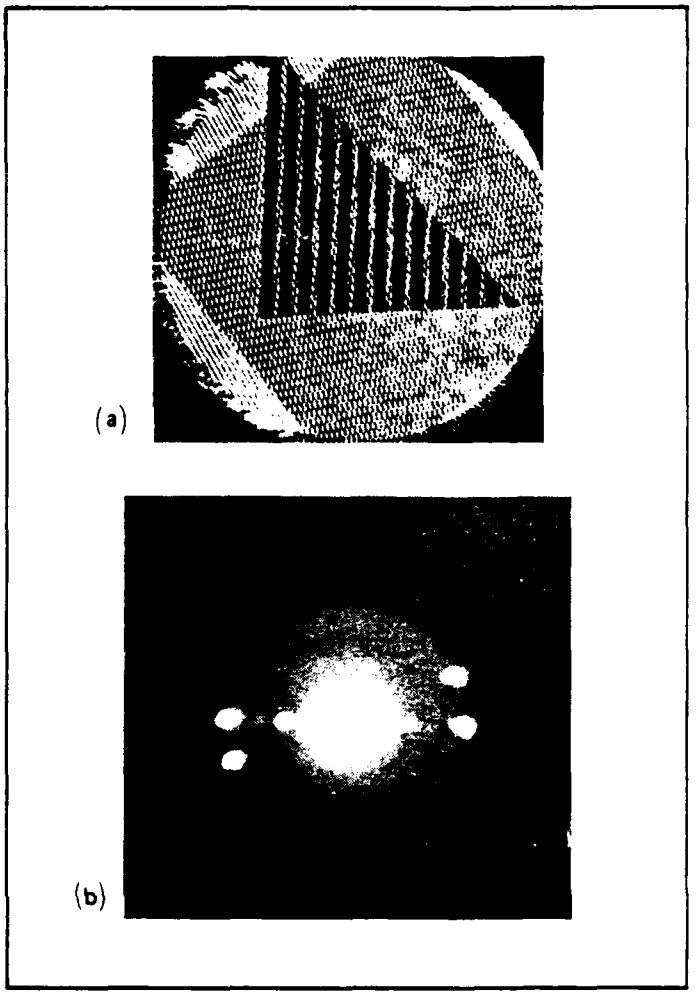

Fig. 5. Spectrum analysis by means of the Radon transform. (a) Input function. (b) Output obtained from apparatus of Fig. 4. The fundamental spatial frequencies of the fine gratings and three orders from the coarse grating are visible.

5. RADON IMPLEMENTATION OF THE 4-D WDF

To compute the 4-D WDF of a 2-D real function $t(\mathbf{r})$, it is necessary to form the product function $t[\mathbf{r}_0 + (\mathbf{r}'/2)]\,t[\mathbf{r}_0 - (\mathbf{r}'/2)] = m(\mathbf{r}_0,\mathbf{r}')$ for all values of $\mathbf{r}'$ and then Fourier transform over $\mathbf{r}'$. We can apply the Radon transform to this computation in the following manner. First, we take line-integral projections of the product function

$$\lambda(p,\mathbf{r}_0,\phi) = \iint d^2\mathbf{r}'\,m(\mathbf{r}_0,\mathbf{r}')\,\delta(p - \mathbf{r}'\cdot\hat{\mathbf{n}}) \qquad (9)$$

The geometry of the projection is shown in Fig. 6. Taking the 1-D Fourier transform of $\lambda(p,\mathbf{r}_0,\phi)$ yields [by the central-slice theorem, Eq. (4)] one line through the 2-D *slice* of the WDF evaluated at $\mathbf{r}_0$. By rotating the azimuth ϕ, we can build up the 2-D slice in exact analogy to the 2-D spectrum analyzer. By sampling over the two coordinate dimensions, the complete 4-D WDF can be computed. The geometry for the Radon transform calculation of one line through the WDF is shown in Fig. 7.

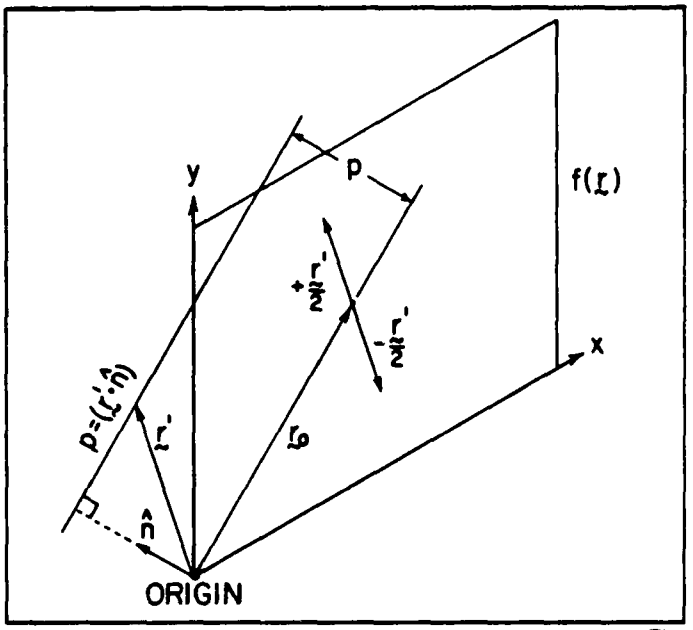

Fig. 6. Line-integral projections of the Wigner distribution function. The integration is made over the line $p = \vec{r} \cdot \hat{n}$.

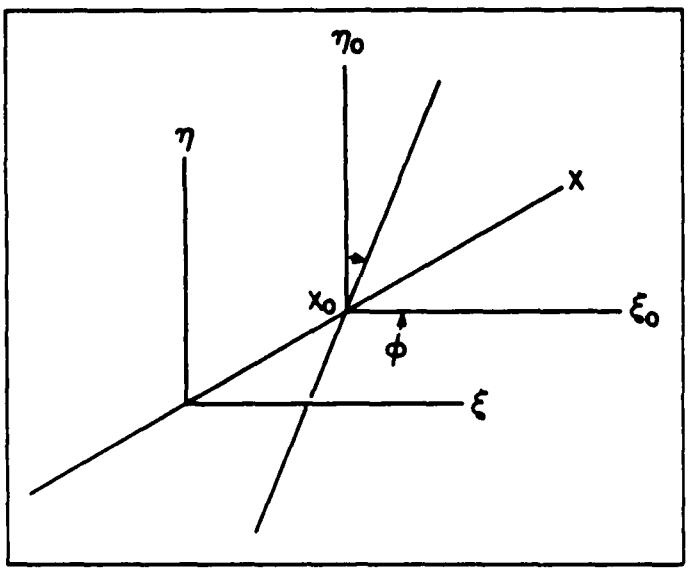

Fig. 7. Orientation of one output line of the WDF. Consider a line-integral projection of the product function at an angle ϕ to the x-axis at a point $(x_0,0)$. The line of the WDF so obtained is oriented in 4-D WDF output space as shown, where the y-coordinate axis has been ignored.

To produce the line-integral projection of the product function, the technique used by Bamler and Glünder[10] was adapted as pictured in Fig. 8. The input transparency is placed in the flying line scanner with the optic axis passing through the point r_0 of the transparency. The transmitted light is collected by a lens, focused on a mirror, and reimaged by the lens back on the transparency. The doubly transmitted light is reflected out of the system by a beam splitter, collected, and detected by the PMT. The PMT output current is proportional to the line integral of $m(r_0,r')$. As the flying line is scanned across the transparency, the temporal signal out of the PMT is proportional to the integral of $m(r_0,r')$ for different values of r'. The signal is Fourier transformed, yielding one line through the WDF. Other values of r_0 may be interrogated either by moving the transparency relative to the optic axis or by tilting the mirror. Using a galvanometer scanner,

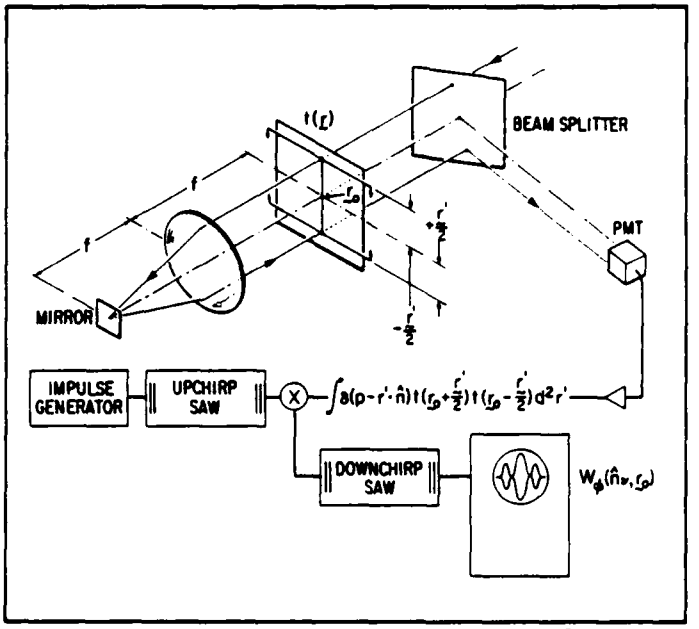

Fig. 8. Hybrid system to generate the WDF of a real input $t(\vec{r})$. The line of light from the flying line scanner passes through the beam splitter onto the transparency centered at $\vec{r}_0 + (\vec{r}'/2)$. The light transmitted is refocused onto the transparency by the lens-mirror system, but is now centered at $\vec{r}_0 + (\vec{r}'/2)$. The output is reflected by the beam splitter onto the PMT. The PMT output is Fourier transformed by the SAW filter as before and yields one line through the WDF of $t(\vec{r})$.

mirror tilting may be done quite rapidly. Results are shown in Fig. 9.

This method offers an advantage over that of Bamler and Glünder in some applications. Since the Fourier transformation is not optical, coherent illumination is not required if an appropriate scanning technique is used.

6. COMPUTATION OF THE CROSS-WIGNER DISTRIBUTION FUNCTION AND ITS RELATION TO THE SLIDING-WINDOW SPECTRUM

The sliding-window spectrum of a function f(r) windowed by a function g(r) is defined as[10]:

$$S_{fg}(r',u) = \int_{-\infty}^{\infty}\int_{-\infty}^{\infty} f\left(r + \frac{r'}{2}\right) g^*\left(r - \frac{r'}{2}\right) e^{-2\pi i u \cdot r}\, d^2r \,. \quad (10)$$

From Eq. (2), we can define a cross-Wigner distribution function (CWDF) to be

$$W_{fg}(r,u) = \int_{-\infty}^{\infty}\int_{-\infty}^{\infty} f\left(r + \frac{r'}{2}\right) g^*\left(r - \frac{r'}{2}\right) e^{-2\pi i u \cdot r'}\, d^2r' \,. \quad (11)$$

By changing variables in Eq. (11) to $q = r'/2$, we obtain

$$W_{fg}(r,u) = 2 \int_{-\infty}^{\infty}\int_{-\infty}^{\infty} f(r+q) g^*(r-q)\, e^{-2\pi i (u \cdot 2q)}\, dq^2 \,. \quad (12)$$

Assuming a symmetric window function [$g(r) = g(-r)$] and using Eq. (10), we find

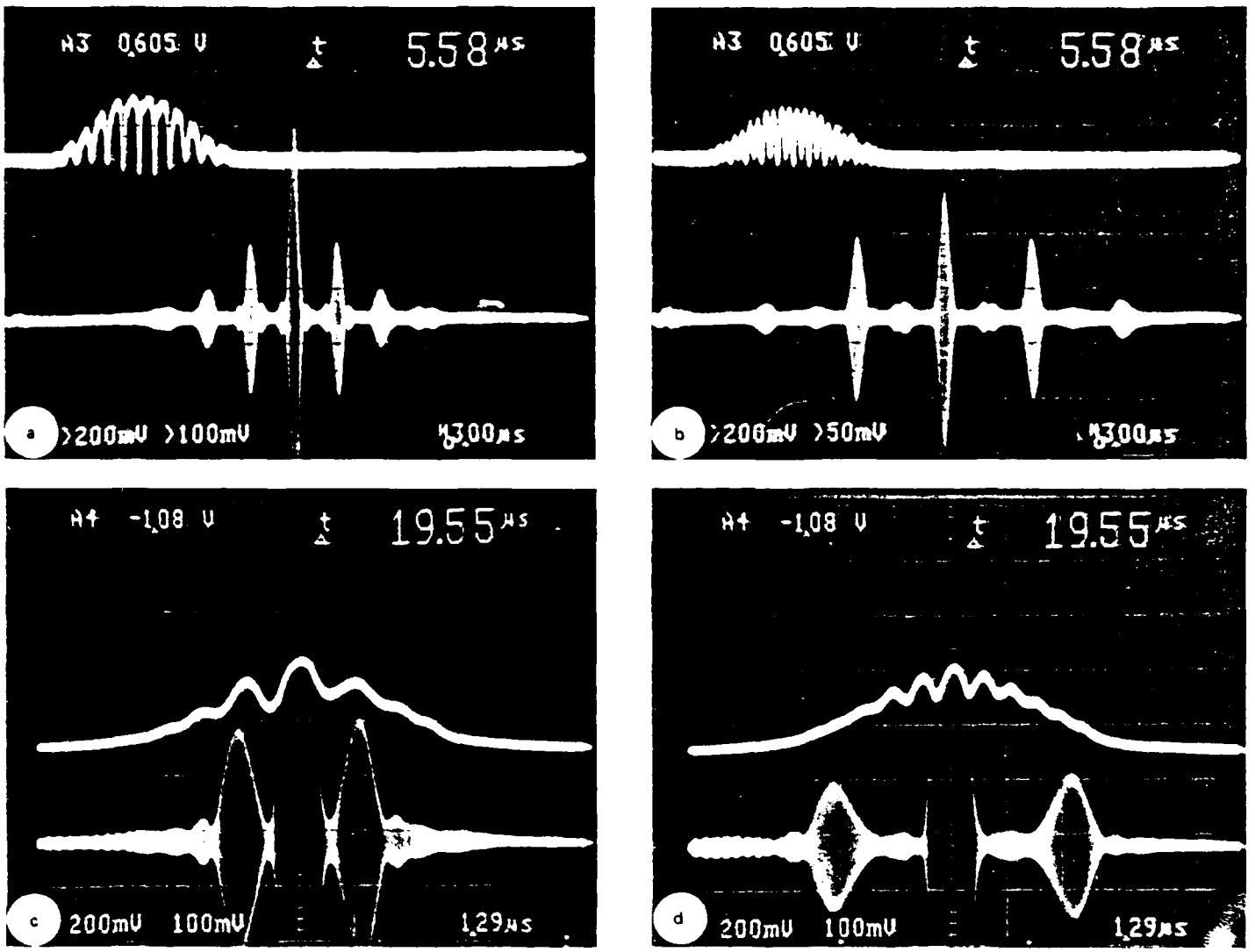

Fig. 9. 1-D slices through the 4-D WDF of two 2-D objects. In each case, the upper trace is the signal from the PMT, representing $\lambda(\rho,\phi)$ [Eq. (5)]. The lower trace is the output of the chirp Fourier transformer. Since there was no postmultiply chirp, the magnitude of the transform modulates the carrier frequency. In (a) and (b), the object is a grating of 25% duty cycle (25% opaque, 75% transparent) in a circular aperture. The envelope of the upper trace is due to the line-integral projection of the circular aperture. In (a), the grating is positioned with the optic axis centered on an opaque grating line [defining $\vec{r}_0$ in Eq. (2)]. The components of the product function exactly "overlay," and the WDF at this coordinate is dominated by the fundamental frequency of the grating. In (b), the object has been shifted (varying $\vec{r}_0$) so that an opaque grating line of one shifted function "overlays" the transparent region in the other shifted function. Hence the WDF is dominated by a frequency twice that of the fundamental of the grating. In (c) and (d), the object is a Fresnel zone plate, and the coordinate displacement is normal to the scanning line. Shifting one zone plate relative to the other results in a linear moire whose spatial frequency increases linearly with increased shift.

$$W_{fg}(\mathbf{r},\mathbf{u}) = 2\int_{-\infty}^{\infty}\int_{-\infty}^{\infty} f(\mathbf{q}+\mathbf{r})g^*(\mathbf{q}-\mathbf{r})\,e^{-2\pi i(2\mathbf{u})\cdot\mathbf{q}}\,d^2q$$

$$= 2S_{fg}(2\mathbf{r},2\mathbf{u}) \qquad (13)$$

Thus, by computing the CWDF of a function using a symmetric window, we can find a scaled version of the sliding-window spectrum. This is useful in some pattern-recognition applications where the local frequency spectrum is of value.[18]

Evaluation of the CWDF is also possible using the Radon transform. The setup is shown in Fig. 10. It is similar to the system for finding the WDF except that the reflecting telescope arrangement has been replaced with a second lens and transparency to supply the window function. As before, one line through the spectrum is calculated at a time. In cases of directional texture, this will result in a reduced throughput of insignificant data. Results for an Air Force three-bar chart are shown in Fig. 11.

7. CONCLUSIONS

We have demonstrated a hybrid optical analog electronics processor that can rapidly compute 1-D lines through the Wigner distribution function and cross-Wigner distribution function of real-valued 2-D inputs. In certain pattern-recognition applications, such as recognition and classification of scenes with directional texture, this technique offers advantages over digital processors in speed and over other optical processors in output configuration.

8. ACKNOWLEDGMENTS

We would like to thank H. H. Szu for a helpful discussion. This research was sponsored by the Air Force Office of Scientific Research, contract number AFOSR-82-0249.

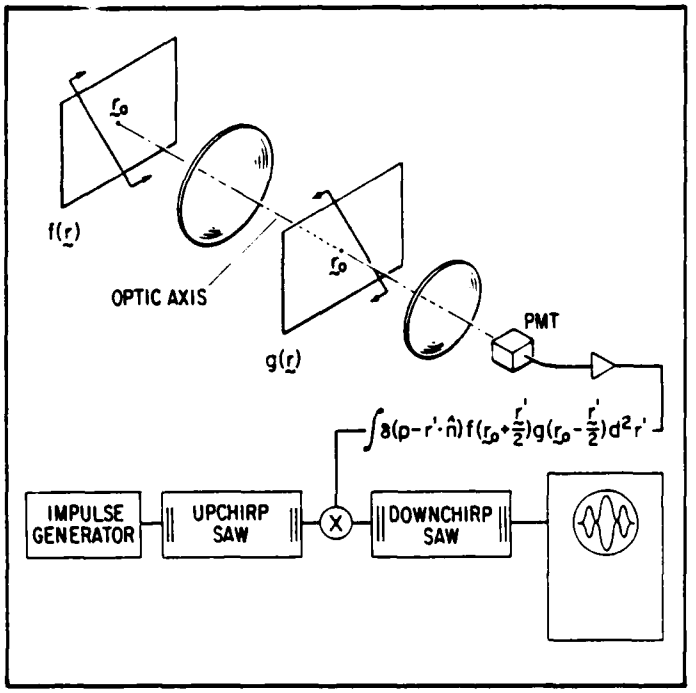

Fig. 10. Setup to compute the cross-Wigner distribution function. The line of light incident on f($\vec{r}$) is reimaged on g($\vec{r}$). The total light incident on the PMT is proportional to the line integral of f[$\vec{r}_0 + (\vec{r}'/2)$]g[$\vec{r}_0 - (\vec{r}'/2)$]. The Fourier transform with respect to $\vec{r}'$ gives the CWDF.

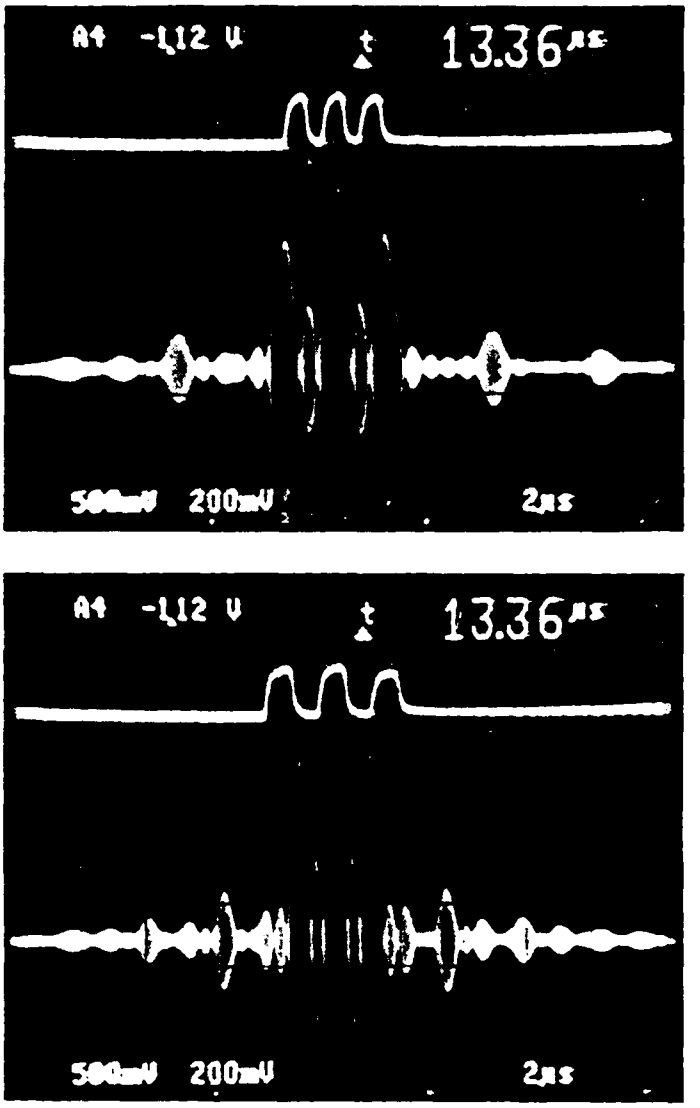

Fig. 11. 1-D slices of the 4-D CWDF of a 2-D Air Force three-bar resolution chart. The window function was a square aperture and was shifted to examine two areas of the chart.

9. REFERENCES

1. E. Wigner, Phys. Rev. 40, 749 (1932).
2. B. V. K. Kumar and C. Carroll, in *10th Int. Optical Computing Conference*, S. Horvitz, ed., Proc. SPIE 422, 130 (1983).
3. H. H. Szu and J. A. Blodgett, AIP Conf. Proc. 65, 355 (1981).
4. H. H. Szu, Opt. Eng. 21(5), 804 (1982).
5. T. A. M. C. Claasen and W. F. G. Mecklenbräuker, Phillips J. Res. 35, 217 (1980).
6. M. J. Bastiaans, AIP Conf. Proc. 65, 292 (1981).
7. H. O. Bartelt, K.-H. Brenner, and A. W. Lohmann, Opt. Commun. 32, 32 (1980).
8. R. A. Athale, J. N. Lee, E. Larry Robinson, and H. H. Szu, Opt. Lett. 8, 166 (1983).
9. K.-H. Brenner and A. W. Lohmann, Opt. Commun. 42, 310 (1982).
10. R. Bamler and H. Glünder, Opt. Acta 30, 1789 (1983).
11. S. R. Deans, *The Radon Transform and Some of Its Applications*, John Wiley & Sons, New York (1983).
12. H. H. Barrett, "The Radon Transform and Its Applications," in *Progress in Optics*, Vol. 21, E. Wolf, ed., North-Holland, Amsterdam (1984).
13. H. H. Barrett, in *Transformations in Optical Signal Processing*, W. T. Rhodes, J. R. Fienup, B. E. A. Saleh, eds., Proc. SPIE 373, 179 (1984).
14. R. L. Easton, Jr., H. H. Barrett, and A. J. Ticknor, Proc. of 1983 IEEE Ultrasonics Symposium, B. R. McAvoy, ed., p. 185, IEEE, New York (1983).
15. G. R. Gindi and A. F. Gmitro, Opt. Eng. 23(5), 499 (1984).
16. J. Radon, Ber. Sächsische Akademie der Wissenschaften, Leipzig, Math-Phys. Kl. 69, 262 (1917). Translated in S. R. Deans, *The Radon Transform and Some of Its Applications*, John Wiley & Sons, New York (1983).
17. A. A. Oliner, ed., *Acoustic Surface Waves*, Springer-Verlag, New York (1978).
18. R. P. Kruger, E. L. Hall, and A. F. Turner, Appl. Opt. 16, 2637 (1977).

TOMOGRAPHIC TRANSFORMATIONS IN OPTICAL SIGNAL PROCESSING

Roger L. Easton, Jr.
Harrison H. Barrett

Optical Sciences Center
University of Arizona
Tucson, AZ 85721

I. Introduction and definitions

A. History, development

B. Basic theory
   1. forward Radon transform, projections
   2. central-slice theorem
   3. filter theorem
   4. inverse Radon transform

C. Application to optical signal processing
   1. Optical Radon transformer
   2. 1-D processor technologies
      a. electronic systems
      b. charge-transfer devices
      c. acousto-electric devices
      d. acousto-optics (AO)
   3. Optical Implementation of filtered back-projection

II. Applications

A. Operations on 2-D Signals
   1. Fourier transformation
      a. power spectrum
      b. complex transforms
      c. Hartley transform
   2. filtering and correlation
   3. pattern recognition
      a. image moments
      b. Hough transform
   4. image coding and bandwidth compression
   5. spectrum estimation
   6. linear, space-variant operations
   7. bilinear and nonlinear operations

B. Operations on 3-D signals
   1. 3-D spatial and 2-D spatial + 1-D temporal data
   2. 2-D spatial + 1-D spectral data

III. Summary and Conclusions

1. Introduction and Definitions

Traditionally, the motivation for processing signals by optical means is due primarily to two factors. The first is the ability of coherent optical systems using spherical elements to perform the Fourier transform, while the second is the inherent capability of optical systems to operate on two-dimensional (2-D) data planes. For 2-D signals (e.g. images), optical processing is of obvious utility, but even if the signals to be processed are one-dimensional (1-D), optical techniques may allow parallel processing of several channels. The increased system throughput thus obtained may make optical processing attractive relative to more precise (but as yet slower) digital electronic technologies.

The main thrust of research in optical signal processing has been directed at applying either or both of the capabilities of rapid Fourier transformation and parallelism. However, there are problems restricting the utility of optical processing that are well-known to those working in the field and which diminish its attractiveness relative to digital electronic processing. Primary among these are the limitations of available 2-D input/output devices (spatial light modulators and detector arrays), and (for coherent systems) speckle noise. These limitations are responsible for restricting the use of optical processing to a few applications in which they are not significant (e.g. off-line synthetic aperture radar processing). In marked contrast to the situation for 2-D hardware, signal-processor technology for temporal (1-D) signals is quite advanced in capability and flexibility, and hence it may be profitable to apply that 1-D technology to 2-D operations, if possible. In effect, this would allow a trade-off between rapid parallel processing and precise serial processing in a hybrid system. Several algorithms are available to derive 1-D signals from a 2-D input and reconstruct the 2-D processed signal. A familiar example of such an operation is the television raster, which creates a 1-D temporal signal from 2-D imagery by scanning and rederives the 2-D image by stacking segments of the temporal signal (Rhodes,

1981b). The raster transduction was used in optical signal processing by Thomas (1966) to generate a 2-D array from a long 1-D temporal signal to use as input to a 2-D optical processor. Several other dimensional transduction operations were considered by Bartelt and Lohmann (1981). One that is becoming more familiar can be called a tomographic transformation, where a 1-D data set is derived from a 2-D signal by integration along sets of parallel lines. The relation between these two sets of data has some nice mathematical properties that make the transformation potentially very useful in both analog and digital signal processing.

I.A. History and Development

The mathematical basis for the tomographic transformation was derived in 1917 by Johann Radon, an Austrian mathematician. Radon proved that the complete set of 1-D projections of continuous 2-D or 3-D functions with compact support contain all of the information in the original function. The projections are derived by integration of the 2-D function over sets of parallel lines, or by integration of the 3-D function over parallel planes. The derivation of the 1-D projections from the function is the forward Radon transform. Radon also derived expressions for reconstruction of the function from its projections--the inverse Radon transform. Generalization of the theory has made it applicable to functions of higher dimensionality (John, 1955). Another development was made by Cormack (1963, 1964), who formulated the mathematical expansion of projections into circular harmonics, i.e. a discrete angular Fourier series representation of the projection data.

Radon was primarily interested in using projections to find solutions of Poisson's differential equation in electrostatics, but his work has been applied to a myriad of scientific disciplines since the 1950s, including crystallography, radio astronomy, geophysics, nuclear magnetic resonance, radiative scattering, and diagnostic radiology. This explosion

of interest is evident by the number of publications on the subject, especially in the last 15 years or so. For a good discussion of applications and an extensive bibliography, see Deans (1983). No doubt the application of the Radon transform most familiar to the lay public is in diagnostic radiology. The new fields of x-ray computed tomography (CT), emission computed tomography (ECT), and magnetic resonance imaging (MRI), which enable imaging of cross-sectional slices of the body of a patient from sets of projection data, have received much attention in the popular press. Indeed, the medical application of Radon's theory is the source of its now familiar name; "tomography" is derived from the Greek word for slice. Each of these new medical wonders owes its existence to Johann Radon and the subsequent researchers who generalized and applied the mathematical theory.

In each of the applications listed above, Radon's mathematical theory is used to solve an inverse problem, where the source function is mathematically reconstructed from the projection data. Of course, the complete infinite set of projections is never collected, making it impossible to uniquely reconstruct the source function; only some "best" estimate may be found. We shall not overly concern ourselves here with such niceties, as they are somewhat removed from the purpose at hand and have been considered at length elsewhere (Rowland, 1979) (Barrett and Swindell, 1981). Rather, we wish to investigate the use of the Radon transform as a dimensional transducer in signal processing. The discrete nature of the data set will still be of some concern to us, mainly due to nonuniform sampling of Cartesian space by the transformation, but our main purpose is the identification of signal processing operations that are possible and profitable to perform via a tomographic transformation. For some of these, the processed 1-D data alone may be sufficient for the task at hand, but often it will be desirable to reconstruct the processed 2-D signal from the processed projections and so some consideration will be given to optical methods of generating the inverse Radon transform.

I.B. Basic Theory

In the literature, there are several extensive mathematical developments of the theory of the Radon transform, e.g. Helgason (1980), Deans (1983), and Barrett (1984) . Consequently, we shall keep our discussion brief and emphasize applicability rather than completeness or mathematical rigor. Also, we shall generally restrict our treatment to the 2-D problem, with occasional remarks about application to 3-D when warranted.

I.B.1. Forward Radon Transform, Projections

Given a 2-D function $f(\mathbf{r}) = f(x,y)$ (as is common, we shall denote vectors by boldface characters), a single projection along an azimuth angle ϕ can be derived by integration along all lines at azimuth $\phi + \pi/2$. The one-dimensional function thus generated has as independent variable the perpendicular distance of the integration line from the origin. This distance is the magnitude of the vector p, where $\mathbf{p} = (p,\phi)$ in polar coordinates. It is also useful to define a unit vector $\hat{\mathbf{n}} = \frac{\mathbf{p}}{|\mathbf{p}|} = (1,\phi) = [\cos\phi, \sin\phi]$ (n.b. square brackets denote Cartesian coordinates and parentheses denote polar coordinates). Naturally, for each set of integration lines at different angles relative to the x-axis, a different projection is derived. A common notation for a projection is $\lambda(p,\phi)$, implying that λ is a 2-D function. But since all operations on the projection will act on the spatial coordinate p alone, we can consider the projection to be a 1-D function parametrized by the azimuth angle ϕ. Depending on one's mathematical preference, $\lambda(p,\phi)$ can be defined in a number of equivalent ways For example, we can consider a projection to be obtained by integration over lines parallel to the y'-axis in a system of coordinates [x',y'] rotated at angle ϕ relative to the original [x,y] axes. However, there are distinct advantages obtained by defining a projection as a 2-D integral transform whose kernel is a 1-D Dirac delta function which selects the projection azimuth, as shown in Figure 1. Consider a

projection azimuth ϕ defined by the polar unit vector $\hat{\mathbf{n}} = (1,\phi)$. We wish to determine the value of the projection coordinate p that will be influenced by a point in the 2-D function located at $\mathbf{r} = (|\mathbf{r}|,\theta) = [r\cos\theta, r\sin\theta]$. As is apparent from Figure 1, $\mathbf{r}$ must be located on the line normal to $\hat{\mathbf{n}}$ at a perpendicular distance from the origin defined by

$$p = r\cos(\theta-\phi) = (r\cos\theta\cos\phi + r\sin\theta\sin\phi) = \mathbf{r}\cdot\hat{\mathbf{n}}. \qquad (1)$$

Hence, multiplying $f(\mathbf{r})$ by $\delta(p - \mathbf{r}\cdot\hat{\mathbf{n}})$ collapses the area integral to a set of line integrals for the azimuth defined by $\hat{\mathbf{n}}$, giving

$$\lambda(p,\phi) = \int_{-\infty}^{\infty}\int_{-\infty}^{\infty} d^2r\, f(\mathbf{r})\,\delta(p - \mathbf{r}\cdot\hat{\mathbf{n}}). \qquad (2)$$

The transformation has mapped the Cartesian coordinates [x,y] to a new system (p,ϕ), which is called Radon space. We have a choice about the limits on the new coordinates. If we consider p to be bipolar ($-\infty \leq p \leq \infty$), then $\lambda(p,\phi) = \lambda(-p,\phi+\pi)$. We may therefore limit ϕ to the region ($0 \leq \phi \leq \pi$). If we require p to be positive, then ϕ runs over 2π radians. The former choice is usually preferred, since it simplifies the mathematical development. A plot of the Radon transform in (p,ϕ) space (Figure 2) is termed a sinogram, since a point in Cartesian space maps to a sinusoid in Radon space. From eq. (2), it is easy to see that the Radon transform is linear and space-variant. It is often convenient to express the projection operation in operator notation, e.g. $R_2[f(\mathbf{r})] = \lambda(p,\phi)$, where the subscript $_2$ denotes that the function being transformed is two-dimensional.

The projection operation described by eq. (2) can be easily extended to functions of higher dimensionality (Barrett, 1984). For example, a 1-D projection of a 3-D function can be obtained by integration over parallel 2-D planes. Hence the 1-D Dirac delta function in eq. (2) now reduces the volume integral to a planar integral. The transform collapses the 3-D function f(x,y,z) to a set of 1-D projections (e.g. $\lambda(p,\phi,\theta)$) parametrized by the two

angles defining the unit normal to the planes of integration.

I.B.2. Central-Slice Theorem

Now that the forward Radon transform has been defined, we need to investigate its properties that may be useful for signal processing. Foremost of these is the central-slice theorem, which relates the Fourier transform of a 2-D function to the 1-D Fourier transforms of its projections. The theorem arises because the kernel of the Radon transform is a Dirac delta function of the scalar product of the conjugate variables r and ρ, as the kernel of the Fourier transform is a function of the scalar product of conjugate variables r and ρ. As is customary, we define the Fourier transform of a 2-D function f(r) as

$$\mathcal{F}_2 [f(r)] \equiv F(\rho) = \int_{-\infty}^{\infty}\int_{-\infty}^{\infty} d^2r\, f(r)\, e^{-2\pi i \rho \cdot r}, \tag{3}$$

where $\mathcal{F}_2$ is the 2-D Fourier transform operator from coordinate $r = [x,y]$ to spatial frequency $\rho = [\xi,\eta]$. In this notation, functions denoted by a lower-case character are the coordinate-space representation (e.g. f(r)), while the corresponding frequency-space representation is signified by the upper-case character (e.g. F(ρ)). If we perform the 1-D Fourier transform of the projection defined by eq. (2), we obtain

$$\mathcal{F}_1 [\lambda(p,\phi)] \equiv \Lambda(\nu,\phi) = \int_{-\infty}^{\infty} dp\, \lambda(p,\phi)\, e^{-2\pi i p \nu}. \tag{4}$$

Substitution of eq. (2) into eq. (4) yields

$$\Lambda(\nu,\phi) = \int_{-\infty}^{\infty} dp \left[\int_{-\infty}^{\infty}\int_{-\infty}^{\infty} d^2r\, f(r)\, \delta(p - r \cdot \hat{n})\right] e^{-2\pi i p \nu}. \tag{5}$$

Exchanging the order of integration, we obtain

$$\Lambda(\nu,\phi) = \int_{-\infty}^{\infty}\int_{-\infty}^{\infty} d^2r\, f(r) \int_{-\infty}^{\infty} dp\, \delta(p - r \cdot \hat{n})\, e^{-2\pi i p\nu}$$

$$= \int_{-\infty}^{\infty}\int_{-\infty}^{\infty} d^2r\, f(r)\, e^{-2\pi i \hat{n}\nu \cdot r}. \qquad (6)$$

Comparing eq. (6) and eq. (3), we can identify the relation between $\Lambda(\nu,\phi)$ and $F(\rho)$:

$$\Lambda(\nu,\phi) = F(\rho)\Big|_{\rho=\hat{n}\nu} = F(\hat{n}\nu). \qquad (7)$$

So the 1-D Fourier transform of a Radon projection at azimuth angle ϕ relative to the x-axis yields one line through the origin of the 2-D Fourier transform of the function $f(r)$. This line (central slice) in Fourier space is oriented at the same azimuth angle ϕ, but relative to the ξ-axis (Figure 1). The central-slice theorem can be represented in operator notation by:

$$\mathcal{F}_2 = \mathcal{F}_1 R_2. \qquad (8)$$

It is important to note that the 2-D frequency-space representation generated via the Radon-Fourier transform has a sampling density in Cartesian space that falls off as ν^{-1} (Figure 3). This sampling nonuniformity must be compensated whenever a Cartesian-space representation is derived from a Radon-space representation, e.g. for display of the 2-D Fourier transform, or (as will be shown) when reconstructing the 2-D source function via the inverse Radon transform. Also note that the duality of coordinate- and Fourier-space representations ensures that a dual to the central-slice theorem exists. That is, the inverse Fourier transform of a projection in Fourier space is a central-slice of the coordinate space representation of the 2-D function.

A theorem similar in nature to central-slice relates parallel projections weighted by a phase factor to parallel, rather than meridional, lines of the 2-D Fourier transform (Farhat

et al., 1983). If a weighted projection is defined as

$$q(x,n_\theta) = \int_{-\infty}^{\infty} dy\ f(x,y)\ e^{2\pi i n_\theta y}\ , \tag{9}$$

the 1-D Fourier transform of the weighted slice is found to be:

$$\int_{-\infty}^{\infty} dx\ q(x,n_\theta)\ e^{2\pi i \xi x} = \int_{-\infty}^{\infty}\int_{-\infty}^{\infty} dx\ dy\ f(x,y)\ e^{2\pi i(\xi x + n_\theta y)}$$

$$= Q(\xi,n_\theta)\ . \tag{10}$$

Systems for optically generating and processing weighted projections have been proposed (Gmitro et al., 1983), but are substantially more complicated than comparable systems for central slices.

I.B.3. Filter Theorem

Another very useful attribute of the Radon transform may be derived easily via the central-slice theorem. Consider the convolution of two 2-D functions f(r) and g(r). Using operator notation, we can take the 2-D Fourier transform of the convolution:

$$\mathcal{F}_2[f(r) * g(r)] = \mathcal{F}_2\,[f(r)] \times \mathcal{F}_2\,[g(r)]\ . \tag{11}$$

Eq. (11) can be rewritten using the operator notation for the central-slice theorem [eq. (8)], giving:

$$\begin{aligned}\mathcal{F}_2[f * g] &= \mathcal{F}_1 R_2\,[f * g] \\ &= \mathcal{F}_1 R_2\,[f] \times \mathcal{F}_1 R_2\,[g] \\ &= \mathcal{F}_1[\lambda_f(p,\phi)] \times \mathcal{F}_1[\lambda_g(p,\phi)] = \Lambda_f(\nu,\phi) \times \Lambda_g(\nu,\phi)\ ,\end{aligned} \tag{12}$$

where the subscripts f and g are used to denote which function is being projected at the common azimuth angle ϕ. Applying the inverse 1-D Fourier transform operator to eq. (12) yields:

$$\mathcal{F}_1^{-1}\,\mathcal{F}_1 R_2\,[f * g] = R_2\,[f * g] = \lambda_{f*g}$$

$$= \mathcal{F}_1^{-1} [\Lambda_f \times \Lambda_g] = \mathcal{F}_1^{-1} [\Lambda_f] * \mathcal{F}_1^{-1} [\Lambda_g]$$

$$= \lambda_f * \lambda_g , \qquad (13)$$

where the common coordinate variables have been suppressed. In words, this shows that the projection of a 2-D convolution of two functions is the 1-D convolution of the projections of the functions. From this conclusion, it is just a very short conceptual hop to the realization that the same relationship holds for 2-D correlations. Thus, we now have the mathematical capability of deriving the projection of a 2-D filtering or correlation operation simply by performing 1-D filtering or correlation of the projections of the original functions. This is a very powerful result and holds much promise for application to optical processing.

I.B.4. Inverse Radon Transform

Since most of the research into the Radon transform has been directed at the solution of inverse problems, there has been a plethora of publications devoted to the inverse Radon transform. Therefore we shall limit our mathematical discussion to a straightforward derivation of the inverse transform, with some comments made about algorithms appropriate to optical reconstruction methods. Readers interested in an in-depth mathematical development should consult some of the other literature, notably Rowland (1979), Deans (1983), and Barrett (1984).

The inverse Radon transform is most easily derived by applying the central-slice theorem to the polar form of the inverse 2-D Fourier transform:

$$\mathcal{F}_2^{-1}[F(\boldsymbol{\rho})] \equiv f(\mathbf{r}) = \int_{-\pi}^{\pi} d\theta_\rho \int_0^{\infty} d\rho \; \rho \, F(\boldsymbol{\rho}) \, e^{+2\pi i \boldsymbol{\rho} \cdot \mathbf{r}} . \qquad (14)$$

Invoking the central-slice theorem [eq. (7)], we set $\boldsymbol{\rho} = \hat{\mathbf{n}}\nu$, $\rho = \nu$, $\theta_\rho = \phi$, and $F(\boldsymbol{\rho}) = F(\hat{\mathbf{n}}\nu) = \Lambda(\nu,\phi)$ in eq. (14), yielding:

$$f(\mathbf{r}) = \int_0^{\pi} d\phi \int_{-\infty}^{\infty} d\nu \, |\nu| \, \Lambda(\nu,\phi) \, e^{+2\pi i \nu \hat{\mathbf{n}} \cdot \mathbf{r}}$$

$$= \int_0^{\pi} d\phi \, [\, \mathcal{F}_1 \, [\, |\nu| \, \Lambda(\nu,\phi)]]\Big|_{p = \mathbf{r} \cdot \hat{\mathbf{n}}} \, . \qquad (15)$$

This is one form of the inverse Radon transform. In words, it reconstructs a 2-D function $f(\mathbf{r})$ from a complete set of projections $\lambda(p,\phi)$ by the following steps:

(1) 1-D Fourier transform $\lambda(p,\phi)$, yielding $\Lambda(\nu,\phi)$;

(2) multiply by $|\nu|$;

(3) inverse 1-D Fourier transform the product $[|\nu| \, \Lambda(\nu,\phi)]$;

(4) smear this 1-D function perpendicular to the line defined by $p = \mathbf{r} \cdot \hat{\mathbf{n}}$;

(5) sum over all angles ϕ.

Step 4 generates a 2-D function from the 1-D projections and is referred to as "back-projection" since it is the complementary operation to projection. Step 2 is a filtering operation in Fourier space to correct for the sampling nonuniformity of the transformation from Cartesian to Radon space mentioned previously.

It is instructive to rearrange the steps to obtain another recipe for the inverse transform. Back-projection and summation (steps 4 and 5) may be performed first to generate a 2-D unfiltered summation image (sometimes called a "layergram"). The point spread function of the layergram has been shown to be $p(\mathbf{r}) = |\mathbf{r}|^{-1}$ (Peters, 1974), which implies a transfer function $\mathcal{F}_2 \, [\, |\mathbf{r}|^{-1} \,] = |\boldsymbol{\rho}|^{-1}$. This distortion may be corrected by filtering in 2-D with transfer function $|\boldsymbol{\rho}|$, an operation commonly known as "rho-filtering" (often, albeit imprecisely, the 1-D filter $|\nu|$ in step 2 is also referred to as a rho-filter). In reality of course, the noise dominant at high spatial frequencies requires either filter to be rolled-off, or "apodized." Since our rationale for signal processing in Radon space was

to avoid unnecessary 2-D operations, we shall not consider implementations of the alternative recipe. Interested readers should consult Barrett and Swindell (1977, 1981) or Barrett (1984).

We can also express the inverse Radon transform in operator notation (Barrett, 1984), expanding the operator R_2^{-1} into the sequences:

$$R_2^{-1} = B_2 \mathcal{F}_1^{-1} |\nu| \mathcal{F}_1$$

$$= \mathcal{F}_2^{-1} |\rho| \mathcal{F}_2 B_2 \quad , \tag{16}$$

where B_2 is the operator notation for back-projection.

The inverse Radon transform algorithm [eq. (15)] can be recast into a more concise form by invoking the filter theorem of Fourier transforms to create a convolution of functions instead of a product of their Fourier transforms. That is,

$$\mathcal{F}_1^{-1} \left[|\nu| \Lambda(\nu,\phi) \right] = h(p) * \lambda(p,\phi), \tag{17}$$

where $h(p) = \mathcal{F}_1^{-1} \left[|\nu| \right]$ is the filter function in the coordinate space representation. Lighthill (1962) showed that $h(p) = \mathcal{F}_1^{-1} \left[|\nu| \right] = -\frac{1}{2\pi^2 p^2}$, where the singularity at the origin requires that it be interpreted as a generalized function which has a Dirac delta function at the origin. A realizable interpretation is (Gmitro et al., 1980)

$$h(p) = \lim_{\epsilon \to 0} \begin{bmatrix} -\frac{1}{p^2} & |p| \geq \epsilon \\ \frac{1}{\epsilon^2} & |p| < \epsilon \end{bmatrix}. \tag{18}$$

Note that h(p) is bipolar. We can now represent the inverse Radon transform in one equation, with the important proviso that the true nature of the filter function be recognized:

$$f(r) = -\frac{1}{2\pi^2} \int_0^{\pi} d\phi \left[\lambda(p,\phi) * \frac{1}{p^2} \right]_{p = r \cdot \hat{n}}. \tag{19}$$

The operations required to implement this algorithm for the inverse Radon transform are the source of its common name, filtered back-projection. Integration of the convolution product by parts yields other possible expressions for filtered back-projection (Barrett, 1984):

$$f(r) = \frac{1}{2\pi^2} P\left[\int_0^{\pi} d\phi \left[\lambda'(p,\phi) * \frac{1}{p}\right]\right]_{p = r \cdot \hat{n}} \tag{20}$$

$$= \frac{1}{2\pi^2} \int_0^{\pi} d\phi \left[\lambda''(p,\phi) * \ln|p|\right]_{p = r \cdot \hat{n}} \tag{21}$$

$$= \frac{1}{2\pi^2} \int_0^{\pi} d\phi \left[\frac{\partial^2}{\partial p^2} \left[\lambda(p,\phi) * \ln|p|\right]\right]_{p = r \cdot \hat{n}} , \tag{22}$$

where $P[\int dx]$ denotes the Cauchy principal value of the integral, and the primes (e.g. $\lambda'(p,\phi)$) represent derivatives of the function with respect to p. Each representation of the inverse Radon transform [eq. (19-22)] requires a bipolar filter function, a fact having important consequences for optical implementation. Which representation is optimum depends strongly on the limitations of the signal and available hardware. For instance, the dynamic range of the 1-D filter function $\ln|p|$ in eqs. (21-22) is much less than that of $-p^{-2}$ or $P[p^{-1}]$, thus reducing the dynamic range required of the 1-D convolver at the cost of increased noise inherent in taking the second derivative of the projection.

An alternative development of the reconstruction problem was made independently by Cormack. Though not as straightforward in application as filtered back-projection, we shall discuss it briefly because it can potentially be implemented by optical methods (Ein-Gal, 1974) (Hansen and Goodman, 1978). Cormack's development is based on the periodicity in angle of every physically realizable object, i.e. $f(r,\theta) = f(r,\theta + 2\pi)$. As a result, $f(r,\theta)$ can be expanded in a discrete Fourier series of angular basis functions, which are called circular

harmonics:

$$f(r,\theta) = \sum_{n=-\infty}^{\infty} f_n(r)\, e^{in\theta} \tag{23}$$

where

$$f_n(r) = \frac{1}{2\pi} \int_{-\infty}^{\infty} d\theta\, f(r,\theta)\, e^{-in\theta}. \tag{24}$$

Cormack expanded the projections $\lambda(p,\phi)$ in the same manner and derived the space-variant transformation between these two representations. The transformation can be made space-invariant via a Mellin transform (Casasent and Psaltis, 1977), and can then be processed by optical methods (Hofer, 1979) (Hansen, 1981a, 1981b). However, the Cormack reconstruction algorithm is not directly applicable to our task at hand, so we shall not consider it further.

I.C. Application to Optical Signal Processing

To summarize the mathematical development, we have demonstrated that the classic 2-D signal-processing operations of Fourier transformation and convolution (filtering) can be performed via the equivalent 1-D operations on the Radon projections, producing central slices of the 2-D Fourier transform or projections of the 2-D convolution. Of course, there are optical methods available for performing these 2-D operations as well. Coherent computation of the of the 2-D Fourier transform has always been the basis of optical signal processing, but limitations of speckle noise and performance of available spatial light modulators have generally restricted application to static film transparencies in liquid gates. By placing the input in the front focal plane of the transform lens, the correct magnitude and phase of the 2-D Fourier transform are produced in the back focal plane (limited by lens aberrations). However, the phase of the transform is coded in the relative

phases of the coherent wavefront at the various locations in the Fourier plane. Preserving this phase information requires a very precise and stable optical configuration, and square-law detection necessitates heterodyne techniques to decode it. Optical convolution/correlation can be performed by spatial filtering in the Fourier plane or by a joint transform arrangement (Weaver and Goodman, 1966) (Rau, 1966). Problems still abound, however. The stability and positioning requirements are stricter yet, generation of a true complex (magnitude and phase) spatial filter is nontrivial, and deriving the phase of a complex convolution remains difficult. Incoherent optics avoids the speckle noise problems, and architectures are available for performing Fourier transformation and convolution (Rogers, 1977) (Monahan et al., 1977), but representation of negative quantities requires a bias or two signal channels.

On the other hand, the corresponding 1-D operations of Fourier transformation and convolution can be performed readily and rapidly by devices based on electronics, acoustic interactions, or charge transfer. By constructing optical systems to perform the dimensional transduction to and from Radon space, we can utilize these technologies to perform the corresponding 2-D operation. By so doing, we may be able to loosen the constraints on signal input format and system stability, at the cost of some processing parallelism. The resulting hybrid systems can emphasize the strengths and minimize the weaknesses of each technology. If the optical dimensional transducers and the 1-D processors are fast enough, we may still be able to perform the complete 2-D processing operation at a usefully rapid rate, e.g. 30 frames/second.

I.C.1. Optical Radon Transformer

The forward Radon transform [eq. (2)] is generated by integrating the input function $f(r)$ along the set of lines perpendicular to the azimuth ϕ. This can be done optically in several ways, depending on the format of the input data and the type of signal processor to

be used. Radon projections can be generated as temporal data by scanning the input function with a line of light (usually from a laser) and integrating the resultant intensity on a detector. This method is suitable for transmissive or reflective input data. At one instant, the detector signal is proportional to the line integral of input transmittance or reflectance. Sweeping the line of light perpendicular to itself generates a temporal signal proportional to one line-integral projection. The azimuth of the scan can be optically rotated (e.g. by a dove prism) to sequentially derive the complete set of projection data. For obvious reasons, this optical Radon transformer is called a flying-line scanner, and is shown schematically in Figure 4 (Easton et al., 1984). Since the light transmitted or reflected by the 2-D input is integrated on the detector, speckle noise is irrelevant, and a laser can be usefully employed as a light source. Indeed, the coherence of the laser becomes an advantage, as it allows the use of a fast acousto-optic beam deflector, or a slower and cheaper holographic deflector ("hologon scanner"). The technology of optical scanners and image rotators permits a system to be built capable of performing Radon transforms at video rates with video resolution (30 frames/sec, 500x500 points). This would require scanning 500 azimuth angles with 500 resolvable data points per scan every 30 mS. Acousto-optic Bragg-cell scanners capable of resolving more than 1000 points per 10 μS scan have been reported (Gottlieb et al., 1983). To preserve the phase of the projection, the temporal center of the flying line scan must intersect the image rotation axis each time, i.e. the optical rotation axis of the prism must not wobble. Scanning a full projection set in 30 mS requires an image rotation rate of $180^{\circ}/30$ mS = 900 RPM, implying a prism rotation rate of 450 RPM. Such systems have been constructed and demonstrated (Gmitro and Gindi, 1985). Indeed, much higher rotation rates have been reported while preserving holographic image quality (Stetson and Elkins, 1977). Radon transformers based on the flying-line scanner are most useful for 2-D signals on transparencies (e.g. movies)

or for real reflective scenes.

Projection data can also be generated by "collapsing" an image of the 2-D signal onto a linear array or imaging detector with anamorphic optics (Figure 5). The anamorphic optical element can be a cylindrical lens (Gindi and Gmitro, 1984), or a coherent optical fiber bundle (Farhat et al., 1983). Alternatively, if an N-element 1-D linear array detector can be obtained with an aspect ratio of N:1, anamorphic imaging is unnecessary. An array detector samples the projection, making this arrangement especially useful if the data is to be processed digitally. An image rotator is still required and hence the projections are again generated sequentially. This type of system is adaptable to naturally illuminated scenes or to self-luminous signals, as from a CRT.

I.C.2. 1-D Signal Processor Technologies

As was demonstrated in eqs. (19-22), the inverse Radon transformation requires convolution of the projection data with a bipolar 1-D filter function. Therefore we shall now shift gears somewhat to investigate the types and capabilities of available 1-D signal processors. These will be lumped into four categories: electronic devices (both digital and analog), charge-transfer devices (mainly CCDs), acousto-electric devices (primarily those based on surface acoustic waves, or SAWs), and acousto-optics (AO). In the first case, the Radon transform allows direct application to 2-D problems of the very technologies that optical methods are supposedly competing against on the signal-processing battlefield.

I.C.2.a. Electronic Systems

Electronic systems (analog and digital) for processing temporal signals are no doubt familiar to the reader. They can be as simple as an RC filter or as complex as a digital supercomputer. The accuracy, precision, stability, and flexibility of electronics are products of many decades of theoretical and engineering effort, with the result that electronic systems are generally preferred for signal-processing applications. This is the

target at which proponents of optical signal processing must aim, but it is moving ahead all the time. New materials, such as GaAs, and new fabrication technologies, such as x-ray lithography, promise further improvements in packing density, speed, and cost of electronic devices. Even the traditional advantage of parallelism offered by optical processing is fading, as new algorithms and chip architectures are adding parallel capability to the electronic world.

Electronic signal processing is generally divided into analog and digital domains, each having its own advantages and disadvantages. Analog processing represents signal amplitudes by proportional voltages that can be added, subtracted, and divided. Some nonlinear operations (e.g. thresholding) are easily performed as well. Analog processing with active and passive components can be fast, with bandwidths reported to ≈ 2 GHz for silicon devices and up to 20 GHz for GaAs (Bierman, 1985). More complicated operations (e.g. multiplication, root finding) are possible with special analog modules, but operation is much slower and subject to severe limitations in linearity, stability, and precision. For some applications, the restrictions can be eased by using the analog voltage signal to modulate a radio-frequency (RF) carrier. RF devices capable of several useful operations are available, including multiplication, phase shifting, and phase detection. Though still limited in linearity and stability, these devices can be profitably used for analog signal processing.

The advantages of digital systems are well known--probably too well known to the optical processing community. But they have their limitations too, lack of speed and large power consumption being two of the most important. Sampling limits system bandwidth and subjects the sampled signal to aliasing. A/D and D/A conversions may have to trade speed for precision and dynamic range. Clock rates are limited to ≈500 MHz for silicon-based logic. However, improvements are being made continuously. For instance, the increased

mobility of gallium arsenide charge carriers allows clock rates up to several GHz with lower power consumption (Bierman, 1985). Generally the limited disadvantages of digital processing have been more than offset by its inherent noise immunity and linearity. An unlimited variety of signal-processing operations are amenable to solution by digital means, and new special-purpose hardware promises to increase speeds dramatically. The very-high-speed integrated circuit (VHSIC) program of the Department of Defense is stimulating the design and production of new devices, such as the Westinghouse complex arithmetic vector processor, which can perform a 1024-point 16-bit complex Fourier transform in 130 μS, compute one point of a 256-element 16-bit correlation in 6 μS, and multiply a 64x64 16-bit matrix by a 64-element vector in 35 μS (Marr, 1982). Digital parallel operation is becoming more economical as design costs drop and fabrication yields increase, but cost is still a significant limitation for such devices and is likely to remain so.

I.C.2.b. Charge-Transfer Devices

Charge-transfer devices can store and manipulate packets of electronic charge using two structurally different circuit technologies. The older "bucket-brigade" device is a series of MOS transistors and capacitors, where the charge is moved between capacitors by alternate switching of the transistors. These have been largely superseded by charge-coupled devices (CCDs), where minority charge carriers are stored under closely-spaced electrodes. Charges are moved to detectors at the edges of the array by sequential pulsing of the electrodes. The most familiar use of CCD devices has been as 1-D and 2-D optical detector arrays, where the amount of charge in a detector cell is proportional to the photon flux. However, it is also possible to use them as signal processors, where the sampled data values are denoted by the varying amounts of charge . By moving, summing, and detecting the charge packets in various ways, a variety of processing operations can be performed. The resulting devices are an interesting hybrid of analog and digital qualities, since the

amplitude of each discrete sample is a continuous variable. CCDs can obviously be used as delay lines, with applications to signal time and bandwidth compression. Tapped delay lines and fixed-transversal filters can be constructed by spacing nondestructive charge detectors along the charge pathway and summing the tapped signals (Buss et al., 1973) (Beynon and Lamb, 1980). With variable weights, the filter is programmable. Multiplying adjacent tapped signals from two CCD delay lines and summing the products allows computation of a discrete convolution. The useful dynamic range of these CCD devices is limited by the quantum noise floor and the saturation level, with typical specifications of 60-70 dB (30 dB for the convolver). The bandwidth of the CCD devices is determined by the analog electronics and the sampling clock rate, ranging from a few Hz to 5 MHz.

By combining the CCD devices described above, a wide variety of 1-D signal-processing operations is possible. The utility of fixed and programmable CCD transversal filters and of the CCD convolver for signal processing is obvious. Using two or three filters with linear FM (or chirp) impulse responses, the chirp z-transform algorithm can be implemented (Rabiner et al., 1969). This algorithm will be discussed in some detail later. CCD spectrum analyzers using the chirp z-transform algorithm have been demonstrated which are capable of computing a 512-point z-transform at a 5 MHz sampling rate.

I.C.2.c. Acousto-Electric Devices

Piezoelectric materials distort when placed in an electric field, and also they generate a field when mechanically stressed. By applying a modulated RF electric field to a piezoelectric medium, a corresponding acoustic distortion is generated which can be processed and detected. This acoustic wave propagates in the medium at a characteristic velocity $v_s \approx 10^{-5}$ c. Thus, the acoustic wavelengths are much shorter than the electromagnetic wavelengths, allowing signal processing devices that are many wavelengths long to be constructed in small packages. Components based on acoustic waves in bulk

materials, such as the quartz oscillator and delay line, have been used for many years. More recently, however, much attention has been paid to using acoustic waves on the surface of a medium (surface acoustic waves or SAWs) due to their accessibility. Once a wave has been generated on the surface of a medium, it can be sampled at any point in its journey along the surface. A diagram of a simple SAW device is shown in Figure 6. A pair of conductive transducers is deposited on the surface of the piezoelectric crystalline medium. The input signal (often on a carrier) is applied to the input transducer, consisting of a set of interleaved 'fingers' connected to buss bars. The field distorts the medium piezoelectrically, and the acoustic wave travels along the surface of the crystal to a similar transducer where it generates an electric RF signal.

If we think of the SAW device in Figure 6 as a delay line, the sampling of the acoustic wave by the output transducer is a tapping and summing operation performed in parallel for many points in the acoustic wave. Hence, the SAW device is another example of a transversal filter. Variation of the spacing and overlap of the transducer fingers produces different impulse responses, allowing a wide variety of operations to be performed. The utility of SAW filters is such that several design procedures have been developed (Matthews, 1977) (Gerard, 1978), and the filters themselves are manufactured by standard photolithographic techniques (Smith, 1978). SAW bandpass filters are available for center (carrier) frequencies from 10 MHz to 2 GHz and bandwidths from $\leq$100 kHz up to 50% of center frequency (Morgan, 1985). The noise-limited dynamic range is typically 70 dB, comparable to that available from CCDs. Indeed, it is interesting that CCDs and SAW devices are so complementary, offering similar signal processing capability over a wide range of input frequencies (Roberts, 1977).

Linear FM, or chirp, SAW filters are easily made and have found wide application to radar systems (Klauder et al., 1960) (Gerard et al., 1973). More recently, they have been

employed in spectrum analyzers and Fourier transformers (Jack and Paige, 1978) (Jack et al., 1980). The transducers are designed such that the impulse response of the filter is a signal of linearly increasing or decreasing frequency. SAW interdigital chirp filters are limited to bandwidths of about 500 MHz, dispersion times of 50 μS, and effective time-bandwidth products of about 1000 (Morgan, 1985). Frequency dispersion can also be achieved by spacing acoustic reflectors on the substrate. These so-called reflective array compressors (RACs) have been reported with bandwidths to 180 MHz, dispersion times to 90 μS, and time-bandwidth products of 16,200 (Gerard, et al., 1977).

Other useful SAW signal processors can be made by utilizing the nonlinear response of the substrate to severe distortions. If strong acoustic signals are applied to each end of a substrate, the two waves will interact nonlinearly to generate higher harmonics. The second harmonic of the carrier frequency contains information about the product of the two signal amplitudes. Integration of the second harmonic frequency over the substrate by an area electrode produces a temporal signal proportional to the convolution of the input signals. Since second harmonic generation is inefficient, the convolution signal will be weak, typically 80 dB below the input signal levels. Even so, noise-limited dynamic ranges of 60 dB, and spurious-signal-limited dynamic ranges of 30 dB have been reported (Ash, 1978). Acoustic convolvers are available commercially with time-bandwidth products approaching 2000 (Morgan, 1985).

I.C.2.d. Acousto-optics

Acousto-optic processors are reviewed in detail elsewhere in this volume, so we shall discuss their capabilities only briefly. As mentioned above, an RF electromagnetic wave can be transformed into an acoustic wave in a medium via the piezoelectric effect. The variation in material density modulates the refractive index, producing a phase grating which can diffract light. Devices based on the interaction of sound and light have long

been used in signal processing as efficient 1-D spatial light modulators and beam deflectors (Korpel, 1981). Developments in materials and architectures in the last 15 years or so have led to new applications for bulk A-O devices in signal processing, including time-integrating and space-integrating correlators/convolvers (Berg et al., 1979) (Rhodes, 1981a) (Abramovitz et al., 1983), Fourier transformers (Lee et al., 1982) (Pancott and Reeve, 1985), and generation of 1-D time-frequency representations (e.g. the Woodward ambiguity function) (Athale et al., 1983) (Casasent, 1983). The interaction of light and surface acoustic waves has also been applied to various signal processing operations (Das and Ayub, 1982) (Casseday et al., 1983). Indeed, AO devices and SAW devices are inherently compatible, for the obvious reason that the processing mechanism is so similar. Limits on carrier frequency, bandwidth, and dispersion time are comparable for both types. AO materials support carrier frequencies in the range of ($1\ \text{MHz} \leq \nu_0 \leq 1\ \text{GHz}$), with bandwidths of up to 500 MHz, interaction times of up to 80 μS, and time-bandwidth products greater than 10,000 (Berg et al., 1979).

I.C.3. Optical Implementation of the Inverse Radon Transform

Having discussed the technologies available for 1-D signal processing, we are now ready to describe methods for reconstructing the 2-D processed signal from the 1-D projections. Two mathematical algorithms for reconstruction have already been discussed: filtered back-projection and circular harmonic expansion. As stated, the latter is more complicated to implement and not as appropriate for signal processing applications, and so will not be considered further here. Interested readers should consult the work of Hansen and Goodman (1978), Hofer (1979), Hofer and Kupka (1979), and Hansen (1981a, 1981b).

In our mathematical development of filtered back-projection, we stated that 1-D filtering can be performed before back-projection, or 2-D filtering afterwards. Optical reconstruction systems have been built which filter in 2-D (Peters, 1974), but again we are

more concerned with application of 1-D technologies to the problem. Several hybrid optical systems have been proposed or built to implement 1-D filtered back-projection, and we shall give a brief overview of those systems here. Readers desiring more detail should consult the original papers or the review articles by Barrett and Swindell (1977) and Gmitro et al. (1980). To lessen problems associated with coherent noise, these systems used incoherent illumination. However, it is essential to recall that the filtered projection is bipolar, requiring that any reconstruction scheme preserve sign information. Because of this constraint, systems based on incoherent optics must place the projection signal on a bias or employ two signal channels. Neither of these alternatives is desirable; biased signals reduce the contrast of the reconstruction, and dual-channel systems are subject to differential signal errors.

After 1-D filtering, the algorithms of eqs. (19-22) require two more steps: back-projection and summation. Back-projection, i.e. generation of a 2-D function from a 1-D projection by 'smearing' perpendicular to the projection azimuth, has been demonstrated by anamorphic optics. The projection is written on the face of a 1-D display device (e.g. a CRT or LED array) located one focal length from a cylindrical lens, and imaged onto an integrating 2-D detector or display device. As this operation is performed for each projection, the reconstructed image is built-up at the output plane. Any integrating 2-D detector can be used for summation of the back-projections (e.g. photographic film, video camera, or human eye if the system is fast enough).

The hybrid optical-electronic reconstruction schemes have differed greatly in detail and degree of success. The system of Duinker et al. (1978) was mostly based on analog electronics, with only filtering performed optically. The projections were displayed in sequence on a CRT and imaged onto two area-weighted optical masks representing the positive and negative parts of the filter function. The images of the projections were

swept across the filter masks by electronic deflection, and the integrated transmitted signals electronically subtracted to obtain the bipolar temporal filtered signals. Back-projection and summation were performed electronically. Edholm et al. (1978) stored the Radon projections on film in sinogram format $\lambda(p,\phi)$. A filtered, biased sinogram was generated by sandwiching a positive image of $\lambda(p,\phi)$ and a negative image of $\lambda(p,\phi) * h_-(p)$, where $h_-(p)$ represents the negative part of the filter function in eq. (18). Back-projection was performed for each line of the sinogram by a cylindrical lens, with summation on a suitably rotated piece of photographic film. Despite the dynamic range limitation inherent in the use of a bias, this system produced some good reconstructions.

Probably the most successful incoherent optical reconstruction systems synthesized the required filter function by OTF synthesis. This method is based on the fact that the OTF is the autocorrelation of the pupil function (Lohmann, 1977) (Rhodes, 1977) (Rhodes and Lohmann, 1978) (Stoner, 1978). Two pupil functions are calculated for which the difference of the autocorrelations is the Fourier transform of the required filter point spread function. An infinite number of pairs of pupil functions are theoretically possible, with the optimum choice determined by system requirements such as light throughput or noise considerations. Since the required positive part of the filter psf is a delta function [eq. (18)], a clear pupil in the positive channel is appropriate. Two negative-channel pupils successfully demonstrated are the so-called Ronchi pupil (Barrett, Greivenkamp et al., 1979), and a logarithmic phase plate (Barrett, Chiu et al., 1979). The envelope of the point spread function of either pupil falls off as $1/p^2$, as required. Optical reconstruction systems based on OTF synthesis include the drum processor (Gordon, 1977) (Gmitro et al., 1980), the loop processor (Greivenkamp et al., 1981), and a hybrid digital-optical system (Gmitro et al., 1980). An example of image reconstruction with the loop processor is shown in Figure 7.

A reconstruction system that is most applicable to tomographic signal processing tasks was proposed recently by Gmitro and Gindi (1985). It is capable of performing a 500 x 500 point reconstruction of projection data at video rates. The system, depicted in Figure 8, implements the algorithm of eq. (19). Filtering is performed by a space-integrating acousto-optic convolver, as shown in Figure 9, though a SAW convolver could be used as suggested in section I.C.2.c. The projection data are stored in a fast digital memory and read out line-by-line to a fast D/A converter. The analog signal modulates an RF carrier and is then impressed on a Bragg cell. The diffracted light is Fourier transformed by a lens and filtered by a spatial binary transmission mask. The diffracted light is retransformed, collected by the detector, and demodulated. The filtered projection is displayed on a CRT and back-projected by a cylindrical lens. Azimuth selection for the back-projection is accomplished by an image-rotating prism, and the 2-D image is collected by a video camera and displayed on a conventional CRT. The image data are read out rapidly enough for operation at video rates (30 reconstructed frames/second). The design goal is to process projections at video rates with a dynamic range of 12 bits, implying a signal-to-noise ratio of about 4000. Preliminary results are presented in Figure 10.

II. Applications

II.A. Operations on 2-D signals

As was evident from our mathematical development, the application of the Radon transform to signal processing primarily exploits the central-slice and filter theorems, which allow operations based on Fourier transforms and/or convolutions to be performed on the 1-D projections. Useful operations of this type include the Fourier transform and its relative, the Hartley transform, 2-D filtering, some pattern-recognition algorithms, bandwidth compression, and spectrum estimation. Some of these operations require the flexibility of digital operation but are included to indicate the scope of application of Radon methods. Since application of projection operations to signal processing is a field that has yet to be fully plowed, much of our treatment will deal with feasibility rather than actual results.

II.A.1. Fourier Transformation

Since it is a signal-processing staple, and also because of its close relationship to the Radon transform via the central-slice theorem, it seems natural to commence our discussion of applications with 2-D Fourier transformation. After having been generated by one of the systems described in section I.C.1., each projection is Fourier transformed and the result is displayed in the polar format required by the central-slice theorem. To perform the 1-D Fourier transform, we introduce the chirp transform algorithm, which is derived by decomposing the Fourier kernel:

$$e^{-2\pi i\nu t} = e^{-i\pi(\frac{\nu}{\beta})^2} \times e^{-i\pi(\beta t)^2} \times e^{+i\pi(\frac{\nu}{\beta} - \beta t)^2}. \qquad (25)$$

The three complex exponentials are quadratic phase terms or linear FM signals, i.e. the instantaneous frequency of each varies linearly with time. Such signals are commonly called chirps by the radar community. The factor β, with dimensions of temporal

frequency, has been introduced to rationalize the units of the exponent. A 1-D temporal Fourier transform can now be written:

$$F(\nu) = \int_{-\infty}^{\infty} dt\, f(t)\, e^{-2\pi i \nu t}$$

$$= e^{-i\pi(\frac{\nu}{\beta})^2} \int_{-\infty}^{\infty} dt \left[[f(t)\, e^{-i\pi(\beta t)^2}] \times e^{+i\pi(\frac{\nu}{\beta} - \beta t)^2} \right]$$

$$= e^{-i\pi(\beta t)^2} \times [[f(t)\, e^{-i\pi(\beta t)^2}] * e^{+i\pi(\beta t)^2}]\Big|_{(\nu = \beta^2 t)} . \qquad (26)$$

Thus, by employing three temporal chirp signals (one with positive exponential term, or upchirp, and two with negative terms, or downchirps), the Fourier transform of f(t) can be implemented in three steps:

(1) multiplication of f(t) by a downchirp;

(2) convolution of the product in a filter with an upchirp impulse response;

(3) multiplication by a downchirp.

The resulting temporal signal is a scaled version of the Fourier transform, where the frequency is related to the output temporal coordinate by $\nu = \beta^2 t$. The pre- and postmultiplication chirp signals can be generated by applying impulsive inputs to filters with upchirp impulse responses. Note that this analysis has assumed that the chirp signals are complex and of infinite length. If only the power spectrum is required, the postmultiplication in step 3 can be eliminated. Because of the order of operations, this algorithm is usually referred to as the M-C-M chirp transform, for multiply-convolve-multiply. The duality of multiplication and convolution in coordinate and Fourier space imply that the operations can be exchanged to produce a second arrangement for chirp transforms, the C-M-C transform (Jack et al., 1980). It has the disadvantage of requiring three filters even if only the power spectrum is required. For sampled data, Fourier

transformation is equivalent to evaluation of the z-transform on the unit circle. The comparable implementation using sampled chirps is therefore called the chirp z-transform (Rabiner et al., 1969).

It is instructive to reconsider coherent optical Fourier transformation in light of the chirp transform algorithm. Propagation of light in the Fresnel region can be described as convolution of the wavefront with a quadratic-phase impulse response, and the action of a spherical lens on a wavefront is multiplication by a quadratic phase, so the common 2-f coherent Fourier transformer is a version of the C-M-C chirp algorithm. An optical version of M-C-M is also possible (Whitehouse, 1977).

The chirp Fourier or z-transform can be implemented for real 1-D data (as would be obtained from a flying-line scanner) using the technologies described previously, but the analysis differs somewhat from that given in eqs. 25-26. A basic temporal signal filter has a real, finite-length impulse response, often modulating a carrier. For example, the impulse response of a SAW chirp filter is of the form

$$h_{\pm}(t) = A(t) \cos\left[\omega_0 t \pm \frac{\alpha t^2}{2}\right], \tag{27}$$

where $A(t)$ is the apodizing function of the filter, ω_0 is the initial carrier frequency, and α is the "chirp rate", or rate of change of the instantaneous frequency. For SAW filters, the carrier frequency ω_0 is in the RF region ($\approx$15 - 300 MHz). The frequency of $h_+(t)$ rises with time, so this function is again called an upchirp. Using these realizable filters, the chirp Fourier transform may still be implemented, but the phase of the transform is now determined relative to the phase of the carrier (Jack and Paige, 1978). The recipe for the chirp transform becomes:

(1) premultiplication by a downchirp;

(2) convolution (filtering) with an upchirp;

(3) postmultiply by two upchirps separately, with phase difference of $\pi/2$;

(4) low-pass filter both signals from step 3.

The complex transform is thus generated as two parts simultaneously. The signal derived from the in-phase chirp of step 3 is the real part of the complex Fourier transform, or cosine transform. The quadrature signal yields the sine transform, or imaginary part of the Fourier transform. Note that the sign of the slope of the postmultiplication chirp differs for the realizable algorithm relative to that for complex chirps. This is due to double-sideband multiplication of the carrier-borne signals, which yields signals at the sum and difference frequencies of the carriers. By selecting the difference frequency sideband with the low-pass filter, the operation is equivalent to postmultiplication by a chirp of the opposite sign. The output temporal signal maps linearly to frequency with constant of proportionality α. Since the real chirp signals are apodized by A(t), their time-bandwidth product (TBW) is finite, thus limiting the frequency resolution of the transformer. The maximum system TBW is one-fourth the TBW of the convolution chirp (Ash, 1978). It should be noted that the SAW chirp transform algorithm can also be implemented for complex input data by premultiplying the imaginary part of the input signal by a chirp in quadrature to the real-part premultiplication chirp (Jack and Paige, 1978). Using surface acoustic wave reflective array compressive filters, a system capable of transforming signals 60 μS long with 60 MHz bandwidth was demonstrated by Gerard et al. (1977). SAW chirp Fourier transformers are faster and require less power and bulk than all-digital systems, but are less accurate.

The chirp Fourier transform algorithm can be implemented with AO devices as well. Hotz (1984) and Pancott and Reeve (1985) have demonstrated M-C-M transforms using space-integrating architectures incorporating two Bragg cells. The 1-D input is multiplied by an electronically-generated chirp signal in an RF mixer, and the product applied to one

Bragg cell. The +1st diffraction order is selected and imaged on the second Bragg cell, which is driven by the same electronic chirp signal. The -1st diffraction order emerging from the second cell is selected, integrated on a detector, and demodulated. Hotz reports a system bandwidth of 25 MHz for a signal duration of 5 μS, limited by the capabilities of the AO cells and by problems with generating the proper postmultiplication chirp slope. Such a system has similar mechanical stability requirements as other coherent optical systems, but are readily applicable to signal processing in Radon space.

II.A.1.a. 2-D Power Spectra

Ticknor et al. (1984) demonstrated production of 2-D power spectra via the Radon transform and the SAW chirp Fourier transform. Their system is diagrammed in Figure 11. The Radon projection of a 2-D transparency f(r) is generated by a Bragg-cell-driven flying-line scanner. One projection is derived in 10 μS. Premultiplication by the SAW chirp is performed in an RF mixer. This product signal is applied to the convolution chirp filter, whose output is the Fourier transform on an RF carrier. Since the phase of the Fourier transform is not required, the output of the convolution filter is detected incoherently with a diode, producing a unipolar signal proportional to the squared-modulus of the Fourier transform. The SAW filters used had time dispersions of 10 MHz and bandwidths of 20 μS. Power spectra were generated by the system within 28 μS after commencement of the flying-line scan. The spectra were 20 μS long with 50 resolvable frequencies. By the central-slice theorem, the detected signal must be displayed in a polar format to generate one line through the 2-D power spectrum. However, as the 2-D spectrum is built up, the polar raster oversamples the low spatial frequencies, producing a displayed time-averaged intensity that is too bright in the center. Mathematically, this problem is due to the sampling nonuniformity of the Radon transform, and is corrected by rho-filtering, i.e. the central slices of the power spectrum are multiplied by $|\nu|$ in an RF-mixer before detection.

After one transform slice has been displayed, the prism is rotated and a new projection generated. The power spectrum of that projection is displayed at the new azimuth on the CRT. Integration of the result can be done on film, or by eye if the system is fast enough. System speeds up to 5 frames/sec. have been demonstrated, limited by the rotation rate of the stepper motor driving the image rotator in the flying-line scanner. Results for a 2-D function are shown in Figure 12.

II.A.1.b. 2-D Complex Fourier Transforms

The same group (Easton et al., 1985b) added a post-multiplication chirp to their system to generate the complex Fourier transform, as diagrammed in Figure 13. The time delay of the post-multiplication chirp is derived from a digital delay generator (1 ns resolution). To obtain more precise time delay, the phase of the postmultiplication chirp can be varied with a continuously adjustable RF phase shifter. The postmultiplication itself occurs in an RF phase comparator, which generates voltages proportional to the in-phase and quadrature products of two input signals. The in-phase term is the cosine transform, and the quadrature term is the sine transform. Performance of the complex SAW chirp transformer is shown in Figure 14.

Rho-filtering of the complex transform before display is somewhat more difficult than for the power spectrum. The frequency of the demodulated signal is too low for multiplication in RF mixers, and too high for analog multipliers. An integrated-circuit balanced modulator was used instead. The two bipolar complex Fourier transform signals were then biased up before application to the z-axis of the CRT. Results are shown in Figure 15.

Since the phase of the transform is derived from the time differences of the projection signal relative to the chirps, the coherence of the scanner beam is immaterial. This method is therefore applicable to reflective scenes as well as to transparencies. An example of

complex Fourier transformation of a reflective scene is shown in Figure 16.

Another 2-D processing situation where Radon space Fourier transformation may prove very useful is with spatial light modulators whose image quality is relatively poor. Recently, there has been much interest in applying an inexpensive liquid crystal television receiver to optical processing operations (Liu et al., 1985) (McEwan et al., 1985). The poor phase uniformity of the LCTV limits its utility for coherent operations, though various means have been suggested for improvement. Again, this is not a problem when used as input for a flying-line scanner (Easton et al., 1985a). Some results in that application are shown in Figure 17.

Farhat et al. (1983) also demonstrated 2-D complex Fourier transforms via Radon space operations, but utilized a 2-channel incoherent optical correlator to generate the 1-D transforms. A 2-D complex signal was displayed on a CRT in two colors, e.g. real part in red, imaginary part in green. The image was rotated by a dove prism, spectrally filtered to separate channels, and collapsed to 1-D by two coherent optical fiber bundles. The real and imaginary 1-D signals were correlated incoherently with a fixed cosine and sine reference mask, respectively. The 1-D correlator outputs represented the real and imaginary parts of the 1-D Fourier transform, which were then be detected and displayed in the polar raster. The system is fast, but also suffers from the familiar limitations on bandwidth and dynamic range common to other geometrical-optics incoherent correlators (Rogers, 1977).

II.A.1.c. Hartley Transforms

A 2-D operation that is receiving some attention in the signal processing community is the Hartley transform (Bracewell, 1983) (Bracewell et al., 1985). For a 2-D function f(r), the Hartley transform is defined as:

$$H(\rho) = \int_{-\infty}^{\infty} \int_{-\infty}^{\infty} d^2r\, f(r)\, \mathrm{cas}(2\pi r \cdot \rho)\,, \tag{28}$$

where $\mathrm{cas}(x) \equiv \cos(x) + \sin(x)$. The kernel of the Hartley transform is again a function of the scalar product of conjugate variables and is in fact the difference of the real and imaginary parts of the Fourier kernel. Being purely real, the Hartley transform may be preferred over the Fourier transform for digital computation, since the storage requirements could be halved. Being a linear combination of the real and imaginary parts of the 2-D Fourier transform, and hence of the 1-D Fourier transform of the Radon projections, the Hartley transform is easily implemented in Radon space. By subtraction of the real and imaginary outputs of the SAW chirp transformer with a simple difference amplifier, the 1-D central slices of the Hartley transform are generated. They are displayed in the same fashion as the Fourier transform.

II.A.2. Filtering and Correlations

The filter theorem demonstrates that a projection of a 2-D convolution (correlation) is the convolution (correlation) of the corresponding projections of the 2-D functions. Since devices or systems exist to perform 1-D convolutions (SAW devices, CCD convolvers, and AO convolution systems), it is feasible to perform the 2-D operations in Radon space (Gmitro et al., 1983). With a fast 1-D SAW convolver, such an operation can be performed at video rates. A system capable of video-rate 2-D convolution or filtering is depicted in Figure 18. The projections of the filter function may be generated as needed from a 2-D image or stored in digital memory and read out through a fast D/A converter. A simulation of 2-D high-pass filtering is shown in Figure 19, where the projections were generated optically, the 1-D convolutions and rho-filtering performed in a digital computer, and the back-projection again performed optically.

If the projections of the filter function are stored in an addressable digital memory, as suggested above, we have the capability to alter the impulse response of the 2-D filter by updating its digitally stored 1-D projections. This could be useful if filtering a noise signal which varies over time and would enable the application of 1-D adaptive filtering methods to 2-D situations. For example, consider a signal corrupted by noise. An adaptive filter acts on noise in a reference channel (correlated in some unknown way with the noise in the signal channel) to maximize the output signal-to-noise ratio. This is accomplished by adjusting the filter's impulse response to minimize an appropriate error signal. The filter parameters are derived from correlations between the signals in the input and reference channels--operations that can be legitimately performed on the Radon projections of 2-D signals. In 1-D, the technique has been successfully applied to a number of problems, e.g. telephone echo cancellation (Gritton and Lin, 1984), electrocardiography, and antenna sidelobe interference (Widrow et al., 1975). To the knowledge of the authors, there is only one demonstrated example of 2-D adaptive filtering. Tao and Weinhaus (1985) applied adaptive noise cancellation techniques to removal of periodic signal-dependent noise in digital imagery. By filtering the Radon projections with 1-D updatable stored functions in a 1-D convolver, these adaptive algorithms can be implemented while avoiding the limitations of available 2-D hardware.

II.A.3. Pattern Recognition

Some very useful pattern recognition operations can be profitably performed in Radon space. We have already demonstrated generation of the 2-D Fourier power spectrum. Gindi and Gmitro (1984) have used optical methods to rapidly extract integrated features of the power spectrum from the Radon projections. They have also demonstrated the feasibility of evaluating a set of invariant moments, deriving the Hough transform, and finding the convex hull of a 2-D input by operations on the Radon projections. Since the

first three operations are probably of most interest, we shall briefly discuss each.

II.A.3.a. Fourier Spectrum Features

Optical computation of features in the Fourier power spectrum has been feasible for some years and has been applied to some industrial uses (Casasent, 1981). The wedge-ring detector was developed for use in a coherent processor to compute the energy in the power spectrum in discrete segments of magnitude and orientation of spatial frequency. By manipulation of the 1-D power spectra in various ways, the same kind of Fourier feature extraction can be performed. Integration of the power spectra of adjacent projections produces information equivalent to that from the wedge segments. Sampling the 1-D spectra and integrating over projections generates information from discrete spatial frequency intervals, corresponding to the annular segments of the wedge-ring detector. Results from a computer simulation by Gindi and Gmitro (1984) are shown in Figure 20.

II.A.3.b. Image Moments

Two decades ago, Hu (1962) described a system of linear combinations of image moments that are invariant to translation, rotation, and scale change. Later, Maitra (1979) modified the system to include invariance to relative image contrast. Six combinations of ten image moments m_{pq} are required, where:

$$m_{pq} = \int_{-\infty}^{\infty} \int_{-\infty}^{\infty} dx\, dy\, x^p\, y^q\, f(x,y)\ . \tag{29}$$

The ten necessary image moments are m_{00}, m_{11}, m_{10}, m_{01}, m_{20}, m_{02}, m_{12}, m_{21}, m_{30}, and m_{03}. Gindi and Gmitro (1984) demonstrated that the ten moments can be computed from four projections spaced $\pi/4$ radians apart. The ten image moments and the linear combinations can be rapidly computed by digital means from optically-generated projections.

II.A.3.c. Hough Transform

The Hough transform was developed as a technique to speed detection of straight line segments in digital imagery. Edges of the object are mapped by the Hough transform to a parameter space, wherein peaks indicate the presence of straight lines in the object. Deans (1981) described the close similarity between the Hough and Radon transforms. For binary pictures, in fact, they are identical. Eichmann and Dong (1983) have proposed a coherent system to generate the Hough transform, while Gindi and Gmitro (1984) demonstrated that 1-D filtering of Radon projections can be used to edge-enhance a 2-D image and derive the Hough transform simultaneously. Their digital simulations of the computation of the Hough transform are shown in Figure 20.

II.A.4. Image Coding and Bandwidth Compression

The potential of x-ray tomography in medical applications led to investigation of the collected data required to obtain good image quality (Rowland, 1979). In turn, this has led to application of the tomographic transformation to reduce image storage and transmission requirements while maintaining image quality (Mersereau and Oppenheim, 1974). Since only 1-D compression operations are required after the projections are collected, rapid coding is possible. To date, the work has been aimed at digital compression of the 1-D projections. Smith and Barrett (1983) truncated and quantized the Fourier components of each projection of a scene to reduce the data from 8 bits/pixel to 1.1 bits/pixel while retaining good image quality. As they point out, the approach works very well with rectilinear scenes, since significant Fourier components will predominate in a limited number of projections. Fraser et al. (1985) investigated the effect of gross reduction of the number of projections used, as well as quantization effects of various spatial frequency ranges. Using 256x256 8-bit images, they obtained good image quality with as few as 0.86 bits/pixel.

II.A.5. Spectrum Estimation

In temporal signal processing, the estimation of frequencies of a signal buried in uncorrelated noise is a classic problem (Robinson, 1982). Averaging and modeling techniques have been developed appropriate for distinguishing various types of signals (Kay and Marple, 1981). Most are based on Fourier transform and/or correlation operations and are hence adaptable to operation in Radon space for 2-D signals. Traditional methods incorporating averaging operations, such as the periodogram and the Blackman-Tukey spectrum estimate, are most useful for detecting the presence of sinusoidal signals. To compute the periodogram, windowed segments of the 1-D input are sampled and padded with zeros. The size of the data window determines the frequency resolution of the periodogram. The power spectra of the segments are computed and averaged. Since the noise is uncorrelated, the signal spectrum should dominate in the periodogram. This approach has become popular since the invention of the FFT algorithm. 2-D periodograms are used in a similar manner for spatial signals (Dudgeon and Mersereau, 1984). For 2-D signals, optical processing techniques can be used to estimate the spectrum. Indeed, one of the success stories of optical processing, Labeyrie stellar speckle interferometry, generates a form of 2-D periodogram where the signal segmentation is over time rather than over space. Computation of the traditional periodogram is readily adaptable to Radon space implementation. The projections of a noisy signal are computed and segmented. The individual segments are padded with zeros and Fourier transformed. The power spectra of the segments of the projection are averaged to derive an estimate of the power spectrum of that one projection. The same procedure is carried out for each projection to generate the 2-D power spectrum estimate.

The Blackman-Tukey algorithm derives a spectral estimate via the Wiener-Khintchine theorem, i.e. the power spectrum of a stochastic signal is the Fourier transform of its

autocorrelation. For a sampled 1-D signal, the autocorrelation is computed for a number of allowed lags (shifts) and Fourier transformed. For a 2-D signal, the calculation of the 2-D autocorrelation makes this approach computationally expensive. However, once the projections have been derived, this approach can be performed in 1-D rapidly and cheaply. By the filter theorem, the projection of the autocorrelation is the autocorrelation of the projections. The 1-D autocorrelation of each projection can be rapidly computed, Fourier transformed, and displayed in sinogram or polar format to give an estimate of the 2-D power spectrum.

II.A.6. Linear, Space-Variant Operations

In recent years, a considerable amount of effort has been directed at developing optical methods of implementing space-variant operations, in order to broaden the applicability of optical processing. For a review of this work, see Goodman (1981). It is natural, therefore, for us to investigate the application of the Radon transform to such operations. We will see that Radon-space implementation of general space-variant operations, though theoretically possible, usually offers little if any advantage over direct processing. For some special cases, however, the Radon approach can be very useful.

A general linear, space-variant operation on a 2-D function $f(\mathbf{r})$ may be expressed as a superposition integral:

$$g(\mathbf{r}) = \int_{-\infty}^{\infty}\int_{-\infty}^{\infty} d^2\mathbf{r}'\, f(\mathbf{r}')\, h(\mathbf{r};\mathbf{r}'), \tag{30}$$

where the kernel $h(\mathbf{r};\mathbf{r}')$ can be regarded as a space-variant impulse response. Since the superposition kernel is a function of both the input and output coordinates, and is therefore 4-D, we cannot derive unique 1-D projections of $h(\mathbf{r};\mathbf{r}')$ in the manner described by eq. (2). We could derive a generalized projection $\lambda_h(p,\phi;p',\phi')$ of $h(\mathbf{r};\mathbf{r}')$ by integration over the

input and output variables and examine the relationship between λ_f and λ_h that yields λ_g. We have already seen some cases, e.g. the Fourier and Hartley transforms, where the close kinship of the space-variant integral kernel and the Radon kernel allow the operations to be directly performed in this manner. But for the general space-variant operation, we will instead consider an alternative treatment made by Bamler and Hofer-Alfeis (1982). They proved that 2-D space-variant operations can be considered to be a special case of 4-D space-invariant convolution, i.e.

$$g(r) = g'(r;r'=0) = [f'(r;r') \text{ **** } h(r;r')]\big|_{r'=0} , \tag{31}$$

where $f'(r;r') \equiv f(r)\ \delta(r + r')$, and the operator **** denotes 4-D convolution. Deriving $f'(r;r')$ involves sampling a 4-D smeared version of $f(r)$, and so is somewhat akin to back-projection. Bamler and Hofer-Alfeis proposed a means of implementing the 4-D convolution optically via sequential 2-D convolutions for the case of a bandlimited space-variant impulse response. By extension of the filter theorem [eq. (13)] to 4-D, the convolution can theoretically be performed via 1-D convolutions in Radon space once the projections of the 4-D functions have been derived. The 4-D generalization of the projection operation [eq. (2)] is obtained in analogous fashion to the 3-D case (Section I.B.1.), i.e. the 1-D projection of a 4-D function is generated by integration over the 3-D volume normal to the 4-D unit vector defining the azimuth of the projection. Three angles (α,β,γ) are required to specify this unit normal. For clarity, we respecify the arguments $(r;r')$ of the 4-D functions by the notation (r_4), where the subscript denotes the dimensionality of the space. Similarly, we define the 4-D volume element $d^4r = d^2r\ d^2r'$. The 1-D projection of the 4-D input function $f'(r_4)$ is therefore:

$$\lambda_{f'}(p,\alpha,\beta,\gamma) = \int_{-\infty}^{\infty}\int_{-\infty}^{\infty}\int_{-\infty}^{\infty}\int_{-\infty}^{\infty} d^4r\ f'(r_4)\ \delta[p - r_4 \cdot \hat{n}_4] . \tag{32}$$

Note that the definition of $f'(r_4) = f(r)\,\delta(r + r')$ allows some simplification of this expression by evaluating the integral over d^2r'. However, the projection of the kernel $h(r_4)$ cannot be so simplified, in general. Extending the filter theorem [eq. (13)] to 4-D, we have

$$g'(r_4) = R_4^{-1}[\lambda_{g'}(p,\alpha,\beta,\gamma)] = R_4^{-1}[\lambda_{f'}(p,\alpha,\beta,\gamma) * \lambda_h(p,\alpha,\beta,\gamma)]\,, \qquad (33)$$

where R_4^{-1} is the 4-D inverse Radon transform. The desired output $g(r)$ of the 2-D space-variant operation is obtained by evaluation of $g'(r_4) = g'(r;r')$ at the 2-D plane defined by $r' = 0$. Since each 1-D convolution influences every point in the 4-D convolution (and hence every point in the 2-D output plane) via back-projection, there are no computational shortcuts--only nonessential 4-D output. In Radon terms, mapping the 2-D input function to 4-D space and performing a 4-D space-invariant convolution avoids the necessity of operating on one projection of the 2-D input $f(r)$ with multiple generalized projections of the 4-D kernel $h(r;r')$ to obtain one projection of the 2-D output $g(r)$. However, performing the forward and inverse Radon transforms of 4-D functions are very intensive computational processes which would require special-purpose hardware if they are to be performed rapidly and economically. To illustrate the scope of the problem, consider that the forward transform requires the calculation of a volume integral for each point in each projection. For a 500 x 500 input $f(r)$, the general space-variant kernel $h(r;r')$ has $500^4 = 6.25 \times 10^{10}$ data points. Calculation of each of 500^4 projections requires 500 volume integrals over 500^3 points. The difficulties of performing the 4-D back-projection are similarly prodigious. As will be discussed, Barrett (1981) proposed a hybrid 3-D Radon-space signal processor that could be adapted to these 4-D applications, but the addition of one more dimension significantly complicates the data storage and manipulation requirements. Hence, performing the general space-variant operation in Radon space via the 4-D convolution algorithm has no obvious advantage over direct digital processing at

this time.

II.A.7. Bilinear and Nonlinear Operations

For 1-D signals, a number of processing algorithms have been developed that operate on the signal in a multilinear or nonlinear manner for such purposes as voice pattern recognition and echo deconvolution. Examples include coordinate-frequency representations (e.g. sliding-window spectrum, Woodward ambiguity function, Wigner distribution function (WDF)), triple correlation (Lohmann and Wirnitzer, 1984), and the cepstrum (Childers et al., 1977). The success of these algorithms for certain 1-D signal-processing tasks has stimulated research into 2-D analogs, but these are usually computationally intensive and hence not often implemented digitally. In some cases, optical processing has been profitably applied, notably for coherent optical computation of the Wigner distribution function of 2-D data (Bamler and Glünder, 1983). Those operations based on Fourier transforms (e.g. WDF) or on nonlinear point processing (e.g. cepstrum) may be implemented in Radon space. Using a fast optical Radon transformer and 1-D analog or fast digital processing, the 2-D operation may be performed profitably. An example of such an operation is coordinate-frequency representation of 2-D functions.

A simultaneous representation of the coordinate and frequency distribution of the energy in a nonstationary signal has proven useful in a number of applications, e.g. radar signal processing (Woodward, 1953) and speech processing (Oppenheim, 1970). Such a representation is intended to give a picture of the "local" frequency spectrum of the signal, i.e. the frequency content of the signal arising from a particular region of coordinate space. Obviously, such a picture requires twice as many dimensions in the representation space as in the signal space. Several such representations have been proposed. The most direct path to a local spectrum is the complex spectrogram (CS), or sliding-window spectrum, where a constant window function is shifted over the signal to specify the region

to be Fourier analyzed, i.e. for a 1-D signal f(t), the complex spectrogram S_{fg} is defined as:

$$S_{fg}(t;\nu) = \int_{-\infty}^{\infty} dt'\, f(t')\, g^*(t' - t) e^{-2\pi i \nu t'}. \tag{34}$$

This representation is easily computed by coherent optics but the output is affected as much by the window g(t) as by the input f(t). This potential problem can be alleviated by using a self-windowed representation, such as the Wigner distribution function (WDF), which is commonly defined as:

$$W_f(t;\nu) = \int_{-\infty}^{\infty} dt'\, f(t + \frac{t'}{2})\, f^*(t - \frac{t'}{2})\, e^{-2\pi i \nu t'}$$

$$= \underset{t' \to \nu}{\mathcal{F}}{}^{-1}\left[f(t + \frac{t'}{2})\, f^*(t - \frac{t'}{2}) \right], \tag{35}$$

where $\underset{t' \to \nu}{\mathcal{F}}{}^{-1}$ is the 1-D Fourier operator transforming coordinate t' to frequency ν. This representation was introduced by Wigner (1932) and introduced into optics by Bastiaans (1978). Another closely related function is the Woodward ambiguity function (AF), which is defined as:

$$A_f(\nu;t') = \int_{-\infty}^{\infty} dt\, f(t + \frac{t'}{2})\, f^*(t - \frac{t'}{2})\, e^{-2\pi i \nu t}$$

$$= \underset{t \to \nu}{\mathcal{F}}{}^{-1}\left[f(t + \frac{t'}{2})\, f^*(t - \frac{t'}{2}) \right]. \tag{36}$$

It is related to the WDF through a double Fourier transform. Several optical methods for computing these representations for 1-D functions have been introduced (Bartelt et al., 1980) (Brenner and Lohmann, 1982) (Eichmann and Dong, 1982) (Athale et al., 1982).

Generation of such representations for 2-D functions presents another problem, since the resultant is a function of four variables. Generally, 2-D slices of the 4-D

representation are produced. Real input functions are assumed, eliminating the need for conjugating the shifted function. In addition, the computation of the bilinear product function is expensive if done digitally, increasing the motivation for optical processing. Of the representations listed, the WDF is most readily computed optically, since the Fourier transform of the product function is over the shifted coordinate variable . Optically, the product function is generated by passing coherent light twice through a transparency of the signal, either by reflecting an image of the transparency onto itself, by overlaying copies (Bamler and Glünder, 1983), or by imaging onto a copy (Conner and Li, 1985). The bilinear product function is then Fourier transformed to generate one slice, $W_f(r_\theta;\rho)$. Shifting the position of the input functions generates 2-D slices for different values of r_θ.

Computation of the WDF can also be performed in Radon space by taking projections of the optically derived bilinear product and Fourier transforming in 1-D. Easton et al. (1984) demonstrated generation of 1-D central slices of the squared modulus of the 4-D WDF and later used the 1-D SAW complex Fourier transformer to produce bipolar 2-D slices of the 4-D WDF of a 2-D real function. An example is shown in Figure 21.

II.B. Operations on 3-D Signals

Earlier, we stated that we would emphasize processing of 2-D signals via a tomographic transform. However, it may be even more profitable to use the Radon transform to reduce 3-D problems to 1-D operations, since digital data manipulation is even more time-consuming in that case. Two kinds of 3-D problems will be discussed: 3-D purely spatial data, and 2-D spatial data with a third dimension (e.g. time or spectrum). We shall briefly describe the required operations, and suggest potential applications.

II.B.1. 3-D Spatial and 2-D Spatial + 1-D Temporal Signals

In Section I.B.1. we described the decomposition of a 3-D function into a set of 1-D projections by integration over parallel planes. The projection operation is identical to eq.

(2), except that the delta function reduces the volume integral to a set of planar integrals. Given a 3-D function f(x,y,z), we wish to integrate the function over a set of planes normal to the 3-D unit vector $\hat{n}$. Two angles are required to define the normal to a plane, commonly the azimuth ϕ and the colatitude θ. The displacement of the parallel plane from the origin is again defined as p, so that $\hat{n} = p/p$. The 3-D projection operation can then be expressed:

$$\lambda(p,\phi,\theta) = \int_{-\infty}^{\infty}\int_{-\infty}^{\infty}\int_{-\infty}^{\infty} d^3r\, f(r)\, \delta(p - r\cdot\hat{n}) \,. \tag{37}$$

The 3-D version of the central-slice theorem states that the 1-D Fourier transform of a projection of a 3-D function yields one line through the origin of the 3-D Fourier transform.

The 3-D back-projection operation is again very similar to the 2-D case, but now the 1-D function is smeared over the original projection plane normal to $\hat{n}$. Repeating this for all directions $\hat{n}$ generates a 3-D summation image b(r). In the filtering step, however, there is a significant qualitative difference between the 2-D and the 3-D cases. Recall that in 2-D, the Fourier space filter for the 1-D projection is $H(\nu) = |\nu|$, and the coordinate space counterpart is $h(p) = -\frac{1}{2\pi^2 p^2}$, which falls off slowly with p. The corresponding filter for the inverse 3-D Radon transform is $H(\sigma) = 2\pi\sigma^2$, where σ is the magnitude of the 3-D spatial frequency vector (ξ,η,ζ) (Barrett, 1981). The coordinate space filter is easily found, since multiplication by $-(2\pi^2\sigma^2)$ in the frequency domain corresponds to taking the Laplacian in the space domain (Gaskill, 1978). The expression for the inverse 3-D Radon transform is therefore:

$$f(r) = -\frac{1}{2\pi}\,\nabla^2[b(r)] \tag{38}$$

where b(r) is the 3-D summation image. Filtering for the 3-D inverse transform is

therefore a local operation, in contrast with the 2-D case.

Barrett (1981) proposed a hybrid 3-D Radon-space signal processor composed of an optical system to derive the projections, digital storage, 1-D signal processing, and optical back-projection. The input function was assumed to be a collection of 2-D image frames, i.e. a movie film, where each frame is assumed to be a 'slice' through the 3-D object. All of the 3-D versions of the operations described in section II.A. could be performed by this system, including 3-D Fourier transformation and convolution. Such a system should be capable of performing 3-D complex Fourier transforms on 500^3 data points in less than 4 hours. A digital system common at the time (PDP 11/34 + array processor) would have required two days.

Such a system can also be applied to 2-D spatial + 1-D temporal signals (e.g. movies) for joint spatial/temporal filtering. A possible application would be to stellar speckle interferometry, allowing the averaging filter impulse response to vary temporally. Such operations are feasible by digital means, but are expensive and time-consuming.

II.B.2. 2-D Spatial + 1-D Spectral Data

Optical detection and display systems are best-suited to 2-D data formats. In white-light images, a third dimension of information has been encoded in the spectrum of each image point. The Radon transform provides a mechanism by which we may use 2-D detectors, signal processors, and display devices to manipulate the spectral data while retaining the ability to regenerate the image. For example, if we have a white light 2-D image, we can derive the set of 1-D projections of that image as described in section I.C.1. The 1-D projections can be spectrally dispersed in the orthogonal dimension, allowing 2-D filtering to be performed on the joint spatial/spectral projection. The 2-D filtered signal can be 'inversely dispersed', to rederive spectrally-filtered 1-D projections, and a 2-D filtered image then reconstructed via the inverse Radon transform. Such a

system could be used for spectral matched filtered imaging (Lohmann and Maul, 1981) (Yu, 1984) or imaging spectroscopy.

III. Summary and Conclusions

We have discussed the reduction of 2-D signal processing operations to 1-D operations via the Radon transform for the purpose of gaining flexibility, precision, and mechanical advantages over direct optical signal processing. This technique is most readily applicable to operations based on Fourier transforms and convolution. Several optical systems were discussed that are capable of performing the forward and inverse dimensional transformations, and a number of applications were considered, some already demonstrated and some postulated. The authors believe that many of the fruits of this technique have yet to be harvested, and we encourage workers in signal processing to investigate the utility of projection operations in their own applications.

Acknowledgements

The authors have benefitted greatly from discussions with many co-workers and colleagues, including Adolf Lohmann, Stanley Deans, John Walkup, H. Harold Szu, Arthur Gmitro, Gene Gindi, Anthony Ticknor, Warren Smith, and Kyle Myers.

REFERENCES

Abramovitz, I.J., N.J. Berg, and M.W. Casseday (1983). In "Acousto-Optic Signal Processing" (Berg and Lee, eds.), pp. 289-323. Marcel Dekker, New York.

Ash, E.A. (1978). In "Acoustic Surface Waves" (A.A. Oliner, ed.), pp. 97-186. Springer-Verlag, New York.

Athale, R.A., J.N. Lee, E. L. Robinson, and H.H. Szu (1983). Opt. Let. 8, pp. 166-168.

Bamler, R. and J. Hofer-Alfeis (1982). Opt. Comm. 43, pp. 97-102.

Bamler, R. and H. Glünder (1983). Optica Acta 30, pp. 1789-1803.

Barrett, H.H. (1981). SPIE Proc., Vol. 373, pp. 179-190.

Barrett, H.H. (1984). In "Progress in Optics" (E. Wolf, ed.), Vol. XXI,pp. 219-286. Elsevier, Amsterdam.

Barrett, H.H. and W. Swindell (1977). Proc. IEEE 65, pp. 89-107.

Barrett, H.H., J. Greivenkamp, S.K. Gordon, A.F. Gmitro, M.Y. Chiu, and W. Swindell (1979). Opt. Comm. 28, pp. 287-290.

Barrett, H.H., M.Y. Chiu, S.K. Gordon, R.E. Parks, and W. Swindell (1979). Appl. Opt. 18, pp. 2760-2766.

Barrett, H.H. and W. Swindell (1981). "Radiological Imaging", Vol. II. Academic Press, New York.

Bartelt, H.O. and A.W. Lohmann (1981). SPIE Proc. Vol. 373, pp. 3-10.

Bastiaans, M.J. (1978). Opt. Comm. 25,pp. 26-30.

Berg, N.J., J.N. Lee, and M.W. Casseday (1979). Opt. Eng. 18, pp. 420-428.

Beynon, J.D.E. and D.R. Lamb (1980). "Charge-coupled Devices and their Applications." McGraw-Hill, London.

Bierman, H. (1985). Electronics 58(48), p. 139.

Bracewell, R.N. (1983). J. Opt. Soc. Am. 73, pp. 1832-1835.

Bracewell, R.N., H. Bartelt, A.W. Lohmann, and N. Streibl (1985). Appl. Opt. 24, pp. 1401-1402.

Brenner, K.-H., and A.W. Lohmann (1982). Opt. Comm. 42, pp. 310-314.

Buss, D.D., D.R. Collins, W.H. Bailey, and C.R. Reeves (1973). IEEE J. Solid-State Circuits SC-8, pp. 138-146.

Casasent, D.P. (1978). In "Optical Data Processing" (D. Casasent, ed.). pp. 241-282.

Casasent, D.P. (1981). In "Optical Information Processing" (S.H. Lee, ed.). pp. 181-233. Springer-Verlag, New York.

Casasent, D. (1983). In "Acousto-Optic Signal Processing" (Berg and Lee, eds), pp. 325-367. Marcel Dekker, New York.

Casasent, D. and D. Psaltis (1977). Proc. IEEE 65, pp. 77-83.

Casseday, M.W., N.J. Berg, and I.J. Abramovitz (1983). In "Acousto-Optic Signal Processing" (Berg and Lee, eds.), pp. 165-203. Marcel Dekker, New York.

Childers, D.G., D.P. Skinner, and R.C. Kemerait (1977). Proc. IEEE 65, pp. 1428-1443.

Cole, B.C. (1985). Electronics 58(50), p. 50.

Connor, M. and Y. Li (1985). Appl. Opt. 24, pp. 3825-3829.

Cormack, A.M. (1963). J. Appl. Phys. 34, p. 2722-2727.

Cormack, A.M. (1964). J. Appl. Phys. 35, p. 2908-2913.

Das, P. and F.M.M. Ayub (1982). In "Applications of Optical Fourier Transforms" (H. Stark, ed.), pp. 289-331. Academic Press, New York.

Deans, S.R. (1981). IEEE Trans. on Pattern Analysis and Machine Intelligence PAMI-3, pp. 185-188.

Deans, S.R. (1983). "The Radon Transform and Some of its Applications." Wiley, New York.

Dudgeon, D.E. and R.M. Mersereau (1984). "Multidimensional Digital Signal Processing." Prentice-Hall, Englewood Cliffs, NJ.

Duinker, S., R.J. Geluk, and H. Mulder (1978) Oldelft Science and Engineering Quarterly 1, pp. 41-66.

Easton, R.L. Jr., A.J. Ticknor, and H.H. Barrett (1984). Opt. Eng. 23, pp. 738-744.

Easton, R.L. Jr., A.J. Ticknor, and H.H. Barrett (1985a). J. Opt. Soc. Am. A 2, p. P108.

Easton, R.L. Jr., A.J. Ticknor, and H.H. Barrett (1985b). Appl. Opt. 24, pp. 3817-3824.

Edholm, P., L.G. Hellstrom, and B. Jacobson (1978). Phys. Med. Biol. 23, pp. 90-99.

Eichmann, G. and B.Z. Dong (1982). Appl. Opt. 21, pp. 3152-3156.

Eichmann, G. and B.Z. Dong (1983). Appl. Opt. 22, pp. 830-834.

Ein-Gal, M. (1974). 'The Shadow Transform: an Approach to Cross-Sectional Imaging.' Ph.D. Dissertation, Stanford University.

Farhat, N.H., C. Yi Ho, and L.S. Chang (1983). SPIE Proc. Vol. 388, pp. 140-150.

Fraser, D., B.R.Hunt, and J.C. Su (1985). Opt. Eng. 24, pp. 298-306.

Gaskill, J.D. (1978). 'Linear Systems, Fourier Transforms, and Optics.' Wiley-Interscience, New York.

Gerard, H.M. (1978). In 'Acoustic Surface Waves' (A.A. Oliner, ed.), pp. 61-96. Springer-Verlag, New York.

Gerard, H.M., W.R. Smith, W.R. Jones, and J.B. Harrington (1973). IEEE Trans. Microwave Theory Tech. MTT-21, pp. 176-186.

Gerard, H.M., P.S. Yao, and O.W. Otto (1977). 'Proc. of IEEE Ultrasonics Symposium.' pp. 947-951.

Gindi, G.R. and A.F. Gmitro (1984). Opt. Eng. 23, pp. 499-506.

Gmitro, A.F., J.E. Greivenkamp, W. Swindell, H.H. Barrett, M.Y. Chiu, and S.K. Gordon (1980). Opt. Eng. 19, pp. 260-272.

Gmitro, A.F., G.R. Gindi, H.H. Barrett, and R.L. Easton, Jr. (1983). SPIE Proc., Vol. 388, pp. 132-139.

Gmitro, A.F. and G.R. Gindi (1985). Appl. Opt. 24, pp. 4041-4045.

Goodman, J.W. (1981). In 'Optical Information Processing' (S.H. Lee, ed.), pp. 235-260. Springer-Verlag, New York.

Gordon, S.K. (1977). 'Analog Reconstruction Methods for Transaxial Tomography.' Ph.D. Dissertation, University of Arizona.

Gottlieb, M., C.L.M. Ireland, and J.M. Ley (1983). 'Electro-Optic and Acousto-Optic Scanning and Deflection.' Marcel Dekker, New York.

Grassl, H.P. (1985). Microwave Journal 27(7), p. 169.

Greivenkamp, J.E., W. Swindell, A.F. Gmitro, and H.H. Barrett (1981). Appl. Opt. 20, pp. 264-273.

Gritton, C.W.K. and D.W. Lin (1984). IEEE ASSP Magazine 1(2), pp. 30-38.

Hansen, E.W. (1981a). J. Opt. Soc. Am. 71, pp. 304-308.

Hansen, E.W. (1981b). Appl. Opt. 20, pp. 2266-2274.

Hansen, E.W. and J.W. Goodman (1978). Opt. Comm. 24, pp. 268-272.

Helgason, S. (1980). "The Radon Transform." Birkhäuser, Boston.

Hofer, J. (1979). Opt. Comm 29, pp. 22-26.

Hofer, J. and W. Kupka (1979). SPIE Proc. 211, pp. 62-65.

Hotz, D.F. (1984). Appl. Opt. 23, pp. 1613-1619.

Hu, M.K. (1962). IRE Trans. Inform. Theory IT-8, pp. 113-121.

Jack, M.A. and E.G.S. Paige (1978). Wave Electronics 3, pp. 229-247.

Jack, M.A., P.M. Grant, and J.H. Collins (1980). Proc. IEEE 68, pp. 450-468.

John, F. (1955). "Plane Waves and Spherical Means Applied to Partial Differential Equations." Interscience, New York.

Kak, A.C. (1985). In "Array Signal Processing" (S. Haykin, ed.), pp. 351-428. Prentice-Hall, Englewood Cliffs, NJ.

Kay, S.M. and S.L. Marple, Jr. (1981). Proc. IEEE 69, pp. 1380-1419.

Klauder, J.R., A.C. Price, S. Darlington, and W.J. Albersheim (1960). Bell System Technical Journal 34, pp. 745-808.

Korpel, A. (1981). Proc. IEEE 69, pp. 48-53.

Lee, J.N., S-C Lin, and A.B. Tventen (1982). In "Real-Time Signal Processing V" (J. Trimble, ed.), SPIE Proc. 341, pp. 86-93.

Lighthill, M.J. (1962). "Fourier Analysis and Generalized Functions." Cambridge University Press, Cambridge.

Liu, H-K., J.A. Davis, and R.A. Lilly (1985). Opt. Lett. 10, pp. 635-637.

Lohmann, A. (1977). Appl. Opt. 16, pp. 261-263.

Lohmann, A. and M. Maul (1981). Angewandte Optik, Annual Report 1981, Physikalisches Institut der Universität Erlangen-Nürnberg, pp. 28-29.

Lohmann, A.W. and B. Wirnitzer (1984). Proc. IEEE 72, pp. 889-901.

McEwan, J.A., A.D. Fisher, P.B. Rolsma, and J.N. Lee (1985). J. Opt. Soc. Am. A 2, p. P8.

Maitra, S. (1979). Proc. IEEE 67, p. 697-699.

Marr, J.D. (1982). In "Real-Time Signal Processing V" (J. Trimble, ed.), SPIE Proc. 341, pp. 245-251.

Matthews, H. (1977). "Surface Wave Filters." Wiley, New York.

Mersereau, R.M. and A.V. Oppenheim (1974). Proc. IEEE 62, p. 1319-1338.

Monahan, M.A., K. Bromley, and R.P. Bocker (1977). Proc. IEEE 65, pp. 121-129.

Morgan, D.P. (1985). "Surface Wave Devices for Signal Processing." Elsevier, Amsterdam.

Oppenheim, A.V. (1970). IEEE Spectrum 7(8), pp. 57-62.

Pancott, B. and C.D. Reeve (1985). J. Opt. Soc. Am. A. 2, p. P38.

Peters, T.M. (1974). IEEE Trans. on Biomed. Eng. 21, pp. 214-219.

Rabiner, L.R., R.W. Schafer, and C.M. Rader (1969), IEEE Transactions on Audio and Electroacoustics AU-17, pp. 86-92.

Radon, J. (1917). "Berichte Sächsische Akademie der Wissenschaften. Leipzig, Math.-Phys. Kl.", 67, pp. 262-267. (translated in Deans (1983)).

Rau, J. (1966). J. Opt. Soc. Am. 56, pp. 1490-1497.

Rhodes, W.T. (1977). Appl. Opt. 16, p. 265-267.

Rhodes, W.T. (1981a). Proc. IEEE 69, pp. 64-79.

Rhodes, W.T. (1981b). Proc. SPIE 373, pp. 11-20.

Rhodes, W.T. and A. Lohmann (1978). Appl. Opt. 17, p. 1141-1151.

Roberts, J.B.G. (1977). In "Impact of Charge-Coupled Devices and Surface Acoustic Wave Devices on Signal Processing and Imagery in Advanced Systems" (Y. Brault, ed.). Proceedings of the Advisory Group for Aerospace Research and Development of NATO, 230, pp. 1.2-1 - 1.2-16.

Robinson, E. (1982). Proc. IEEE 70, pp. 885-907.

Rogers, G.L. (1977). "Noncoherent Optical Processing". Wiley-Interscience, New York.

Rowland, S.W. (1979). In "Image Reconstruction from Projections (G.T. Herman, ed.). Springer-Verlag, New York.

Smith, H.I. (1978). In "Acoustic Surface Waves" (A.A. Oliner, ed.). Springer-Verlag, New York.

Smith, W.E. and H.H. Barrett (1983). Opt. Lett. 8, pp. 395-397.

Stetson, K.A. and J.N. Elkins (1977). "Optical System for Dynamic Analysis of Rotating Structures." Tech. Rep. AFAOL-TR-77-51, United Technologies Research Center, East Hartford, CT.

Stoner, W. (1978). Appl. Opt. 17, p. 2454-2467.

Tao, K.M. and F.M. Weinhaus (1985). Proceedings of the International Conference on Acoustics, Speech, and Signal Processing, pp. 18.9.1-18.9.4.

Thomas, C.E. (1966). Appl. Opt. 5, pp. 1782-1790.

Ticknor, A.J., R.L. Easton, Jr. and H.H. Barrett (1985). Opt.Eng. 24, pp. 82-85.

Vander Lugt, A. (1982). Appl. Opt. 21, pp. 4005-4011.

Weaver, C.S. and J.W. Goodman (1966). Appl. Opt. 5, pp. 1248-49.

Whitehouse, H.J. (1977). Proc. SPIE 118, pp. 118-123.

Widrow, B., J.R. Glover, Jr., J.M. McCool, J. Kaunitz, C.S. Williams, R.H. Hearn, J.R. Zeidler, E. Dong, Jr., and R.C. Goodlin (1975). Proc. IEEE 63, pp. 1692-1716.

Wigner, E. (1932). Phys. Rev. 40, p. 749.

Woodward, P.M. (1953). "Probability and Information Theory with Applications to Radar." Pergamon Press, 1953.

Yu, F.T.S. (1984). Opt. Eng. 23, pp. 690-694.

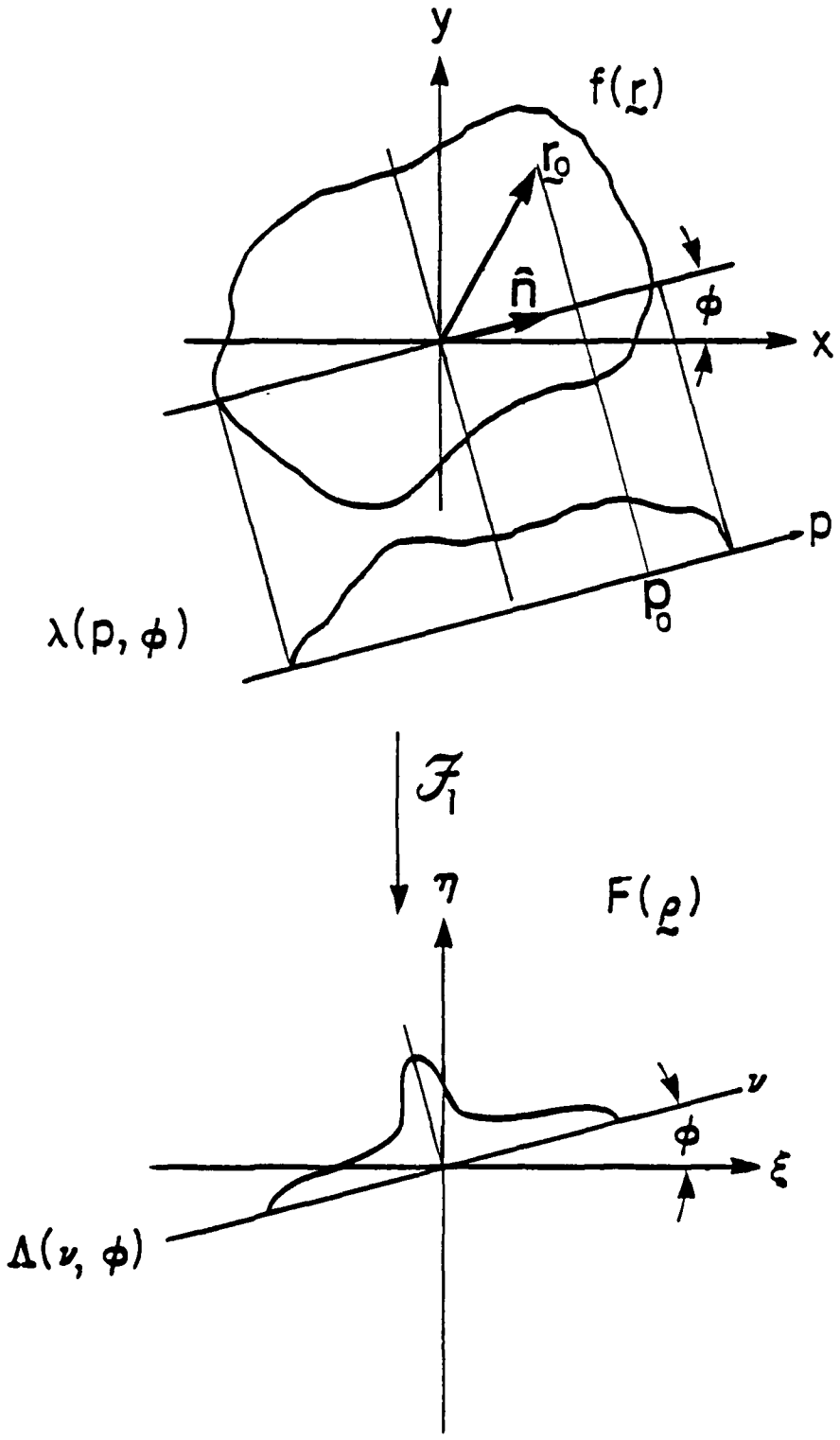

Fig. 1

Fig. 2

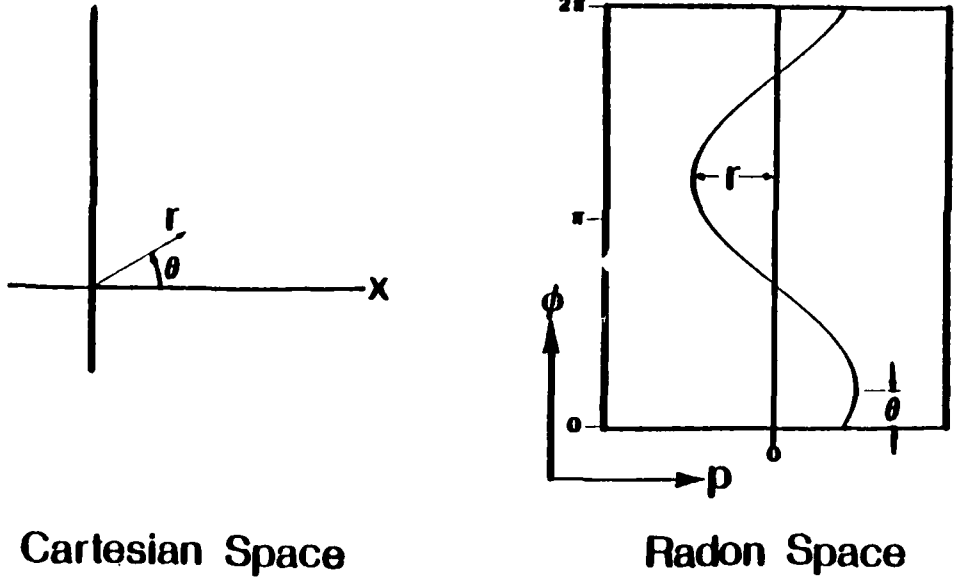

Cartesian Space

Radon Space

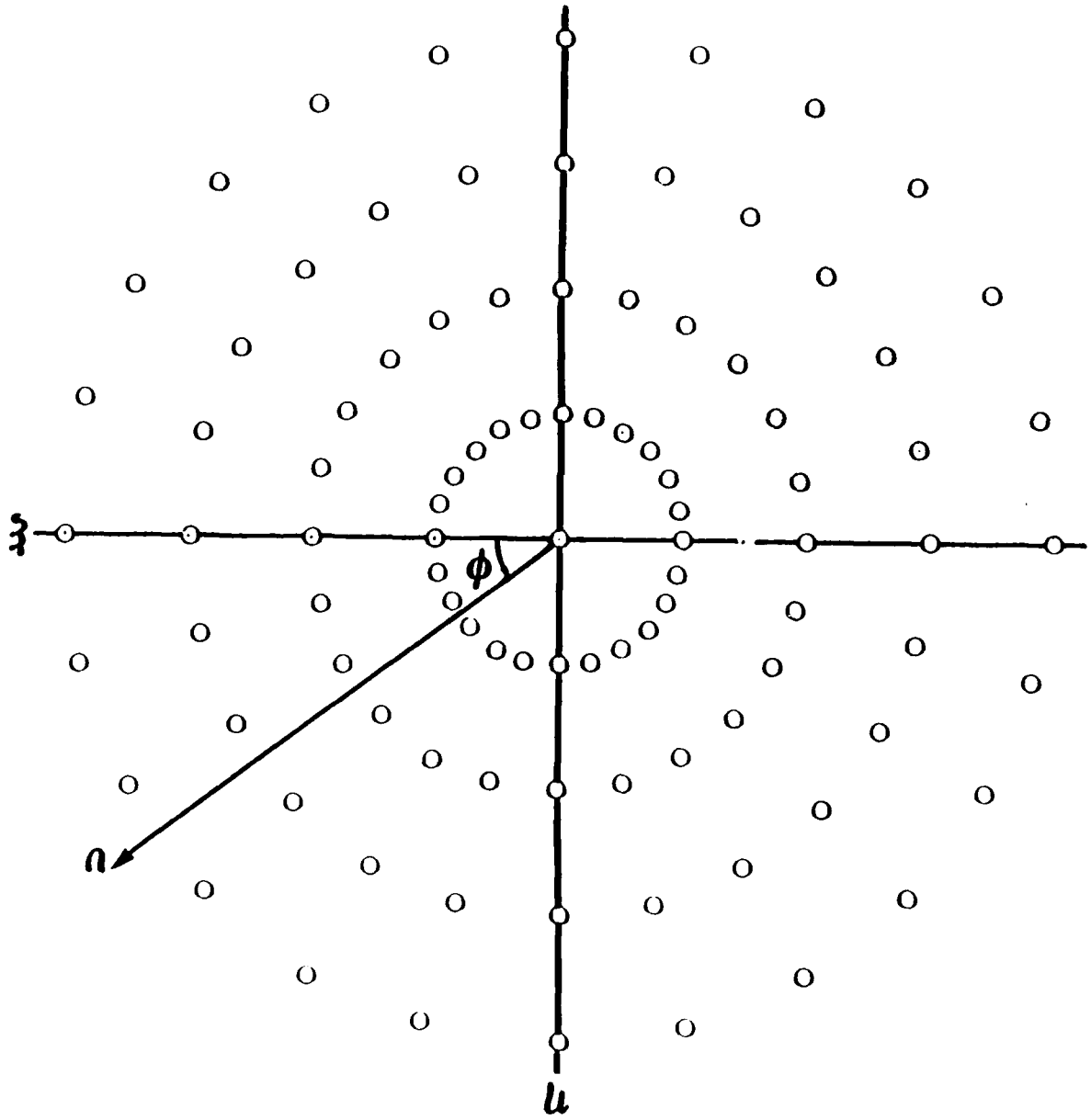

FIG. 3

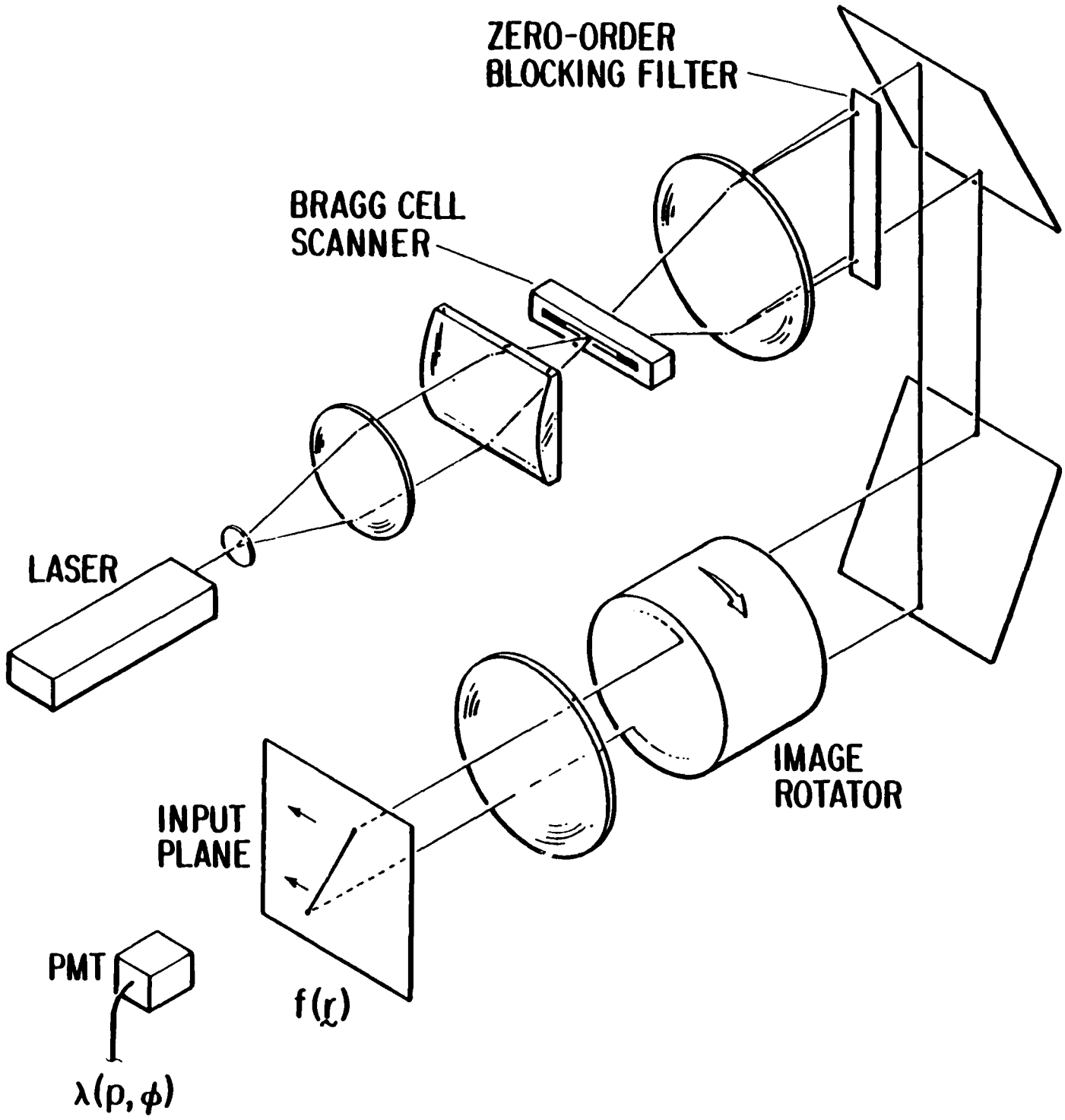
ZERO-ORDER
BLOCKING FILTER
BRAGG CELL
SCANNER
LASER
IMAGE
ROTATOR
INPUT
PLANE
PMT
f(r)
λ(p, φ)

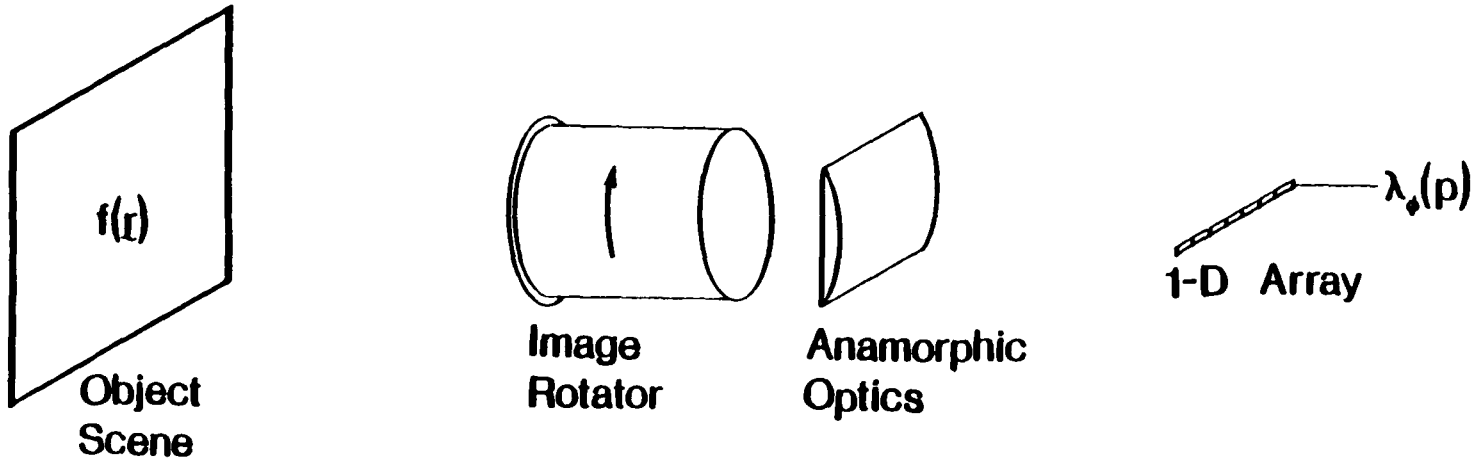
f(r)
Object
Scene
Image
Rotator
Anamorphic
Optics
$\lambda_\phi(p)$
1-D Array

Fig. 5

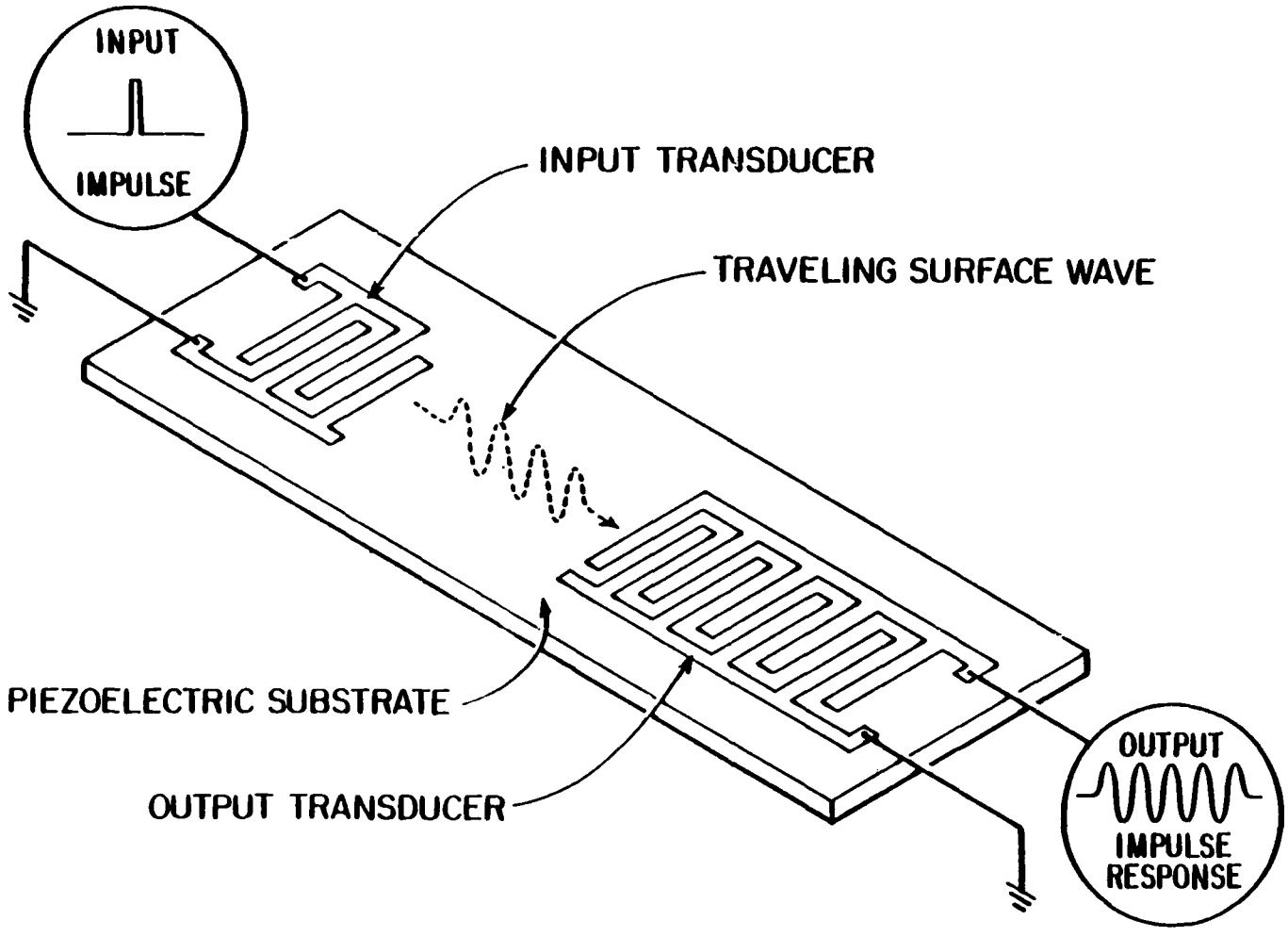
INPUT
IMPULSE
INPUT TRANSDUCER
TRAVELING SURFACE WAVE
PIEZOELECTRIC SUBSTRATE
OUTPUT TRANSDUCER
OUTPUT
IMPULSE
RESPONSE

Fig 6

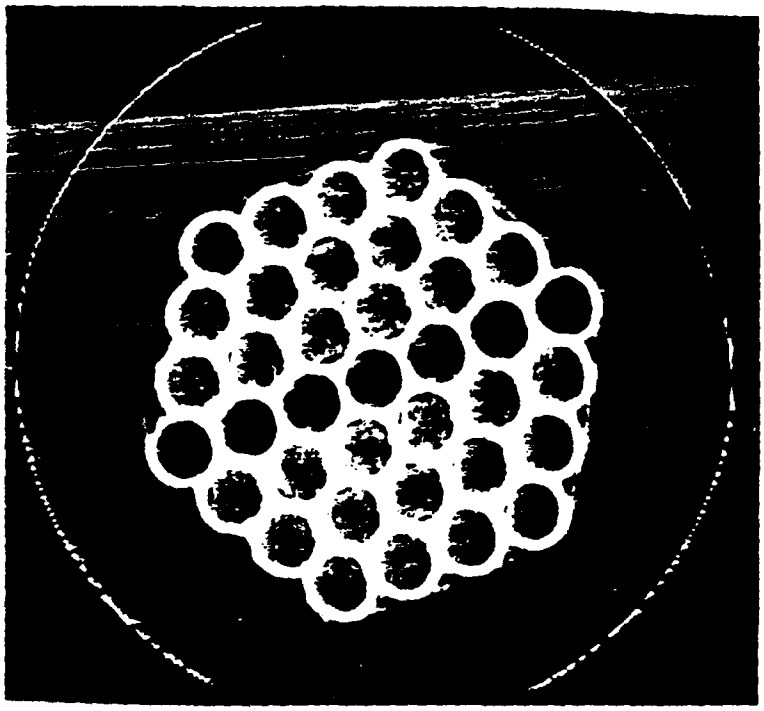

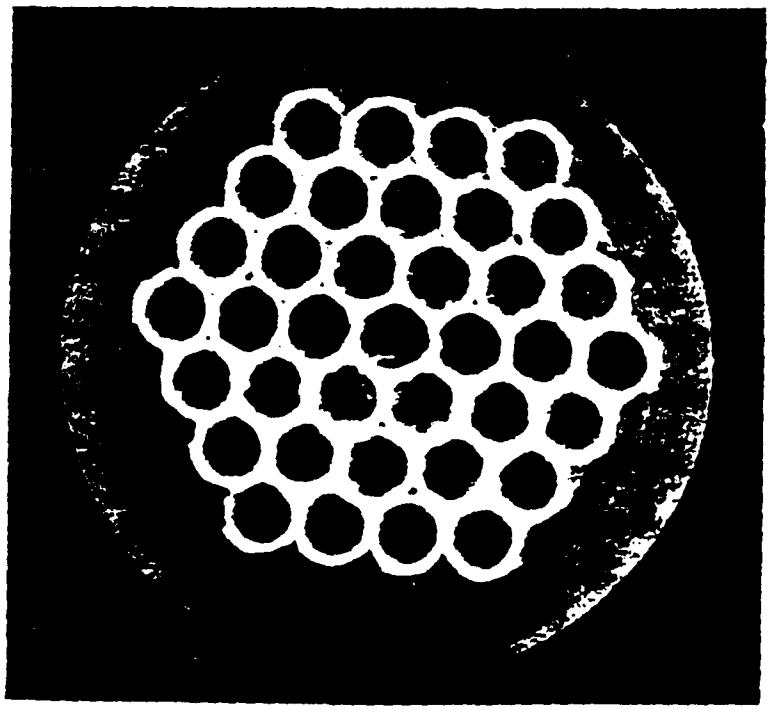

Fig 7

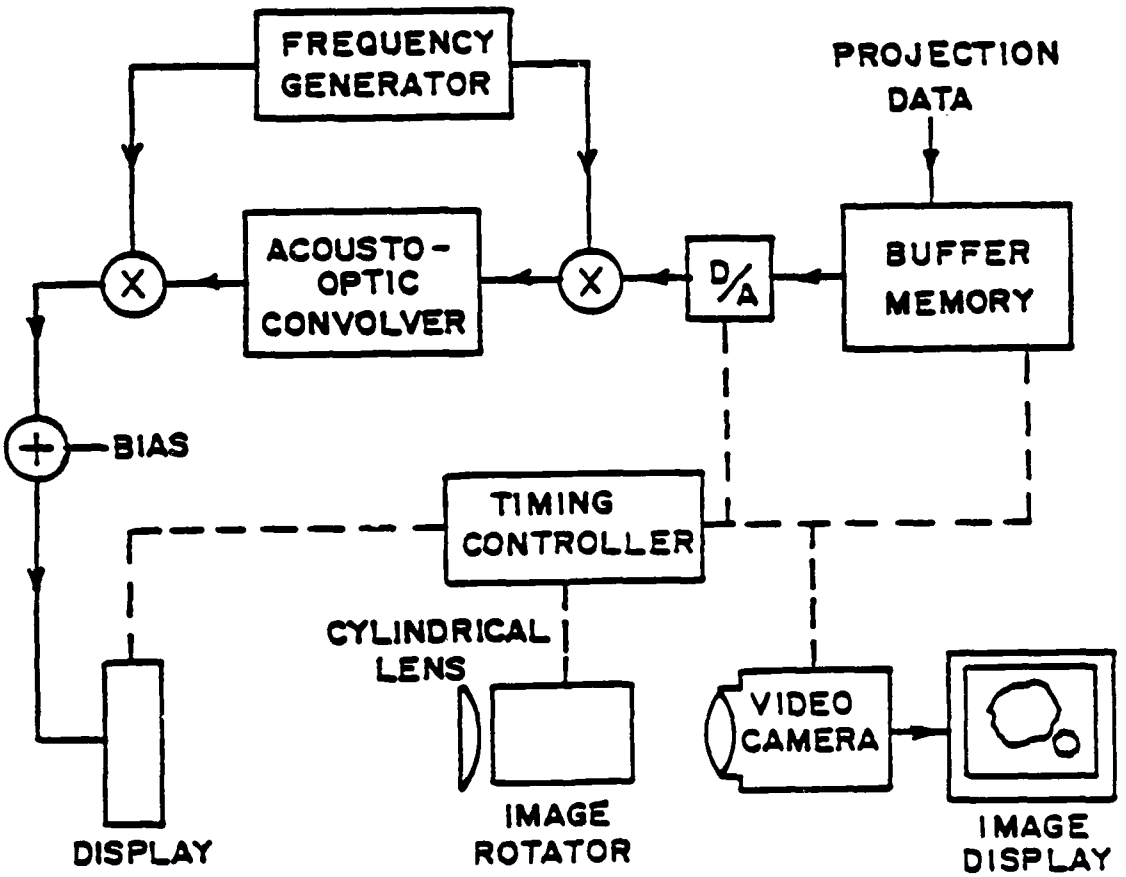
FREQUENCY GENERATOR
PROJECTION DATA
ACOUSTO-OPTIC CONVOLVER
D/A
BUFFER MEMORY
BIAS
TIMING CONTROLLER
CYLINDRICAL LENS
VIDEO CAMERA
DISPLAY
IMAGE ROTATOR
IMAGE DISPLAY

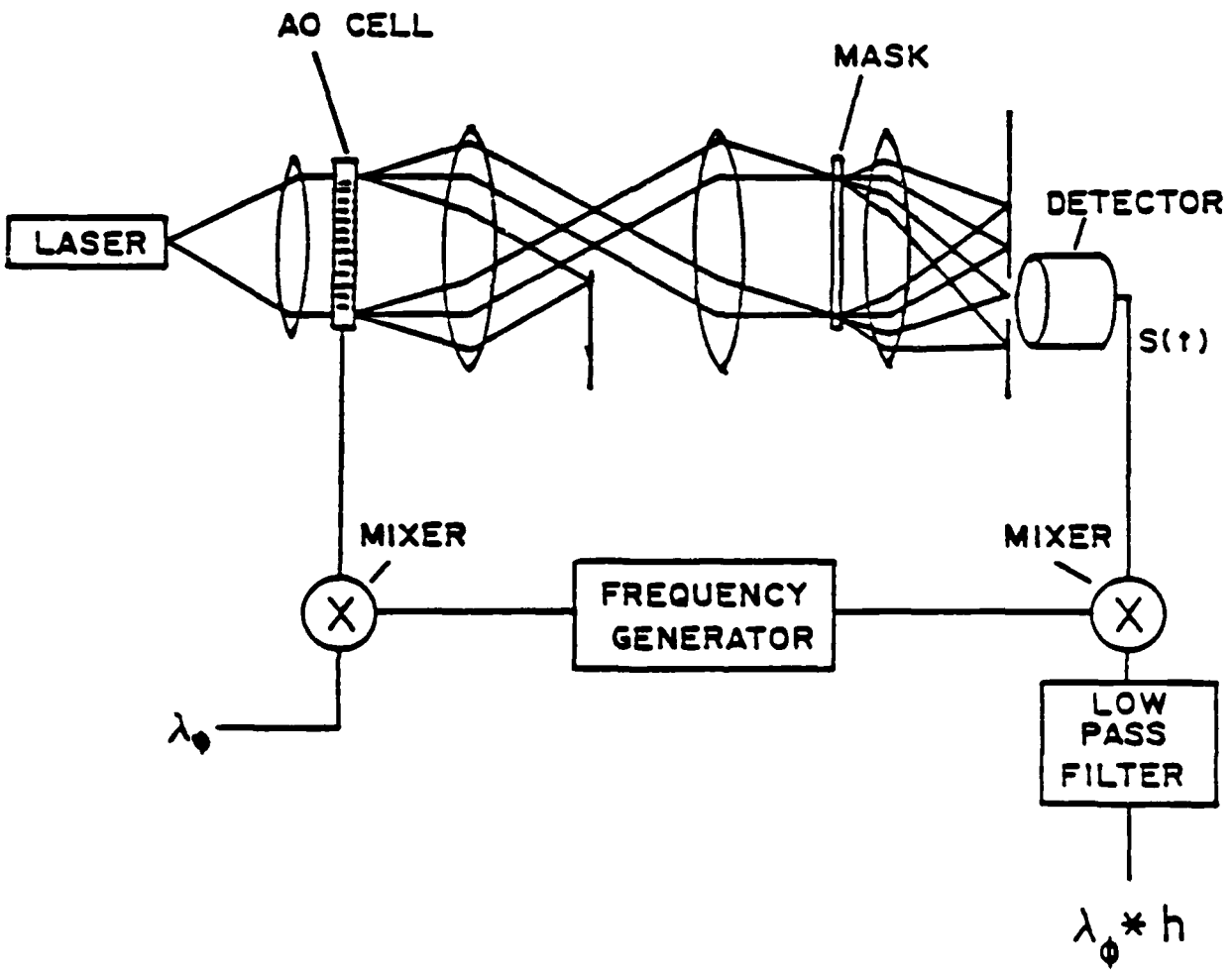
AO CELL
MASK
LASER
DETECTOR
S(t)
MIXER
MIXER
FREQUENCY GENERATOR
LOW PASS FILTER
λ_ϕ
$\lambda_\phi * h$

FIG 9

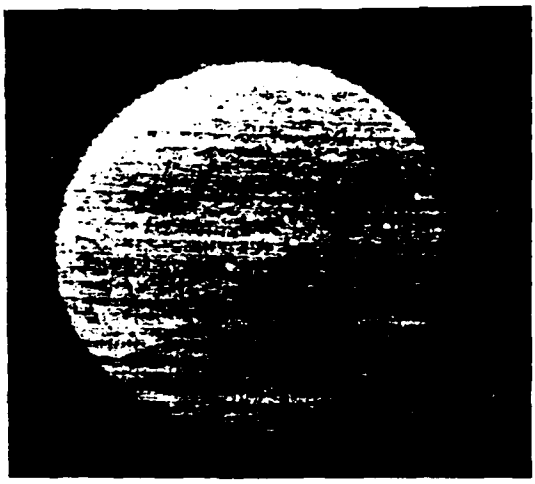

A

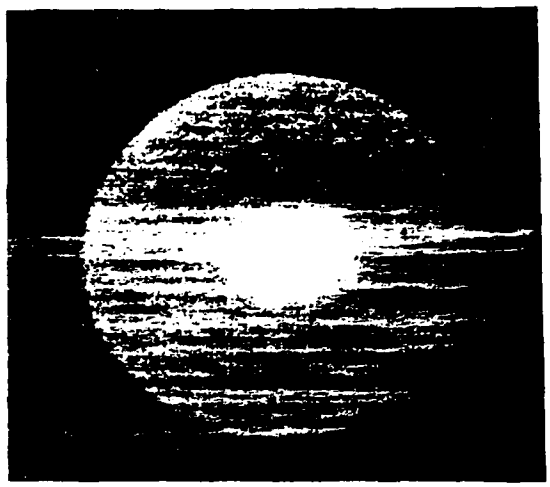

B

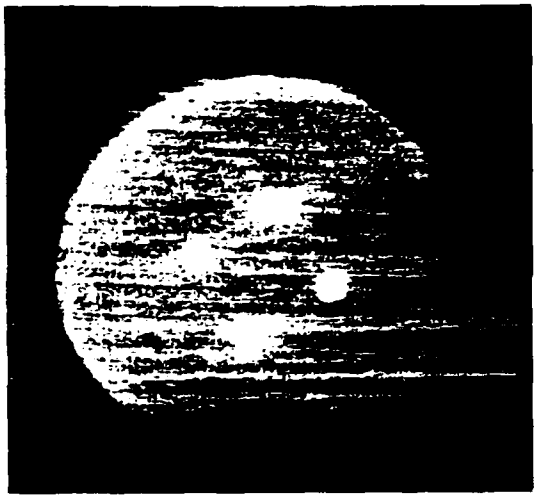

C

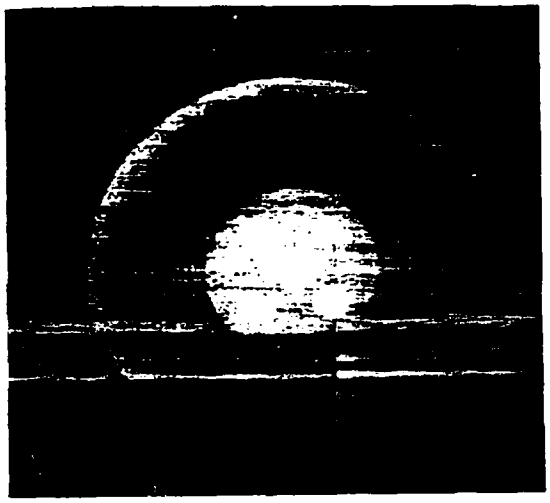

D

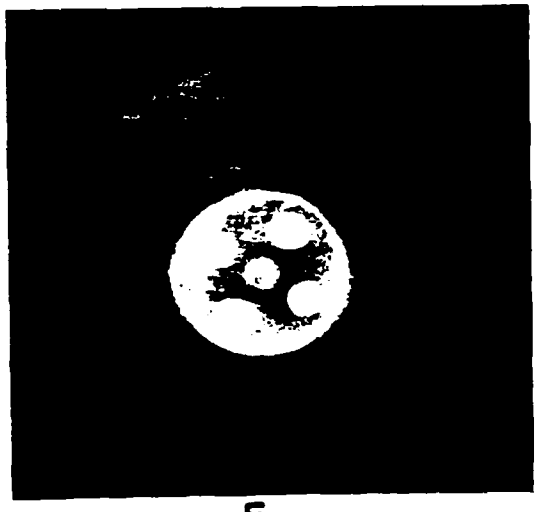

E

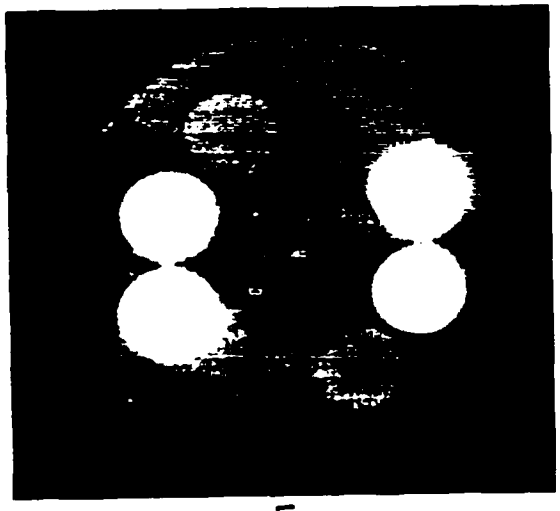

F

Fig. 10

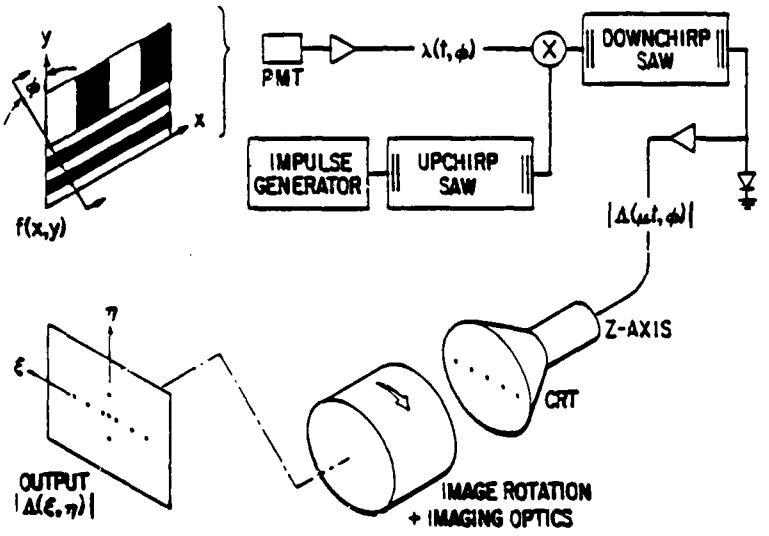
y
x
f(x,y)
PMT
λ(t,φ)
DOWNCHIRP SAW
IMPULSE GENERATOR
UPCHIRP SAW
|Δ(μt,φ)|
Z-AXIS
CRT
η
ξ
OUTPUT
|Δ(ξ,η)|
IMAGE ROTATION
+ IMAGING OPTICS

Fig. 1

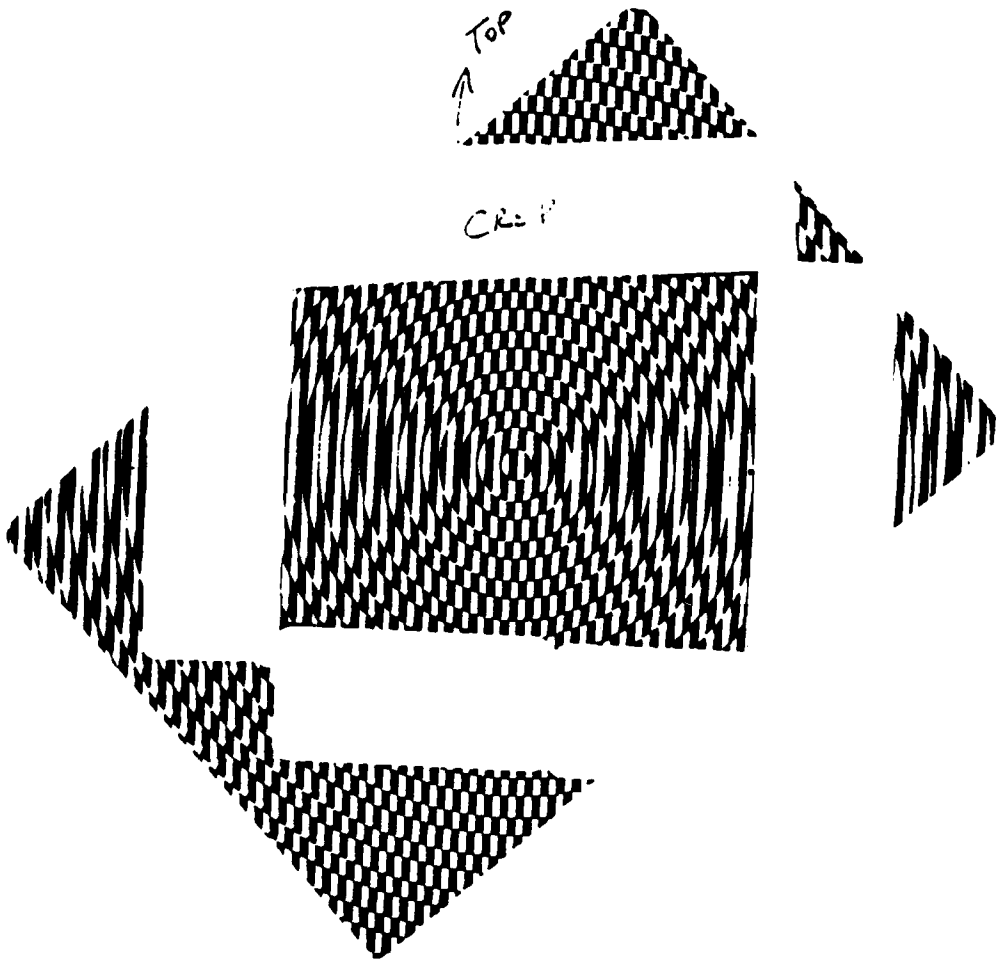

12(a)

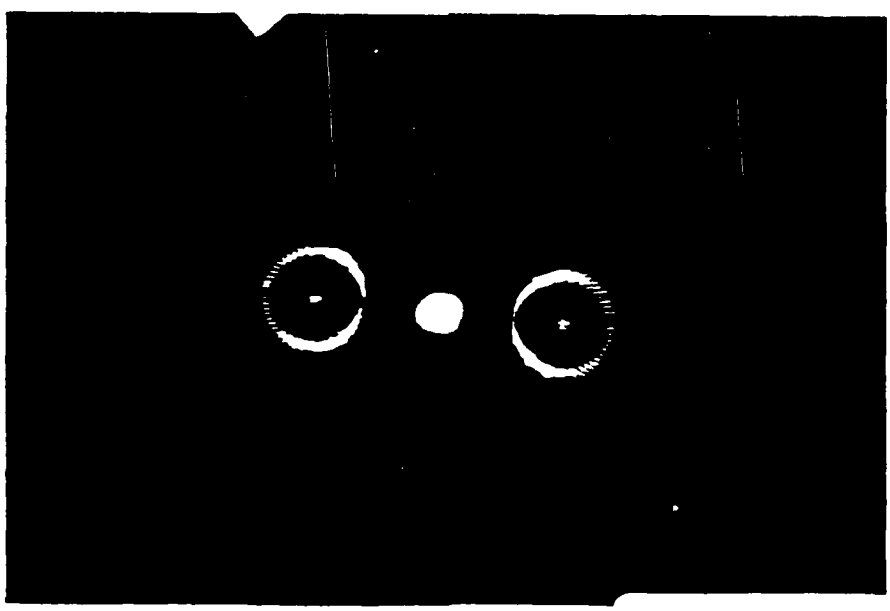

Figure ~~6~~ 12(a)

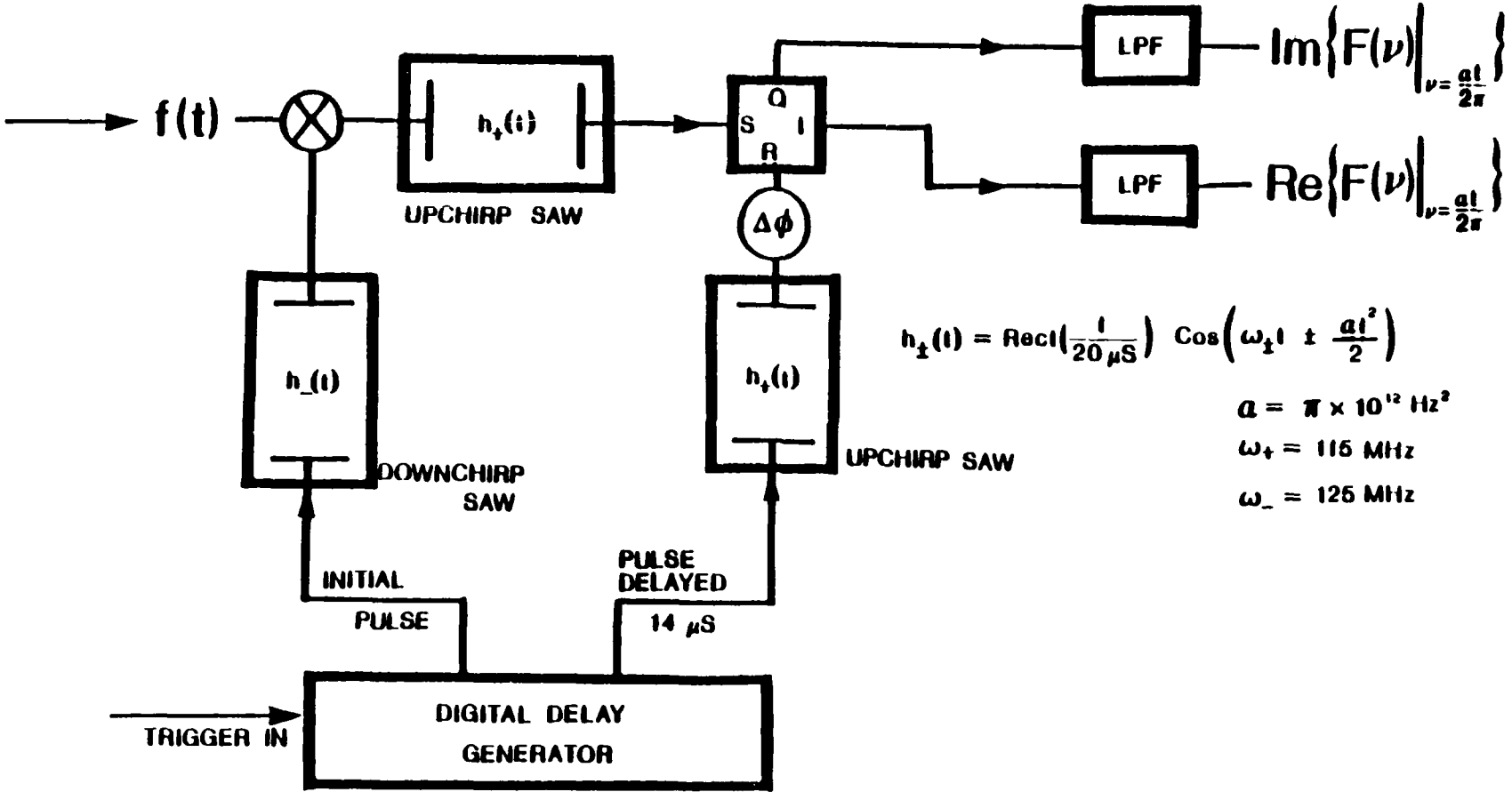
f(t)
$h_+(t)$
UPCHIRP SAW
Q
S
I
R
$\Delta\phi$
LPF
LPF
$\mathrm{Im}\{F(\nu)|_{\nu=\frac{at}{2\pi}}\}$
$\mathrm{Re}\{F(\nu)|_{\nu=\frac{at}{2\pi}}\}$
$h_-(t)$
DOWNCHIRP SAW
$h_+(t)$
UPCHIRP SAW
$h_\pm(t) = \mathrm{Rect}\left(\frac{t}{20\,\mu S}\right)\ \mathrm{Cos}\left(\omega_\pm t \pm \frac{at^2}{2}\right)$
$a = \pi \times 10^{12}\ \mathrm{Hz}^2$
$\omega_+ = 115$ MHz
$\omega_- = 125$ MHz
INITIAL PULSE
PULSE DELAYED 14 μS
TRIGGER IN
DIGITAL DELAY GENERATOR

Fig 13

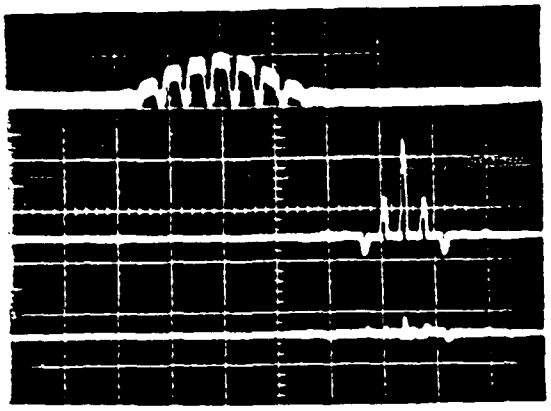

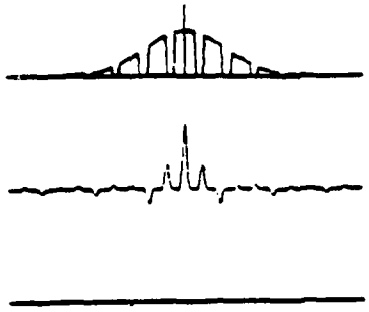

Fig 14

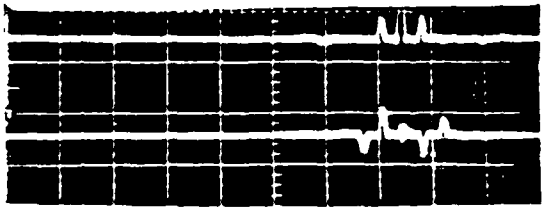

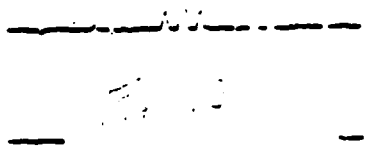

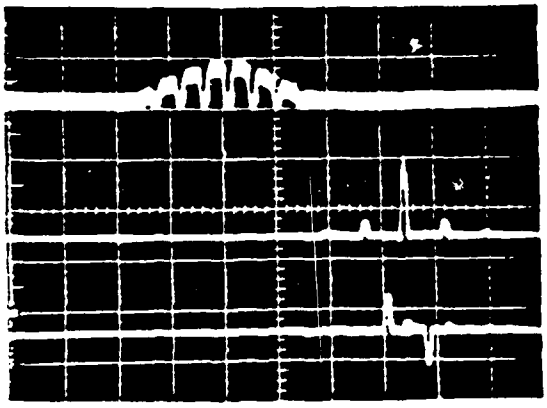

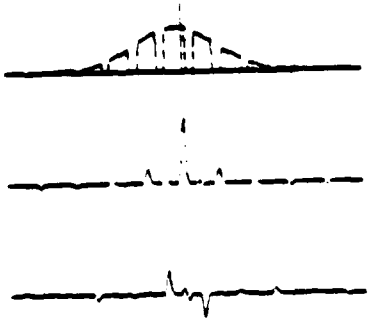

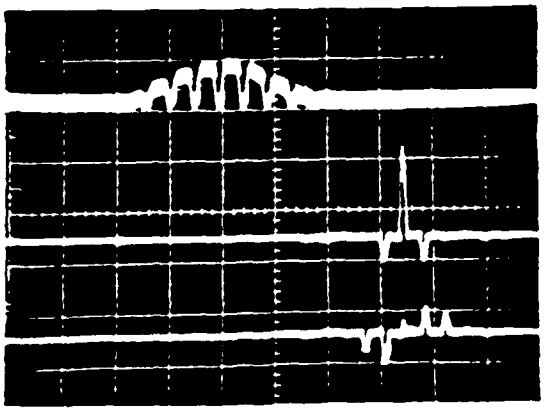

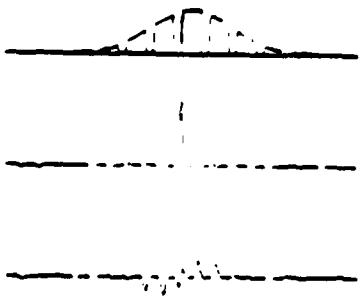

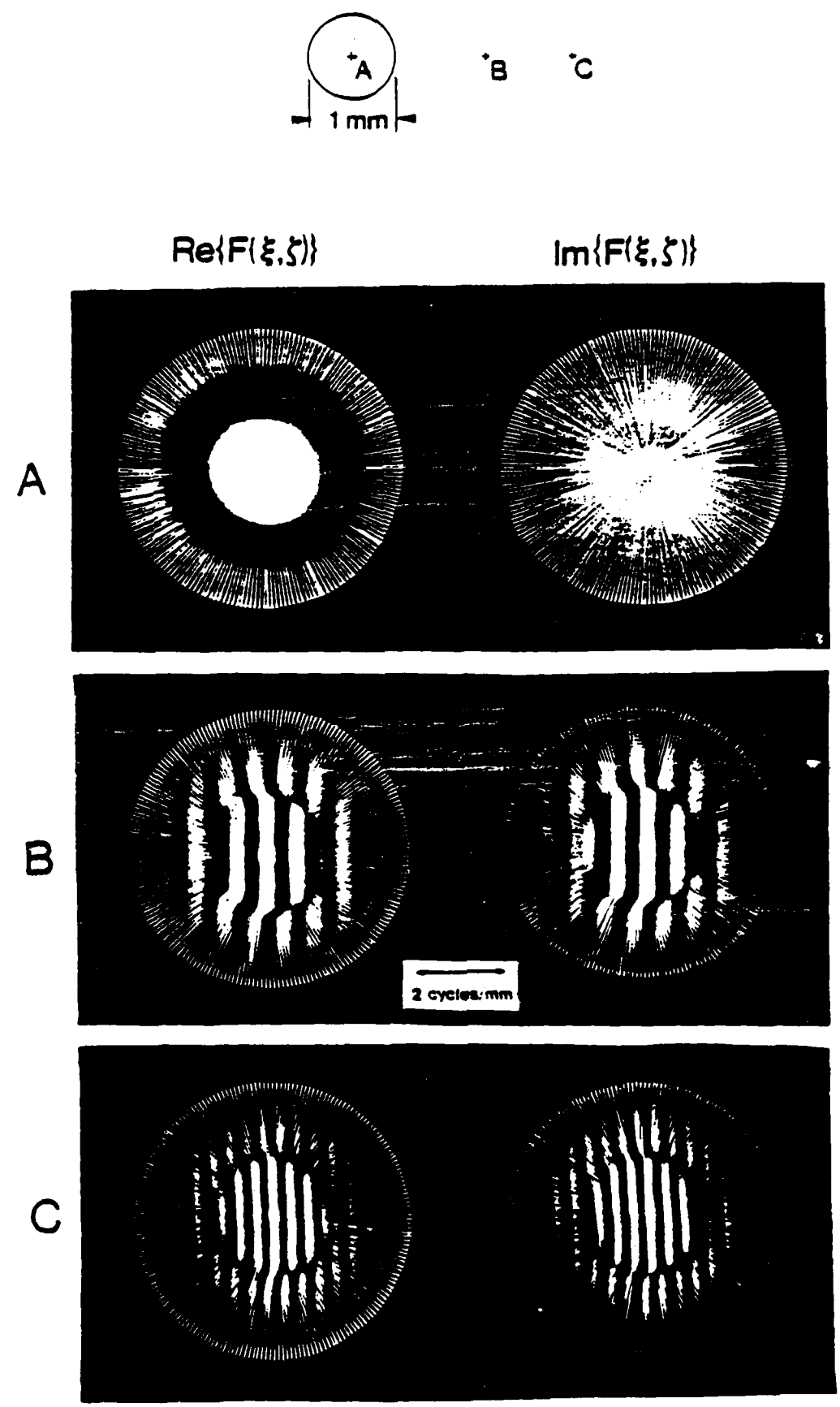

Fig

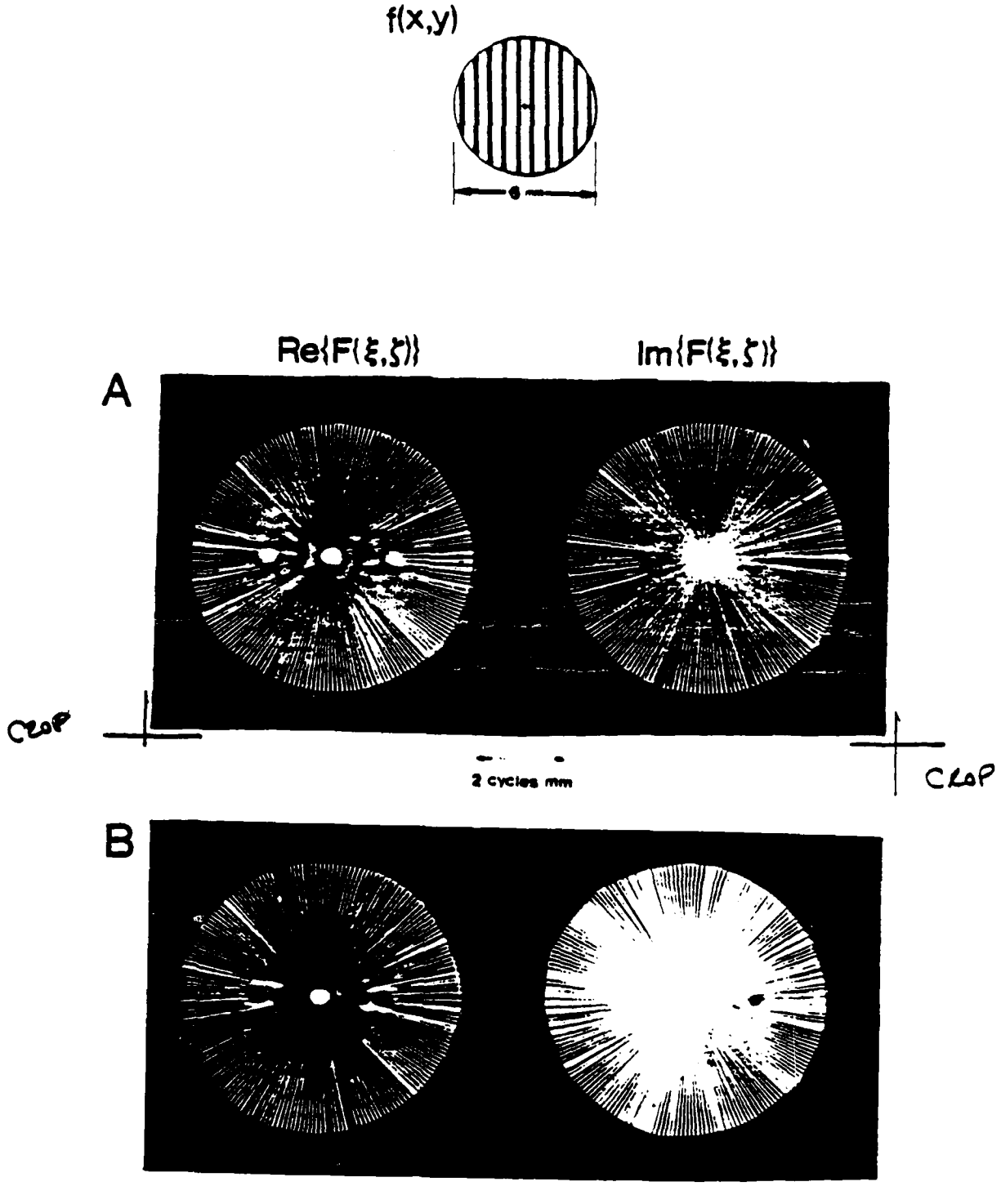

Fig

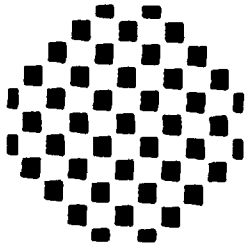

I_d

17a

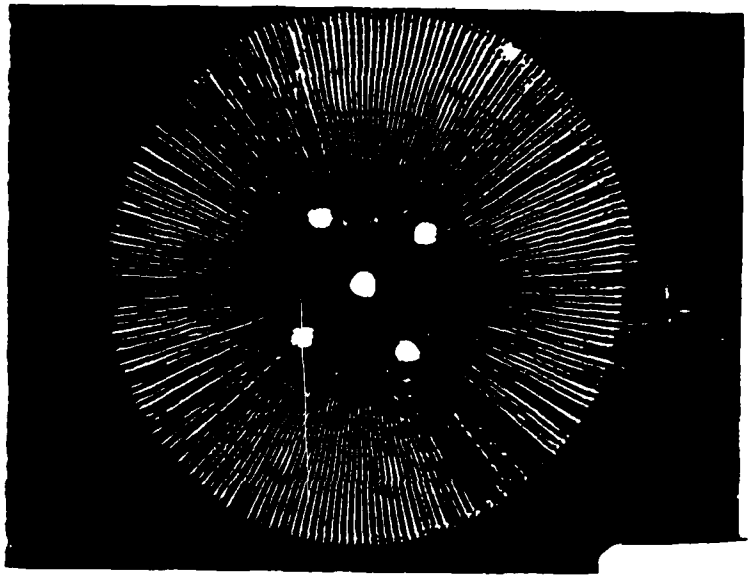

17b

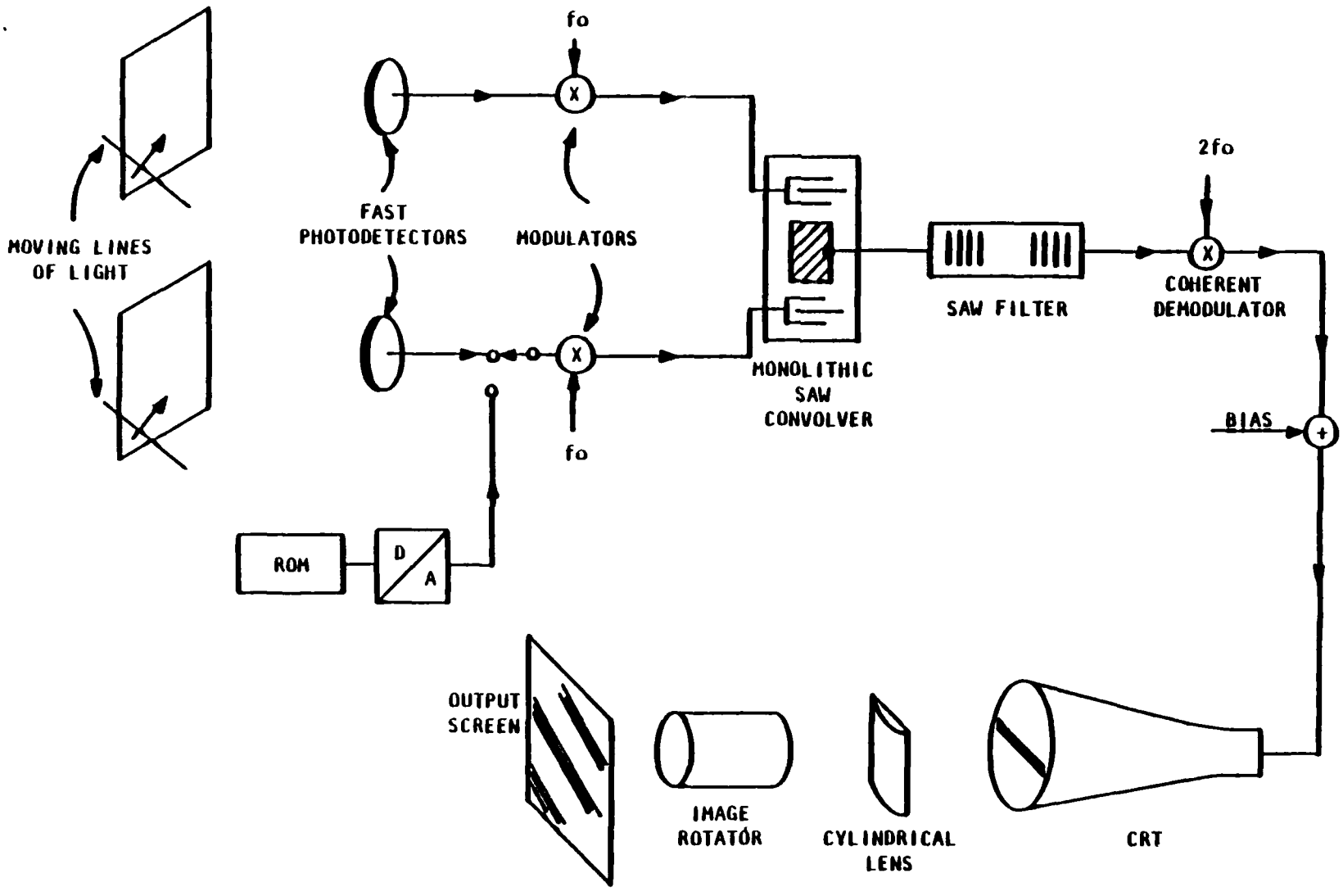
fo
MOVING LINES
OF LIGHT
FAST
PHOTODETECTORS
MODULATORS
MONOLITHIC
SAW
CONVOLVER
SAW FILTER
2fo
COHERENT
DEMODULATOR
BIAS
fo
ROM
D
A
OUTPUT
SCREEN
IMAGE
ROTATOR
CYLINDRICAL
LENS
CRT

Fig 18

Fig 19a

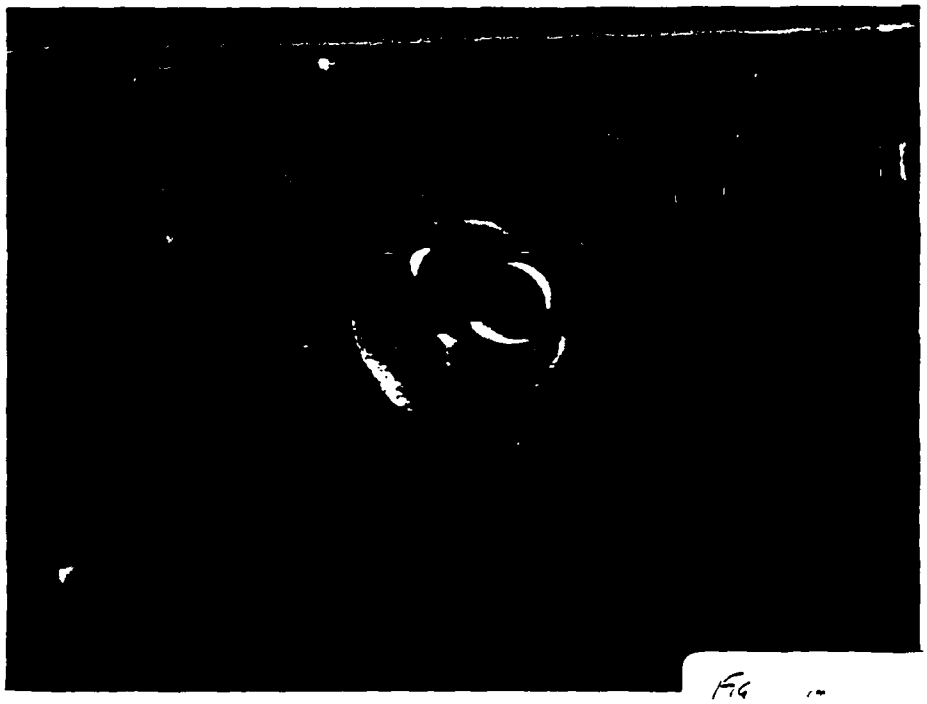

Fig 19b

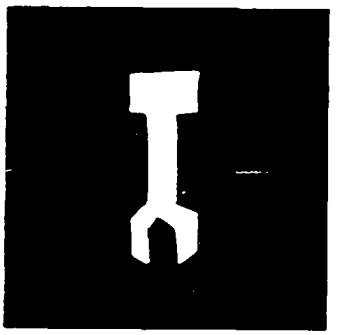

(a)

(b)

(c)

(d)

FIG

20

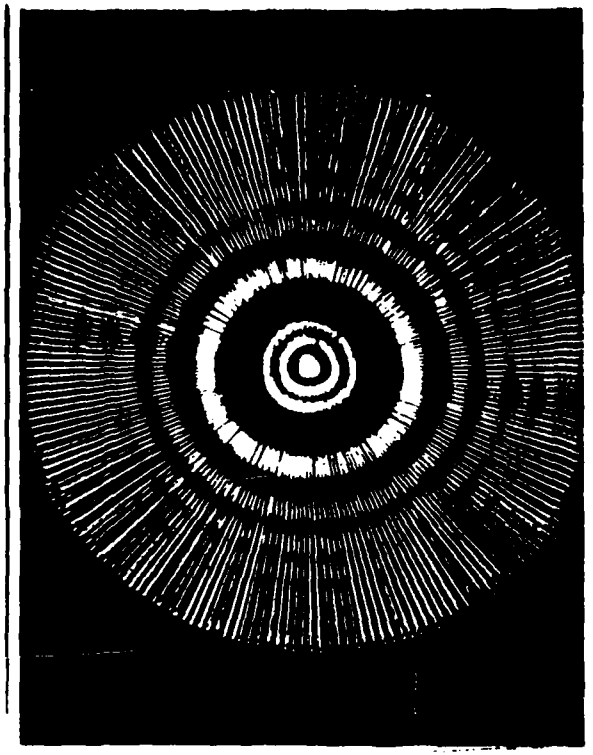

21b

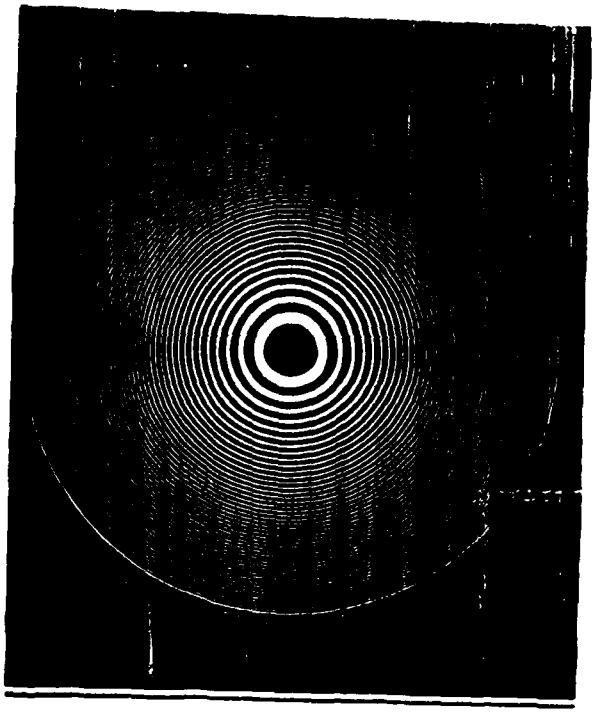

21a

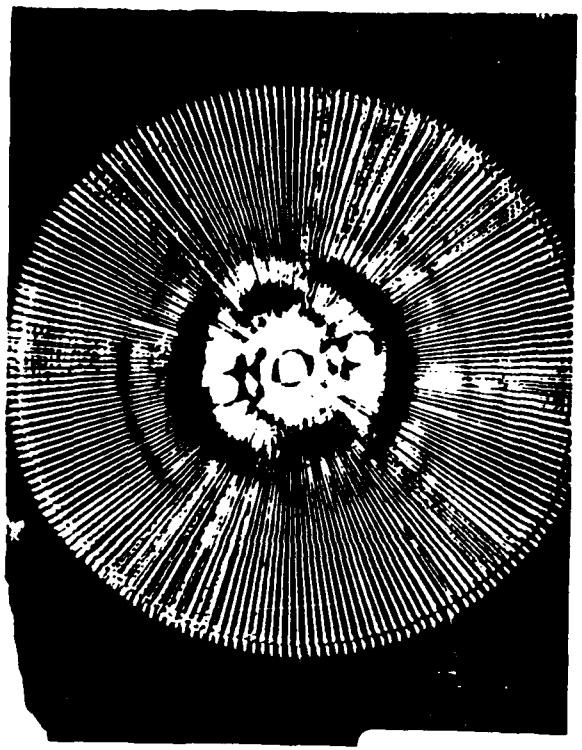

21c

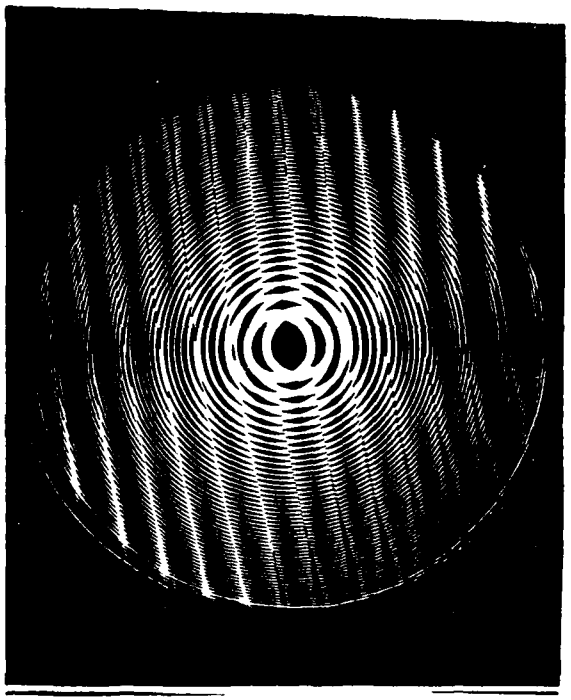

21d.

Reprinted from Applied Optics, Vol. 24, page 3817, November 15, 1985
Copyright © 1985 by the Optical Society of America and reprinted by permission of the copyright owner.

Two-dimensional complex Fourier transform via the Radon transform

Roger L. Easton, Jr., A. J. Ticknor, and H. H. Barrett

A hybrid system has been constructed to perform the complex Fourier transform of real 2-D data. The system is based on the Radon transform; i.e., operations are performed on 1-D projections of the data. The projections are derived optically from transmissive or reflective objects, and the complex Fourier transform is performed with SAW filters via the chirp transform algorithm. The real and imaginary parts of the 2-D transform are produced in two bipolar output channels.

I. Introduction

The utility of the 2-D Fourier transform as a tool for signal processing is well known. Its computation is usually performed digitally or by coherent optics. Other techniques have been demonstrated to compute the 2-D transform using incoherent illumination.[1-9] Each of these methods has inherent advantages and disadvantages. Digital computation on a general purpose computer is precise but slow, even with the FFT algorithm. In addition, it can suffer from aliasing problems if the data are inadequately sampled. The use of special purpose hardware, such as array processors, can speed the process considerably, but digital techniques cannot as yet approach video rates (30 frames/sec) with large arrays. Optical methods to compute the Fourier transform have been developed, but each has disadvantages limiting its utility. We have constructed a system capable of performing complex Fourier transforms of 2-D input data at video rates. The system is based on the Radon transform and the chirp Fourier transform. An optical scanner produces 1-D projections of the input data, which are Fourier transformed in 1-D by a surface acoustic wave chirp transformer. The real and imaginary parts of the transform are produced simultaneously in separate channels. A single projection is derived in 10 μsec, and the complex transform is produced <30 μsec after commencement of the scan. By the central slice theorem, these 1-D transforms are equivalent to lines through the 2-D transform. When the transforms are plotted in polar format on CRT screens, the real and imagination parts of the 2-D Fourier transform of the object are displayed. The system can be used with either transmissive or reflective input data, and the illumination may be incoherent. We have previously reported on the application of this system to computation of power spectra,[10] but results of 2-D complex transformation are given here for the first time.

II. Optical Fourier Transformation

Fourier transformation by coherent optics has been the basis of optical processing for many years and found use even before invention of the laser. Coherent optical systems can compute the squared modulus of the Fourier transform virtually instantaneously but are limited in performance by speckle noise and by the available input transducers (spatial light modulators). Using the proper optical configuration, it is easy to show that the correct amplitude and phase of the transform are produced at the output plane (limited by aberrations in the transform lens), but the necessity of square-law detection makes separation of the amplitude and phase components of the transform (or, nearly equivalently, of the real and imaginary parts) difficult.

A considerable body of work has been done on production of the Fourier transform by incoherent optics with the aim of gaining significant advantages over coherent optics in output noise and flexibility of inputs while retaining the speed advantage over digital computation. Katyl[1] used a temporally incoherent source in the coherent optics format with appropriate dispersion correction. The requirement for spatial coherence remains, and derivation of the complex transform is difficult. Other systems use geometric shadowcasting to image the input on a reference mask of known spatial frequency and phase. The integrated

The authors are with University of Arizona, Optical Sciences Center, Tucson, Arizona 83721.

Received 12 July 1985.
0003-6935/85/223817-08$02.00/0.
© 1985 Optical Society of America.

light at one position in the output plane is proportional to the Fourier coefficient at one spatial frequency. The technique of Mertz,[2] later refined by Richardson,[3] produced the reference masks via the moire pattern created by two Fresnel zone plates. By sequential replacement of the second zone plate with one with spatial frequencies in quadrature, Richardson was able to compute the cosine and sine transforms separately giving the real and imaginary parts of the Fourier transform. This implementation can be analyzed as the chirp algorithm for Fourier transformation, which decomposes the correlation with the Fourier kernel into multiplication and convolution with quadratic phase factors as described later in this paper. Leifer *et al.*[4] used a stored reference mask with a limited range of spatial frequency and orientation in a shadow-casting correlator for alphabetic character recognition. In all these systems, the shift required for correlation of the input with the reference spatial frequency mask is accomplished by optical parallax, and no physical movement is required. The maximum spatial frequency response of these systems is limited by vignetting of the reference masks and by diffraction (since geometric optics is assumed). The vignetting problem may be solved by using a moving correlator at the expense of slower calculation and increased complexity. Even here, the scanning need not be physical motion if an imaging detector is used.[5] However, the geometric optics assumption severely limits the spatial frequency response of these incoherent correlation systems to arrays of 100 × 100 pixels or so. In addition, the spurious terms present in the output plane decrease contrast and reduce output dynamic range.

Other authors have investigated different avenues to Fourier transform computation. Recent work by Tai and Aleksoff[6] has demonstrated production of complex transforms of incoherently illuminated data by selection of the proper output term from a grating interferometer. This approach is limited to 1-D data, however. Xu *et al.*[7] have produced the complex transform of incoherently illuminated 2-D data occupying one-half of the input plane. A symmetric object is synthesized by reflection through the origin and processed through two illumination channels polarized orthogonally. The system performs well, but the restriction on input format limits its utility. George and Wang[8] also have performed Fourier cosine transformation of transmissive or reflective objects in incoherent light by synthesis of a symmetric object followed by an achromatic optical Fourier transform. A double image of the input is produced interferometrically, and the output of the optical system is the cosine transform on a bias. Adjustment of the interferometer allows separate generation of the sine transform. The output signal is detected with a photodiode array for later digital manipulation. The bias could be subtracted electronically or interferometrically. They report system response to 20 cycles/mm, and their results agree very well with calculations. This system has the potential disadvantage of nonsimultaneous generation of the cosine and sine transforms.

Glaser *et al.*[9] have implemented the chirp transform algorithm optically to produce the complex transform. A holographic filter is used to perform the convolution with the quadratic phase factor, thus requiring a temporally quasi-coherent source. Spatial coherence is not required. The optical output is a spatial carrier modulated by the complex transform, from which the real and imaginary parts may, in principle, be derived by digital demodulation at the cost of temporal processing capacity.

III. Radon-Fourier Transformer

All the 2-D Fourier transforming systems discussed above are restricted in utility by limitations on speed, format of input and/or output, space–bandwidth product, or dynamic range. Many of these systems have proven useful in some applications, but none truly fills the need for rapid calculation of the complex 2-D Fourier transform with large space–bandwidth product. Using a different principle, we have constructed a system which can potentially compute complex Fourier transforms of large arrays at video rates. The complex transform is generated as cosine and sine transforms, i.e., the real and imaginary parts of the transform. The two outputs are obtained simultaneously. Operation is based on the Radon transform,[11] which decomposes a function of M-dimensions into the complete set of 1-D projections by integration over $M - 1$ dimensions. For the 2-D case, projections are obtained by integration over sets of parallel lines. The primary theorem of the Radon transform states that a function can be reconstructed from the complete set of its projections and serves as the operating principle of medical computed tomography. The Radon transform has also been shown to be useful in general signal processing, including pattern recognition,[12,13] image filtering,[14,15] bandwidth compression,[16,17] computation of the Wigner distribution function,[18] and Fourier spectrum analysis.[10,19,20]

The utility of the Radon transform for signal processing is due to the central-slice, or projection-slice, theorem, which states that the 1-D Fourier transform of a 1-D Radon projection yields one line through the 2-D Fourier transform of the 2-D function. The 1-D transform passes through the origin of 2-D Fourier space, and its orientation is determined by the orientation of the lines of integration. Since systems exist that can rapidly compute 1-D Fourier transforms (e.g., CCD, SAW, or AO), adopting the Radon transform approach makes possible rapid computation of the 2-D Fourier transform.

The system for producing the Radon transform of the 2-D data has been discussed previously.[10,18,20] Suffice it to say that the projections of the 2-D distribution of intensity transmission (of a transparency) or reflectance (for reflective objects) are derived by projecting a line of light on the input plane and integrating the light transmitted or reflected with a detector. The output of the detector is proportional to the line integral of transmission or reflectance. Sweeping the line of light perpendicular to itself across the input data

AD-A169 612 RADON OPTICAL PROCESSING IN RADON SPACE(U) ARIZONA UNIV 2/2
TUCSON OPTICAL SCIENCES CENTER H H BARRETT 15 JUN 86
AFOSR-84-0188

UNCLASSIFIED F/G 9/3 NL

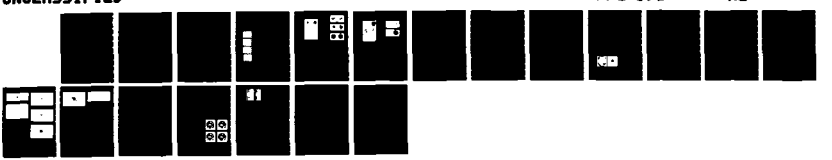

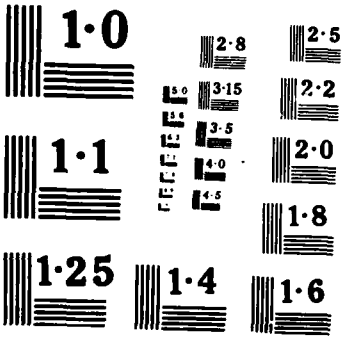
1·0
1·1
1·25
1·4
1·6
1·8
2·0
2·2
2·5
2·8
3·15
3·5
4·0
4·5

produces a temporal signal proportional to one line-integral projection. Rotation of the azimuth of sweep with a prism allows production of the complete Radon transform as a sequence of 1-D temporal signals out of the detector. For obvious reasons, this optical system is termed a flying-line scanner.

From the central-slice theorem mentioned above, the 1-D transform of a projection is one line through a polar plot of the 2-D transform. Farhat *et al.*[21] have adapted both coherent optical transformation and shadow-casting correlation to perform the 1-D Fourier transformation of Radon-transformed data. Their incoherent transformer produces full complex transforms of complex input data by using two-color channels. We have taken a different tack, disposing of optical Fourier transformation altogether, and instead implementing the chirp Fourier transform algorithm with surface acoustic wave filters. The chirp transform results from a decomposition of the Fourier kernel:

$$\exp(-2\pi i\nu t) = \left\{\exp\left[-i\pi\left(\frac{\nu}{\beta}\right)^2\right]\right\} \times \{\exp[-i\pi(\beta t)^2]\} \times \left\{\exp\left[i\pi\left(\frac{\nu}{\beta} - \beta t\right)^2\right]\right\}. \quad (1)$$

Thus the Fourier transform may be written

$$F(\nu) = \int_{-\infty}^{+\infty} f(t)\exp(-2\pi i\nu t)dt = \exp\left[-i\pi\left(\frac{\nu}{\beta}\right)^2\right] \times \int_{-\infty}^{+\infty} \{f(t)\exp[-i\pi(\beta t)^2]\} \times \exp\left[i\pi\left(\frac{\nu}{\beta} - \beta t\right)^2\right] dt$$

$$= [\exp[-i\pi(\beta t)^2] \times (\{f(t)\exp[-i\pi(\beta t)^2]\} * \exp\{i\pi(\beta t)^2\})]_{(\nu=\beta^2 t)}, \quad (2)$$

where * denotes convolution. The complex exponentials are linear FM signals, i.e., the frequency varies linearly with time, and have been named chirps by the radar community. They are also called quadratic phase factors for obvious reasons. The instantaneous frequency of the positive complex quadratic phase term $\exp[+i\pi(\beta t)^2]$ at time t_n is

$$\frac{1}{2\pi} \times \frac{d\phi}{dt}\Big|_{(t=t_n)} = +\frac{\beta^2 t_n}{2},$$

which increases with t_n. Hence, it is called an upchirp, while the negative exponential is a downshirp. Using the three chirps, Fourier transformation can be broken down into the following steps:

(1) multiplication of the signal by $\exp(-i\pi\beta^2 t^2)$, a downchirp;

(2) convolution of the product with an upchirp, $\exp(+i\pi\beta^2 t^2)$;

(3) multiplication of the filtered signal by a downchirp, $\exp(-i\pi\beta^2 t^2)$.

The parameter $\pi\beta^2$ in the chirp signal is called the chirp rate and is the same for all three chirps. The temporal output signal is a scaled version of the Fourier transform of the temporal input signal with the temporal frequency related to the output temporal coordinate via $\nu = \beta^2 t$. If only the modulus of the transform is required, the third step can be deleted. This analysis assumes that the chirps are complex and of infinite length.

One way to obtain the chirp impulse responses necessary to implement the transform is via surface acoustic wave (SAW) chirp filters.[22-24] A SAW filter consists of a piezoelectric crystalline substrate on which two aluminum interdigital transducers (IDTs) have been deposited. When a signal is applied to the input IDT, the electric field across transducer fingers of opposite polarity generates a deformation of the crystal surface via the piezoelectric effect. The deformation travels along the crystal surface as a sound wave. At the output IDT, an electronic signal is regenerated from the sound wave by the inverse piezoelectric interaction. By proper design of the separations and overlaps of the fingers in the IDTs, any of a wide variety of impulse responses can be generated. For a chirp filter, the separations of the fingers are varied to obtain an impulse response $h(t)$ whose frequency increases or decreases from some initial carrier frequency ω_0 at rate α, i.e., of the form

$$h(t) = \cos\left[\left(\omega_0 t \pm \frac{\alpha t^2}{2}\right)\right].$$

Again, the instantaneous frequency of the chirp at time t_n is

$$\nu_n = \frac{1}{2\pi} \times \frac{d}{dt}\left(\omega_0 t \pm \frac{\alpha t^2}{2}\right)\Big|_{(t=t_n)} = \frac{\omega_0 \pm \alpha t_n}{2\pi} = \nu_0 \pm \frac{\alpha t_n}{2\pi}.$$

As before, the positive term is called an unchirp. Realistically, the filter must have a finite temporal response, so the cosine function must be windowed by a function with compact support, e.g., a Rect function or a Hamming window. For chirp Fourier transformation, the premultiplication and postmultiplication chirps can be generated by applying an impulse input to SAW chirp filters of the proper sign (i.e., upchirp or downchirp). The convolution is performed by applying the signal to a similar filter. It is important to note that the SAW chirp filter impulse response is a real function of the form $A(t)\cos(\omega t \pm \alpha t^2)$, not the complex exponential seen above. The function $A(t)$ is an apodization of the chirp, necessitated by the finite output signal length, and ω is the initial angular frequency of the chirp. The chirp transform algorithm may still be implemented,[23] but the steps now become

(1) premultiplication by a downchirp

$$\text{Rect}\left(\frac{t}{\tau_-} - \frac{1}{2}\right) \times \cos\left(\omega_- t - \frac{\alpha t^2}{2}\right).$$

(2) filter this signal with impulse response

$$h(t) = \text{Rect}\left[\frac{t}{\tau_+} - \frac{1}{2}\right] \times \cos\left(\omega_+ t + \frac{\alpha t^2}{2}\right).$$

(3) postmultiply the filtered signal by two upchirps separately:

$$\text{(a) Rect}\left(\frac{t-t'}{\tau_+}-\frac{1}{2}\right)\times\cos\left(\omega_+ t+\frac{\alpha t^2}{2}\right)$$

$$\text{(b) Rect}\left(\frac{t-t'}{\tau_+}-\frac{1}{2}\right)\times\cos\left(\omega_+ t+\frac{\alpha t^2}{2}-\frac{\pi}{2}\right)$$

$$=\text{Rect}\left(\frac{t-t'}{\tau_+}-\frac{1}{2}\right)\times\sin\left(\omega_+ t+\frac{\alpha t^2}{2}\right),$$

(4) low-pass filter both outputs of step (3). The terms τ_+ and τ_- represent the temporal width of the upchirp and downchirp, respectively, and are also called the time dispersions of the chirps. Similarly, ω_+ and ω_- are the initial angular frequency of the upchirp and downchirp.

The output temporal frequency is related to the temporal position in the output signal by the relation

$$\nu=(\omega_+-\omega_-+\alpha t)/2\pi. \tag{3}$$

Since the carrier frequencies in SAW filters are in the rf regime ($\omega \simeq$ 15–300 MHz), multiplications can be performed in rf mixers. The discrepancy in the sign of the two postmultiplication SAW chirps relative to that in the complex chirp algorithm given above results from rf double-sideband mixer multiplication. Such mixers yield product terms as modulations on carriers at the sum and difference frequencies of the original carriers. That is, given two signals $A(t)$ and $B(t)$ modulating carriers at angular frequencies ω_a and ω_b, respectively, the action of the rf mixer is to produce an output:

$$A(t)\cos(\omega_a t)\times B(t)\cos(\omega_b t)=\frac{[A(t)B(t)]}{2}$$

$$\times\{\cos[(\omega_a+\omega_b)t]+\cos[(\omega_a-\omega_b)t]\}. \tag{4}$$

The low-pass filter selects the difference frequency term, and so the sign of the postmultiplication chirp must be the same as that of the convolution filter to obtain demodulation. The signal postmultiplied by the cosine upchirp is the real part of the transform, while that multiplied by the sine upchirp is the imaginary part of the transform.

For maximum time–bandwidth product in the output signal, the requirements on the chirps are that the time dispersions of the premultiplication and the convolution chirp be related by $\tau_- = \tau_+/2$, and that the bandwidth of the convolution chirp be twice that of the multiplication chirps.[23] The two outputs are proportional, respectively, to the real and imaginary parts of the Fourier transform within a time window ($\tau_+/2 \le t \le \tau_+$). The corresponding spectral window spans temporal frequencies

$$\left(|\nu| \le \frac{\alpha\tau_+}{8\pi}\right).$$

The rectangular finite-length window of the convolution filter has the effect of convolving the spectral components with a sinc function, which limits the number of resolvable frequencies in the spectrum to

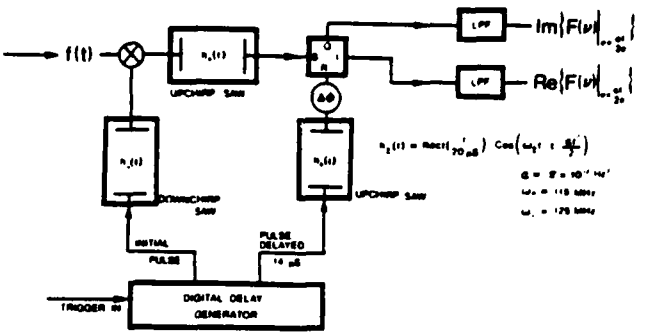

Fig. 1. Schematic of the 1-D SAW complex Fourier transformer. The temporal signal $f(t)$ from the photomultiplier in the flying-line scanner is proportional to one projection. The impulse response of the SAW filters is $h_\pm(t)$. The microcomputer controller sends a trigger signal to the digital delay generator, which in turn produces a 1-nsec pulse that is applied to the downchirp SAW filter. The resulting impulse-response signal $h_-(t)$ is multiplied by the incoming projection signal in a rf mixer. The product signal is applied to the upchirp SAW filter, and the output goes to the signal-input port of the rf phase comparator. After a delay of 14 μsec (1-nsec resolution), the digital delay generator outputs a second 1-nsec pulse, which is applied to the postmultiplication SAW filter. An rf phase shifter at the SAW filter output allows fine adjustment of the postmultiplication timing. This signal is applied to the reference port of the phase comparator. After low pass filtering, the in-phase I output of the phase comparator is proportional to the real part of the Fourier transform $F(\nu)$ (i.e., cosine transform) of the input signal $f(t)$. Similarly, the output of the quadrature port Q of the phase comparator is proportional to the imginary part of $F(\nu)$, (i.e., sine transform).

one-fourth of the time–bandwidth product of the convolution filter.[23] SAW chirp filters with other window functions (e.g., Hamming) are available if smaller sidelobes are desired in the output signal. If only the squared-modulus of the Fourier transform is required, square-law envelope detection can be substituted for steps (3) and (4). This is the algorithm we have used previously to perform 2-D spectrum analysis in Radon space.[10]

The complex transform algorithm was implemented as shown in Fig. 1 using SAW chirp filters from Andersen Laboratories (models DS-120-10-20-251A and -252A), which have bandwidths of 10 MHz, maximum time dispersions of 20 μsec, and a resulting time–bandwidth product of 200. The chirp rate $\alpha = 2\pi \times 10$ MHz/20 μsec $= \pi \times 10^{12}$ Hz^2. The filter windows were unweighted. A flying-line scan, producing one Radon projection, is made in 10 μsec and is synchronized with the signal driving the premultiplication impulse generator so that the center of the scan is mixed with the center of the premultiplication downchirp. This time-gates the premultiplication signal for a maximum system time–bandwidth product. After filtering in the upchirp SAW, the signal is coherently demodulated by the postmultiplication upchirp. To obtain 40 dB of rejection of the signal from one channel of the transform from the other channel, the time of the premultiplication chirp impulse must be synchronized to the postmultiplication impulse to an accuracy of

better than 100 psec.[23] The timing interval between impulse inputs to the premultiplication and postmultiplication chirps is the value t' in step (3). A digital delay generator is used to provide the impulse to the postmultiplication chirp filter with temporal resolution of 1 nsec. More precise timing is provided by shifting the phase of the postmultiplication chirp with a continuously adjustable rf hybrid phase shifter. The demodulation is accomplished in an rf phase comparator, a four-port device which produces in-phase and quadrature mixed signals from an input signal and reference. It may be thought of as a combination of a signal splitter, a quadrature hybrid, and two double-sideband mixers. The filtered signal is split and mixed with in-phase and quadrature components of the postmultiplication chirp. After low-pass filtering in each channel, the in-phase signal is the bipolar cosine transform, and the quadrature signal is the bipolar sine transform (each within the frequency window and convolved with the sinc function due to the finite convolution window as described above).

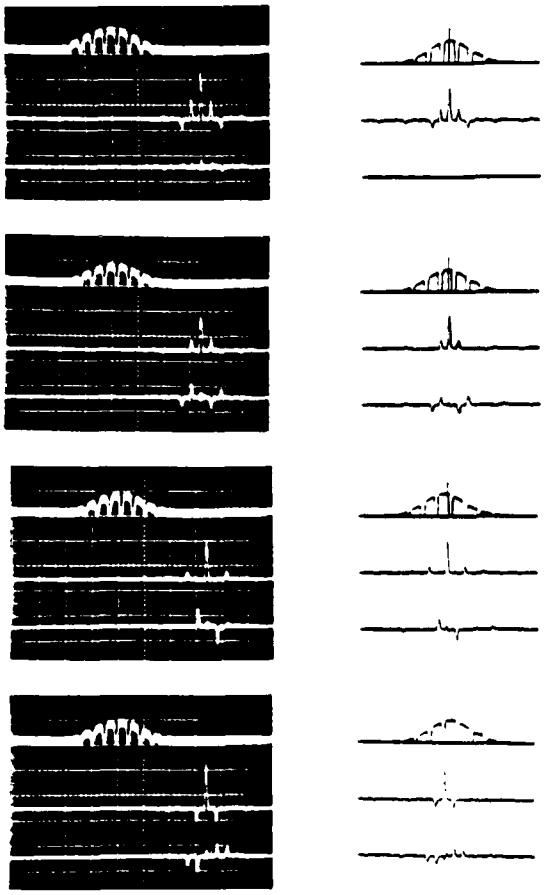

Fig. 2. Performance of the SAW chirp complex Fourier transformer. In each of the four cases shown, the top trace is the signal from the flying-line scanner, i.e., a single projection of the 2-D input. The second and third traces are the cosine transform and sine transform, respectively, produced by the SAW chirp transformer. The traces on the right-hand side are a computer simulation of the same signal. The object was a grating of 25% duty cycle in a circular aperture. In the first case, the grating was centered in the aperture creating a symmetric signal whose Fourier transform is purely real. In the other three cases, the grating was translated relative to the circular aperture giving an asymmetric signal with a complex transform. Each horizontal division in the oscilloscope traces represents 5 μsec, indicating that the complete transform is computed within 30 μsec.

Using the SAW filters described, the chirp transformer resolves fifty temporal frequencies in the window ($|\nu| \leq 2.5$ MHz). When the output of the flying-line scanner is applied to the SAW chirp Fourier transformer, the spatial frequency scaling depends on the scanning speed. Typically, we scan a 25-mm aperture in 10 μsec, giving a spatial frequency range of ±1 cycle/mm with fifty resolvable points. By scanning a 10-mm aperture in the same time, the spatial frequency response is ±2.5 cycles/mm. This by no means is the limit of a SAW chirp filter or optical scanner technology. Using reflective-array SAW chirp filters (RACs), transformers capable of resolving 3600 points within a 60-μsec output window have been reported.[25] Were we to use this chirp transformer and scan a 30-mm diam aperture in 30 μsec, we would obtain 900 resolvable points in a spatial frequency range of ±15 cycles/mm.

The performance of the complex Fourier transformer for a 1-D signal is demonstrated in Fig. 2, where the output is compared to a computer simulation. A grating (75% clear, 25% opaque) was placed in a circular aperture of 20-mm diameter in the flying-line scanner. The azimuth of scan was oriented so that the line of integration was parallel to the grating lines. The grating was mounted on a translation stage so that it could be shifted within the circular aperture. Four cases are shown for both the actual and computed outputs. In each example, the top trace is the output of the flying-line scanner, i.e., the Radon transform of the object for one azimuth. The second and third traces are the cosine and sine transform outputs of the complex Fourier transformer, i.e., one line through the 2-D real part and imaginary part, respectively, of the Fourier transform of the original object, via the central-slice theorem. The scanning time is 10 μsec, and the two transforms have been output within 30 μsec after the beginning of the flying-line scan. In the first case, the grating is centered in the aperture resulting in a symmetric input to the Fourier transformer. The Fourier transform of a symmetric object is purely real, and hence the sine transform vanishes, as shown. Also note that the cosine transform is bipolar and symmetric. In the succeeding three cases, the grating is translated in the aperture, resulting in an asymmetric input to the complex transformer and a nonvanishing bipolar and antisymmetric sine transform. The actual transformer output agrees very well with the computer simulations.

To produce the complex 2-D Fourier transform, the central slice theorem says that it is merely necessary to display the 1-D transforms of the projections in the proper polar format. However, for discrete uniform sampling along both the azimuthal and radial axes, the Fourier space will be densely sampled near the origin

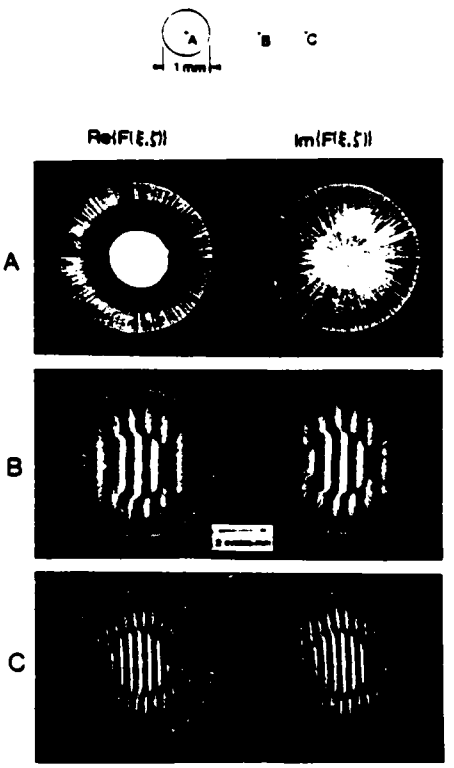

Fig. 3. Two-dimensional complex Fourier transforms of a circular aperture. The object was a single circular aperture of 1.0-mm diameter, as shown at top. The letters denote the origin of coordinates (i.e., the optical axis) for each case. The display was biased up, so that zero amplitude is the brightness level shown in the imaginary part of (A). The brightest areas represent the most positive amplitude of the transform, and the darkest areas represent the most negative amplitude. (A) With the aperture centered at the origin, the transform is purely real. (B), (C) The aperture was translated from the optic axis by ~1.4 and 2.4 diameters, respectively, producing fringes due to the constant phase term.

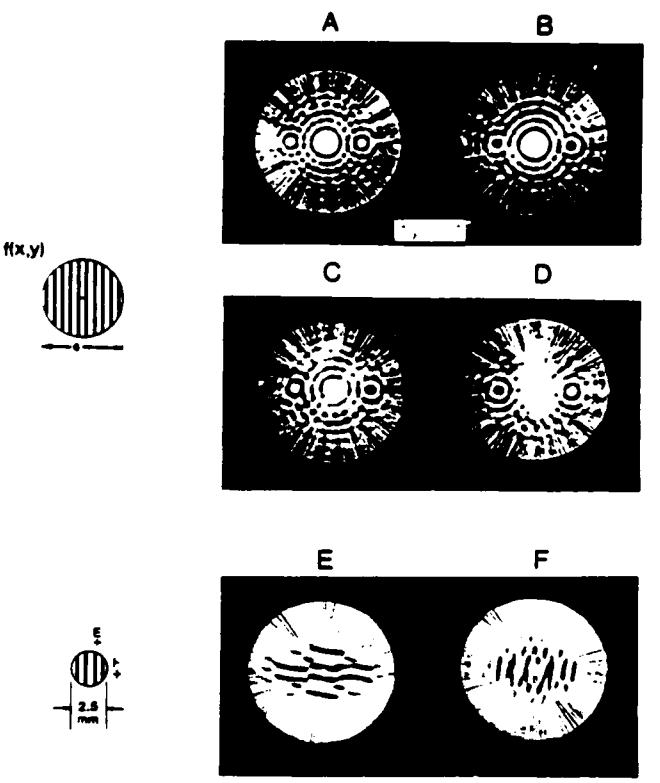

Fig. 4. Two-dimensional complex Fourier transforms of a grating in a circular aperture. The spatial frequency of the grating was 1.5 cycles/mm, with a duty cycle of 80% and the aperture diameter was 6 mm. (A) Cosine transform with the object centered on the optical axis as shown. The transform is even, and the Airy patterns of the circular aperture at the ±1 orders of the grating are clearly seen. (B) Cosine transform after translating the object by one-half of a grating cycle. The linear phase term resulting from the translation has inverted the phase of the Airy patterns. (C), (D) Sine transform of the object after translation by ±one-fourth of a grating cycle, respectively, relative to (A). The transforms are odd, and the Airy patterns at the ±1 orders are out of phase. (E), (F) The aperture diameter was reduced to 2.5 mm, and the center was translated relative the optic axis by a sufficient distance (2 mm) so that several cycles of the linear phase are visible within the central disk of the Airy pattern. (E) is the real part of the transform and is even. (F) is the imaginary part and is odd. Note that the translation was in different directions in the two cases, so that the fringe direction differs.

and sparsely sampled at the high spatial frequencies. The function so obtained is equivalent to $[F(\rho)]/|\rho|$, where ρ is the 2-D frequency vector and $F(\rho)$ is the 2-D Fourier transform of the 2-D input function $f(\mathbf{r}) = f(x,y)$. The radial spatial frequency vector ρ is always non-negative, but we can also consider a radial frequency vector v, which is bipolar. To counter the $1/|\rho|$ weighting, it is necessary to multiply the Fourier transformer output by $|v|$ before display. This V-shaped function is produced electronically by passing a ramp function through an absolute-value amplifier. Since the SNR of the Fourier transformer generally decreases with increasing frequency, the V function is rolled off by current-limiting the output of the V generator. For a signal on an rf carrier, (i.e., the generated magnitude of the Fourier transform that is output by the convolution chirp filter), the multiplication by $|v|$ is easily done in a rf mixer.[10] Multiplication of the coherently demodulated signal is somewhat more difficult in the frequency range of interest (up to 2.5 MHz), which is higher than most analog multiplier modules can handle and not high enough for rf mixers. In their stead, we employed the Motorola balanced modulator–demodulator integrated circuit (MC1496) to multiply the transformer output by $|v|$. The bipolar signal can then be applied to the z axis of a CRT in one of two ways: the signal can be thresholded at ground to display the complex transformation in four parts (positive and negative real and positive and negative imaginary), or the bipolar signal can be biased up to display the complete real or imaginary transform at one time. Since the 1-D cosine and sine transform signals are available simultaneously, they can be displayed simultaneously on separate CRTs.

To display the transform in the polar format, we have used the same system reported previously.[10] The

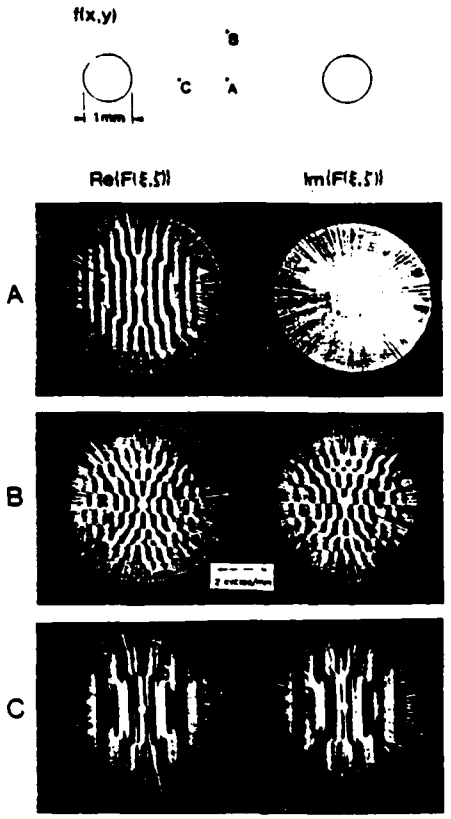

Fig. 5. Two-dimensional complex Fourier transforms of two circular apertures. The diameter of the apertures was 1 mm with their centers separated by 5 mm, as shown at top. Again the letters denote the position of the optical axis in each case. (A) Cosine transform with the optic axis centered on the object's axis of symmetry. Note the phase change as a fringe passes from the central lobe of the Airy disk to the first ring. The faint fringes in the imaginary part of the transform are due to wobble in the image rotating prism. (B) The optic axis was located 1 mm above the symmetry axis producing fringes perpendicular to those from the double aperture. The cosine transform is even, and the sine transform is odd. (C) The optic axis was located on the symmetry axis but displaced from the center of symmetry by 1 mm multiplying the fringes by a linear phase term of lower frequency.

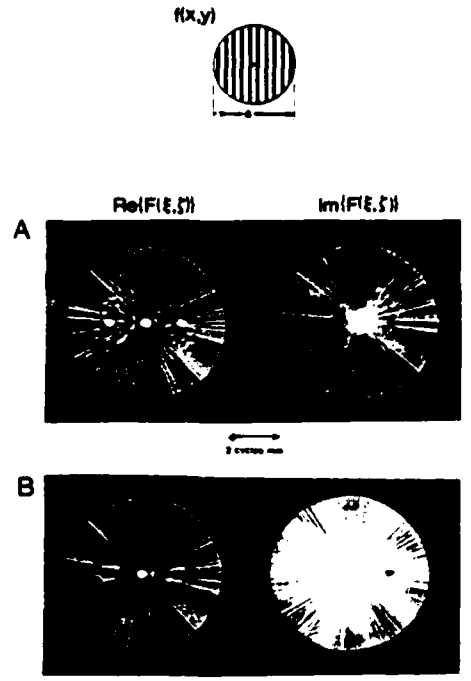

Fig. 6. Two-dimensional complex transforms of a reflective object. A beam splitter was introduced into the flying-line scanner to direct the reflected line onto the detector. Fourier transformation and display were performed as before. The object was a grating in a circular aperture of 6-mm diameter, as in Fig. 4. The main features of the transform are easily seen, i.e., the location and phase of the Airy patterns on the first orders of the grating spectrum. The signal-to-noise is less than in the transmissive case due to the lower reflectance and lower modulation in reflectance. The real and imaginary parts of the Fourier transform of the object centered on the optical axis are shown in (A). Since the object is symmetric in this case, the imaginary part of the transform vanishes. (B) The object was translated by one-half of a grating cycle.

scan azimuth is rotated by an image-rotation prism via a stepper motor resolving 200 steps. The maximum angular resolution in the transform is $\pi/100$ rad. A bipolar ramp function is generated and weighted in two channels by the sine and cosine value of the azimuth angle of the scan. The resulting outputs are applied to the x and y deflections of the CRT scanning spot, which produces a line scan across the screen at the appropriate angle. After completion of the scan, values of the sine and cosine of the new angle are read out of a lookup table for the next scan. The scanning spot is timed to reach the center of the screen when the zero-frequency output of the Fourier transformer is applied to the z axis of the CRT. The complete 2-D transform can now be generated in ~0.1-sec, limited by the rotation rate of the stepper motor. To allow transformation at video rates, the azimuth of the Radon transform would have to be rotated at 30 Hz, corresponding to an easily obtainable prism rotation rate of 7.5 Hz = 450 rpm. Indeed much higher rates have been reported with excellent image quality.[26]

Complex transforms obtained with this system at a rate of 2.5 frames/sec are presented in Figs. 3–6. In each case, the positive part of the Fourier transform is presented; i.e., areas of the transform with amplitude greater than zero are bright, while those areas with amplitude less than zero are dark. Note the difference in the usual presentation of the squared magnitude of the Fourier transform, where areas with amplitude both greater than or less than zero are bright, and the zero-crossings are dark. In Fig. 3, the object was a circular aperture 1.5 mm in diameter. In the first case, the aperture was centered in the flying-line scanner resulting in a symmetric object. The Fourier transform is purely real, and the cosine transform is the well-known Airy pattern. If the aperture is translated in the scanner so that the object is no longer symmetric, a linear phase term in the transform appears as fringes in the output: the greater the shift, the larger the frequency of the linear phase. In Fig. 4, the object

was a circular aperture over a transparent grating whose Fourier transform is the Airy pattern of the circular aperture on the ±1 orders of the grating. Each transform was obtained for a different shift of the grating in the aperture resulting in different phasing of the Airy patterns. In Fig. 5, the object was a pair of circular apertures, each 1 mm in diameter with the centers separated by 5 mm. The first case is the cosine transform of the centered pair. Note the phase shift in the fringes on different rings of the Airy pattern. The other cases are cosine and sine transforms of the pair with the optical axis positioned 1 mm above the center line through the apertures and with the axis located 1 mm along the center line.

Figure 6 demonstrates the capability of this system to compute the complex Fourier transform in reflection. A beam splitter was inserted into the system ahead of the object to direct the reflection of the flying line onto the photomultiplier. The object was identical to that in Fig. 4. Since the overall reflectance is less than the transmittance, and since the modulation in reflectance is less as well, the SNR of the reflective transforms is lower than that in the transmissive case. However, the capability of performing complex reflective transforms with this system is clearly demonstrated.

IV. Conclusions

We have demonstrated a hybrid system to produce the complex 2-D Fourier transform in nearly real time. The transform is presented as real and imaginary parts (i.e., cosine and sine transforms) in separate output channels. Transmissive or reflective functions can be transformed in this manner.

The authors would like to thank Stanley R. Deans, H. Harold Szu, and Adolf W. Lohmann who provided helpful comments.

This work was supported by the Air Force Office of Scientific Research under grant 84-0188.

References

1. R. H. Katyl, "Compensating Optical systems. 3: Achromatic Fourier Transformation," Appl. Opt. **11**, 1255 (1972).
2. L. Mertz, *Transformation in Optics* (Wiley, New York, 1965).
3. J. M. Richardson, U.S. Patent 3,669,528, "Device for Producing Identifiable Sine and Cosine (Fourier) Transforms of Input Signals by means of Noncoherent Optics" (June 1972).
4. I. Leifer, G. L. Rogers, and N. W. F. Stephens, "Incoherent Fourier Transformation: a New Approach to Character Recognition," Opt. Acta **16**, 535 (1969).
5. M. A. Monahan, K. Bromley, and R. P. Bocker, "Incoherent Optical Correlators," Proc. IEEE **65**, 121 (1977).
6. A. M. Tai and C. C. Aleksoff, "Grating-Based Interferometric Processor for Real-Time Optical Fourier Transformation," Appl. Opt. **23**, 2282 (1984).
7. K. Xu, R. Ji, and Z. Zhang, "A New Method for Measuring the Phase of the Fourier Spectrum," Opt. Commun. **50**, 85 (1984).
8. N. George and S. Wang, "Cosinusoidal Transforms in White Light," Appl. Opt. **23**, 787 (1984).
9. I. Glaser, Y. Katzir, and V. Toschi, "Incoherent Optical Two-Dimensional Fourier Transform Using the Chirp-z Algorithm," Opt. Lett. **9**, 199 (1984).
10. A. J. Ticknor, R. L. Easton, Jr., and H. H. Barrett., "A Two-Dimensional Radon-Fourier Transformer," Opt. Eng. **24**, 082 (1985).
11. S. R. Deans, *The Radon Transform and Some of its Applications* (J Wiley, New York, 1983).
12. G. Eichmann and B. Z. Dong, "Coherent Optical Production of the Hough Transform," Appl. Opt. **22**, 830 (1983).
13. G. R. Gindi and A. F. Gmitro, "Optical Feature Extraction via the Radon Transform," Opt. Eng. **23**, 499 (1984).
14. A. G. Gmitro, G. R. Gindi, H. H. Barrett, and R. L. Easton, Jr., "Two-Dimensional Image Processing by One-Dimensional Filtering of Projection Data," Proc. Soc. Photo-Opt. Instrum. Eng. **388**, 132 (1983).
15. H. H. Barrett, "Three-Dimensional Image Reconstruction from Planar Projections with Application to Optical Data Processing," Proc. Soc. Photo-Opt. Instrum. Eng. **373**, 179 (1983).
16. W. E. Smith and H. H. Barrett, "Radon Transform and Bandwidth Compression," Opt. Lett. **8**, 395 (1983).
17. D. Fraser, B. R. Hunt, and J. C. Su, "Principles of Tomography in Image Data Compression," Opt. Eng. **24**, 298 (1985).
18. R. L. Easton, Jr., A. J. Ticknor, and H. H. Barrett, "Application of the Radon Transform to Optical Production of the Wigner Distribution Function," Opt. Eng. **23**, 738 (1984).
19. H. H. Barrett, "Optical Processing in Radon Space," Opt. Lett. **7**, 248 (1982).
20. R. L. Easton, Jr. H. H. Barrett, and A. J. Ticknor, "Using SAW Filters to Process Two-Dimensional Data via the Radon Transform," Proc. IEEE Ultrason. Symp. 185 (1983).
21. N. H. Farhat, C. Y. Ho, and L. Szu Chang, "Projection Theorems and Their Application in Multidimensional Signal Processing," Proc. Soc. Photo-Opt. Instrum. Eng. **388**, 140 (1983).
22. H. J. Whitehouse, "Role of Charge-Coupled Devices and Surface Acoustic Wave Devices in Optical Signal Processing," Proc. Soc. Photo-Opt. Instrum. Eng. **118**, 124 (1977).
23. M. A. Jack and E. G. S. Paige, "Fourier Transformation Processors Based on Surface Acoustic Wave Chirp Filters," Wave Electron. **3**, 229 (1978).
24. M. A. Jack, P. M. Grant, and J. H. Collins, "The Theory, Design, and Applications of Surface Acoustic Wave Fourier-Transform Processors," IEEE Proc. **68**, 450 (1980).
25. H. M. Gerard, P. S. Yao, and O. W. Otto, "Performance of a Programmable Radar Pulse Compression Filter Based on a Chirp Transformation with RAC Filters," Proc. IEEE Ultrason. Symp. 947, (1977).
26. K. A. Stetson and J. N. Elkins, "Optical System for Dynamic Analysis of Rotating Structures," Tech. Rep. AFAPL-TR-77-51 (United Technologies Research Center, East Hartford, Conn., 1977).

USING SAW FILTERS TO PROCESS TWO-DIMENSIONAL DATA BY MEANS OF THE RADON TRANSFORM

Roger L. Easton, Jr., Harrison H. Barrett, and Anthony J. Ticknor

Optical Sciences Center
University of Arizona
Tucson, Arizona 85721

Abstract

It is well known that many mathematical operations on data sets of dimension two or higher may be performed by reducing the data to one-dimensional projections by means of the Radon transform. This is the governing principle of medical computed tomography. In this paper, we describe a system that performs the Radon transform of two-dimensional images and uses SAW devices to perform the data processing. Two processing operations are demonstrated: Fourier transformation of the data by means of the chirp transform, and convolution of the data with a stored filter function by means of a SAW correlator. After processing, a custom SAW filter and an optical system are used to reconstruct the processed image in two dimensions. The resolution of the processor is currently limited by the SAW devices (50 points for the chirp transformer, 300 for the convolver), but better devices are available. This system is capable of performing two-dimensional Fourier transforms at video rates (30 frames/s), which is much faster than current digital systems. An extension of the system to process three-dimensional data is described.

Introduction

The Radon transform has received much attention in the scientific community since the invention of x-ray computed tomography (CT) in the 1960's. It has found application in such diverse disciplines as astronomy, nuclear magnetic resonance, and geophysics. The mathematics of the transform were derived and published by Johann Radon in 1917 (1), where he proved that a mathematical function can be reconstructed from the complete set of its line-integral projections. In the case of CT, measured x-ray transmissions are simply related to the line integral of the x-ray absorption coefficient. By taking an adequately sampled set of one-dimensional data, a two-dimensional map of the x-ray absorption coefficient can be reconstructed, usually by digital means.

We propose to use the Radon transform from a different perspective. Instead of having one-dimensional projections inherent in the data collection, we use the Radon transform to make two-dimensional data susceptible to processing by fast one-dimensional devices. Several types of one-dimensional processors exist; the SAW filter is but one. Many two-dimensional operations can be performed by means of the Radon transform, e.g., spectral analysis, convolution, and Fourier filtering. Such operations can be performed digitally, of course, but the process may be time-consuming and the processor expensive. By operating on the one-dimensional projection instead, it is possible that the processor may be significantly faster and/or cheaper than its digital counterpart. Consider Fourier filtering of a two-dimensional image, for example. Three steps are required: Fourier transformation, filter multiplication, and inverse transformation. This operation may be performed digitally, by coherent optics, or with one-dimensional SAW filters by means of the Radon transform. The invention of the fast Fourier transform (FFT) algorithm and the array processor have dramatically speeded up digital Fourier transform calculations, but the process is still slow. A typical stand-alone minicomputer, the DEC 11/34, requires approximately 10 minutes to Fourier transform a 512 x 512 8-bit array. Adding an array processor speeds this by an order of magnitude at significantly increased cost. The Cray-1, one of the fastest digital computers ever, still requires about 1 second to perform a two-dimensional Fourier transform and is very expensive. Coherent optics can perform Fourier transforms easily, cheaply, and at the speed of light, but the output is noisy, and there are still no fully satisfactory spatial light modulators to allow analysis of rapidly time-varying inputs. We propose to perform two-dimensional Fourier transforms by operating on one-dimensional projections with SAW chirp filters. The resulting processor should be inexpensive relative to the digital system, but more importantly, it should be fast: we envision operation at video rates.

Theory

Mathematical analysis of the Radon transform is straightforward and has been treated in several references (2,3). We shall touch briefly on the main points relevant to the application at hand, i.e., two-dimensional Fourier analysis and filtering.

A one-dimensional projection $\lambda(\phi,p)$ of a two-dimensional function $f(r)$ taken along azimuth direction ϕ (relative to the x axis) is defined as

$$\lambda(\phi,p) = \int_{l=-\infty}^{\infty} d^2r\, f(r)\delta(p - r\cdot\hat{n}). \qquad (1)$$

The one-dimensional delta function reduces the area integral to a line integral along a line at an angle ϕ to the x axis and at a distance p from the origin (Figure 1). The set $[\lambda(\phi,p)]$ for all azimuth angles ϕ is the Radon transform of $f(r)$.

By taking the one-dimensional Fourier transform of a line-integral projection, an important result is obtained:

$$F_1[\lambda(\phi,p)] \equiv \Lambda(\phi,\nu)$$

$$= \int_{-\infty}^{\infty} dp \exp(-2\pi i\nu p) \int\int_{-\infty}^{\infty} d^2r\, f(r)\delta(p - p\cdot\hat{n})$$

$$= \int\int_{-\infty}^{\infty} d^2r\, f(r) \exp(-2\pi i\hat{n}\nu\cdot r) = F(p)\Big|_{p=\hat{n}\nu}^{-\infty},$$

where capital letters denote Fourier transforms of the corresponding lower-case functions. This is the central-slice theorem. In words, the one-dimensional Fourier transform of a projection $\lambda_\phi(p)$ yields one line through the origin of the two-dimensional Fourier transform of the original function $f(r)$ (Figure 1).

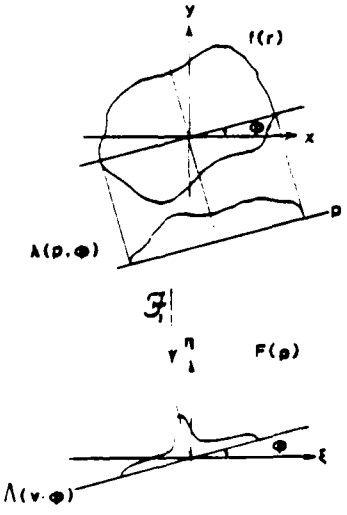

Figure 1 - Geometry of the Radon transform. (a) Derivation of one projection $\lambda(\phi,p)$ by line integrals along azimuth angle ϕ. (b) Central slice theorem: the one-dimensional Fourier transform of a line-integral projection yields one line through the two-dimensional Fourier transform of the original two-dimensional function.

By similar, though more involved reasoning, it can be shown that the original function $f(r)$ may be reconstructed from the projection data by means of the inverse Radon transform

$$f(r) = \int_0^{\pi} d\phi \int_{-\infty}^{\infty} [|N|\Lambda(\phi,\nu)] \exp(2\pi i\nu r\cdot\hat{n}) \quad (3)$$

Again in words, the original function $f(r)$ may be reconstructed from the projections $[\lambda(\phi,p)]$ by: (1) taking the one-dimensional Fourier transform of $\lambda(\phi,p)$; (2) multiplying by the one-dimensional filter $|\nu|$ (ν-filtering); (3) taking the inverse one-dimensional Fourier transform; (4) smearing the function back over the original projection direction (this creates a two-dimensional function from the one-dimensional function and is called back projection); and (5) integrating over ϕ (summation).

If we multiply the one-dimensional Fourier transform data $\Lambda(\phi,\nu)$ by another filter function as well, the reconstructed function is a Fourier-filtered version of $f(r)$.

Other expressions (and hence other procedures for taking the inverse Radon transform exist and are given in Reference 3.

In addition, it can be shown that by convolving line-integral projections from two two-dimensional images, and reconstructing by the procedure of Eq. (3), the resulting two-dimensional image is the convolution of the two input images.

Experiment

We constructed a system using the Radon transform to perform two-dimensional spectral analysis using SAW chirp filters. The apparatus is diagrammed in Figure 3. The Radon transform of the input transparency is derived by scanning it with a line of HeNe laser light. The light transmitted through the transparency is collected on a photomultiplier tube (PMT). At one instant of time, the output of the PMT is proportional to the line integral of the intensity transmission of the transparency along the line of light. By scanning the line perpendicular to itself, the time signal from the PMT is proportional to the line-integral projection along one azimuth. Rotating the direction of scan allows derivation of the complete set of line-integral projections--the Radon transform. For obvious reasons, this device is called a flying-line scanner (FLS).

Recalling the central-slice theorem, we know that the one-dimensional Fourier transform of one projection yields one line through the two-dimensional transform of the original function. By using SAW filters in the chirp Fourier transform algorithm (4,5,6), the Fourier transform of each projection is taken as the projection data are derived. We used SAW dispersive filters for the chirps (Andersen Labs models DS-120-10-20-251A and -252A). The time dispersion of each is 20 μs and the bandwidth is 10 MHz. The time-bandwidth product (TBW) of the entire system is only 50, but filters exist that could boost this to 2000 or more.

In this demonstration, only the modulus of the Fourier transform is computed, but we plan to utilize a third chirp filter to perform the post-multiplication and derive the phase information.

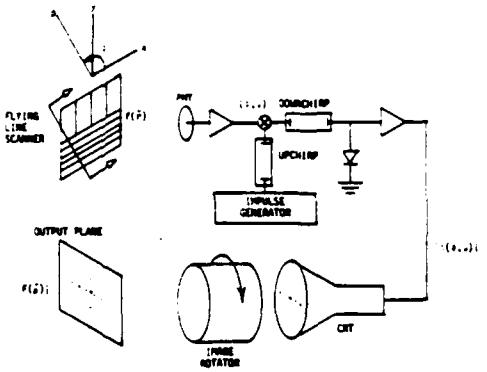

Figure 2 - Diagram of a two-dimensional spectrum analyzer using SAW devices. The projections $[\lambda(\theta,p)]$ are derived by the flying-line scanner. The one-dimensional Fourier transforms of the projections are produced by the SAW chirp filters. The Fourier transform signal modulates the CRT trace. The proper azimuth for display is selected by the image rotator.

To complete the two-dimensional spectral analysis, it is necessary to display the transforms of the projections at the proper orientations. After detection and amplification, the transform of the projection is applied to the z axis of a CRT whose trace is imaged on a photographic film. As the azimuth of scan of the FLS is rotated, the image of the CRT trace is rotated at the same rate, building up the two-dimensional Fourier spectrum modulus on the film. A result from this experiment is shown in Figure 3. The input transparency consisted of three gratings oriented at various angles: two fine crossed gratings overlaid with a section of coarse grating. In the Fourier transform built up from the projection data, the fundamental frequency of the fine gratings and several orders of the coarse grating are visible. This spectrum was built up slowly, but by rapid rotation of the scan direction, we expect to perform two-dimensional spectral analysis at video rates (30 frames/s) or faster.

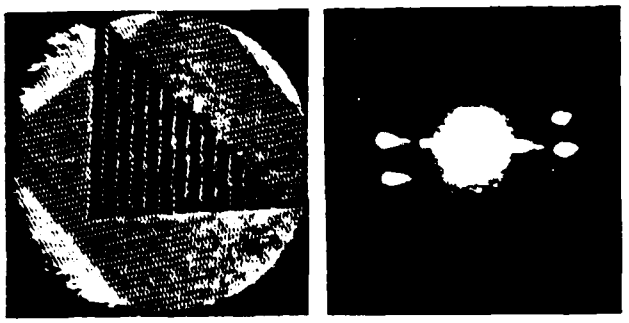

Figure 3 - Results of two-dimensional spectral analysis using SAW devices.
(a) Input transparency consisting of three gratings.
(b) Two-dimensional spectrum, showing the fundamental order of the fine gratings and several orders of the coarser grating.

Extending this system to allow complete Fourier filtering is straightforward and is diagrammed in Figure 4. The Fourier transforms of the projection data are multiplied by a filter function, which can be clocked out of ROM or produced by a function generator. The filtered transforms are then applied to an inverse Radon transformer using the procedure of Eq. (3). The $|\nu|$-filter multiplication is to be done using a custom SAW filter that is presently being constructed in the University of Arizona Microelectronics Laboratory. The inverse one-dimensional Fourier transformation will be done by means of the chirp-transform algorithm and the output applied to the z axis of a CRT. To perform the back-projection (smearing), a cylindrical lens is used to collimate the image in one dimension. The integration over azimuth angle is carried out as before by rotating the image on the recording film.

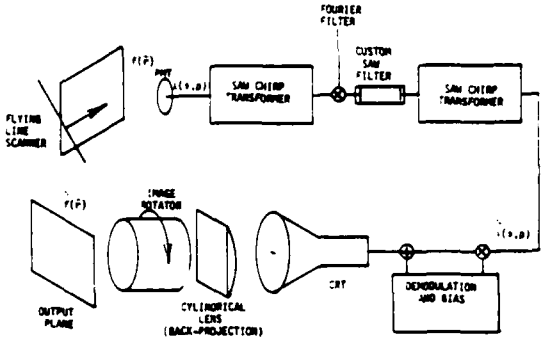

Figure 4 - Block diagram of a two-dimensional system to do Fourier filtering. The signal is filtered in the frequency domain and transformed back to the space domain by the SAW chirp-transform algorithm. The cylindrical lens performs the back-projection (creates a two-dimensional function out of a one-dimensional function), and the proper azimuth is selected by the image rotator.

As mentioned previously, another operation susceptible to Radon transform analysis is the convolution of two two-dimensional functions. The necessary apparatus is diagrammed in Figure 5. Both inputs may be projection data from flying-line scanners, but it is often useful to convolve a two-dimensional function with a stored filter function. This function may be stored in ROM, clocked out to a fast D/A converter, and used to modulate a carrier. The resulting signal is applied to one input of a SAW convolver. The projection data from the FLS modulate the carrier and are applied to the other input of the convolver. The filter function may be varied with azimuth angle by clocking a different function out of ROM for each azimuth.

Reconstruction of the two-dimensional convolution also follows the procedure of Eq. (3). The function is $|\nu|$-filtered in the custom SAW device, demodulated, and biased up to allow display of bipolar output. This signal modulates the CRT and is back-projected and integrated over the azimuth as before.

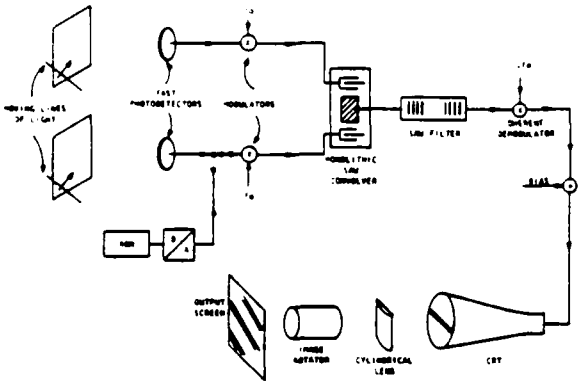

Figure 5 - Block diagram of a system to perform two-dimensional convolution with a SAW convolver. The convolution may be performed between two two-dimensional inputs or between a two-dimensional input and a stored filter function. The SAW convolver output is $|\nu|$-filtered by a custom SAW filter.

Extension to Three-Dimensional Data

The time-consuming nature of three-dimensional data processing is even more extreme than for two-dimensional data. Performing a $(512)^3$ FFT on a minicomputer with array processor and fast disk memory may take two days or more. By applying the principles of the Radon transform, we expect to speed up the computation considerably.

In the three-dimensional case, the Radon transform consists of the complete set of one-dimensional integrals taken over planes of the three-dimensional function. The three-dimensional central-slice theorem states that the one-dimensional Fourier transform of a planar projection yields one line through the three-dimensional Fourier transform of the three-dimensional function (3).

As an example, consider three-dimensional spectral analysis of a function stored as frames of a movie film (512 images, each 512 x 512 pixels, say). We can use SAW chirp filters to compute the three-dimensional Fourier transform. A block diagram is shown in Figure 6. The data manipulation is considerably more complicated than the two-dimensional case, since the Radon transform projections are now parameterized by two angles. But by using a digital video frame store and a flying-line scanner, we can build up the entire Radon transform, sampled at 512 azimuth angles, with 512 passes of the movie film. The digital frame store is then read out through a fast D/A to the SAW chirp-transformer. The projection transforms modulate the CRT as before, and are imaged onto film. We build up the 512 frames of the transform one at a time by selecting only that part of the projection transform relevant to the frame at hand. After reading out the video frame store 512 times, the complete three-dimensional transform is built up. With present video storage technology, the operation is envisioned to take 17 seconds per frame, or less than 4 hours for the complete set. This is an improvement of an order of magnitude

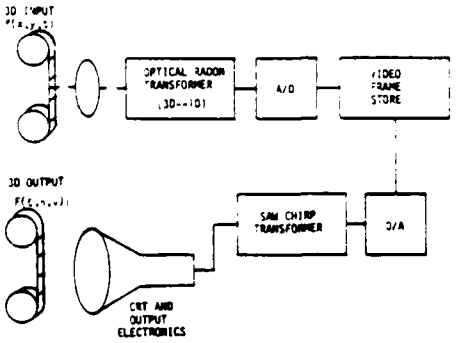

Figure 6 - Block diagram of a three-dimensional spectrum analyzer.

over the digital computer example above. The application of three-dimensional processing is discussed further in Reference 7.

Conclusions

We have demonstrated the ability of one-dimensional processing devices, such as SAW filters, to perform certain two-dimensional processing operations by means of the Radon transform. It is anticipated that this will allow these operations to be performed much more rapidly than is now possible with digital techniques.

We would like to thank Dr. Paul Carr of Rome Air Development Center, Hanscom Field, Massachusetts, for the loan of the SAW correlator. This research was sponsored by the Air Force Office of Scientific Research, contract number AFOSR-82-0249.

References

1. Radon, J., "Über die Bestimmung von Funktionen durch ihre Integrawerte längs gewisser Mannigfaltigkeiten," Berichte Sächsische Akademie der Wissenschaften, Leipzig, Math. Phys. Kl. 69, 262-267 (1917).
2. Deans, Stanley R., The Radon Transform and Some of Its Applications (Wiley, New York, 1983).
3. Barrett, Harrison H., "The Radon transform and its applications," to be published in Progress in Optics.
4. Jack, M. A., and E. G. S. Paige, "Fourier transformation processors based on surface acoustic wave chirp filters," Wave Electronics 3, 299-247 (1978).
5. Jack, M. A., and J. H. Collins, "Fast Fourier transform processor based on the SAW chirp transform algorithm," 1978 IEEE Ultrasonics Symposium Proceedings, IEEE Catalog No. 78 CH 1344-ISU, p. 533.
6. Jack, M. A., P. M. Grant, and J. H. Collins, "The theory, design, and applications of surface acoustic wave Fourier transform processors," Proc. IEEE 68, 450-468 (1980).
7. Barrett, Harrison H., "Three-dimensional image reconstruction from planar projections, with application to optical data processing," Proc. SPIE, to be published.

Two-dimensional Radon-Fourier transformer

Anthony J. Ticknor
Roger L. Easton
Harrison H. Barrett
Optical Sciences Center
University of Arizona
Tucson, Arizona 85721

Abstract. The well-known central-slice, or projection-slice, theorem states that the Radon transform can be used to reduce a two-dimensional Fourier transform to a series of one-dimensional Fourier transforms. In this paper we describe a practical system for implementing this theorem. The Radon transform is carried out with a rotating prism and a flying-line scanner, while the one-dimensional Fourier transforms are performed with surface acoustic wave filters. Both real and imaginary parts of the complex Fourier transform can be obtained. A method of displaying the two-dimensional Fourier transforms is described, and representative transforms are shown. Application of this approach to Labeyrie speckle interferometry is demonstrated.

Subject terms: optical computing; Radon transform; Fourier transform; speckle interferometry.

Optical Engineering 24(1), 082-085 (January/February 1985).

CONTENTS

1. Introduction
2. Producing and transforming the one-dimensional data
3. Displaying the transform
4. Results
5. Speckle interferometry
6. Conclusions
7. Acknowledgments
8. References

1. INTRODUCTION

The two-dimensional Radon transform reduces a 2-D function to a series of 1-D functions by integrating over a series of lines. Although this transform is best known in connection with image reconstruction from projections, as in medical computed tomography, it is also useful in general signal-processing or image-processing applications. Many operations that can be performed on a 2-D function can also be done by performing 1-D operations on the projections. Recent work has demonstrated the usefulness of this approach in calculating Fourier transforms[1,2] and Wigner distribution functions,[3] as well as in pattern recognition,[4,5] image filtering,[6,7] and bandwidth compression.[8]

That these operations are possible in the 1-D Radon domain is a consequence of the celebrated central-slice, or projection-slice, theorem. This theorem states that if a 1-D projection of a 2-D function is formed by integrating over a set of parallel lines, the 1-D Fourier transform of the projection is one line through the 2-D Fourier transform of the function itself (see Fig. 1). This line passes through the origin of the 2-D Fourier space (hence the term *central slice*). By varying the orientation of the lines of integration, the whole 2-D Fourier space can be mapped out in a polar format.

In this paper we describe in detail a practical system for performing 2-D Fourier transforms in the Radon domain. Special attention is given to the electronics for displaying the 2-D Fourier transforms, and several representative transforms are shown. As an illustration of this approach, we demonstrate that the Radon transform can be used to process data from astronomical speckle interferometry.

Invited Paper OP-111 received June 11, 1984; accepted for publication July 30, 1984; received by Managing Editor Sept. 24, 1984.
© 1985 Society of Photo-Optical Instrumentation Engineers.

2. PRODUCING AND TRANSFORMING THE ONE-DIMENSIONAL DATA

In this section we describe the subsystems for producing the Radon transform and the 1-D Fourier transforms. Since these subsystems have been described previously,[1-3] only a brief review is given here.

Assume that the 2-D function to be transformed is in the form of a photographic transparency or print. The projection data $\lambda_\phi(p)$ are derived from the input function $f(x,y)$ by scanning a line of light perpendicular to itself across the function at an angle ϕ (see Fig. 1). The perpendicular distance of the line from the origin is p, and the line is uniquely specified by the variables p and ϕ. The light transmitted or reflected by the object is detected by a photomultiplier tube (PMT). The signal out of the PMT is then proportional to the line integral of the object transmittance or reflectance along the line (p,ϕ). As the line is scanned by means of an acousto-optic deflector, the variable p changes, and one scan produces one projection $\lambda_\phi(p)$. A rotating prism in the system changes the orientation of the line, which is always scanned perpendicular to itself, and provides other projections in the data set. In this way the entire data set, sampled in ϕ but continuous in p, can be formed. This system is referred to as a flying-line scanner.[1-3]

The 1-D Fourier transforms $\Lambda_\phi(\nu)$ are formed by a surface acoustic wave (SAW) chirp transformer[2,9] in which the input signal (the projection) is premultiplied by a chirp produced by impulsing a SAW device. The resulting signal is filtered (convolved) by a second SAW chirp filter in which the chirp rate is equal and opposite to that of the premultiply signal. The signal out of this second filter is coherently detected with a third chirp as a reference. In-phase and quadrature outputs of the coherent detector give, respectively, the real and imaginary parts of the complex Fourier transform. If only the modulus of the transform is desired, the third chirp can be omitted and incoherent detection used.

By the central-slice theorem, $\Lambda_\phi(\rho)$ is also the 2-D Fourier transform of $f(x,y)$ evaluated at polar coordinates (ρ,ϕ) in the 2-D Fourier space, where $\rho = |\nu|$.

3. DISPLAYING THE TRANSFORM

A simple way to display the 1-D Fourier transforms is in the so-called "sinogram" format, in which the radial frequency variable ρ is plotted horizontally and the azimuthal variable ϕ is plotted vertically.

This representation is certainly legitimate and useful in some applications,[8] but it is often desirable to present the data in polar format. This not only makes the transform more recognizable to someone not familiar with sinograms but also presents the data in a form that can be further processed in cascaded systems. A system to accomplish this polar display has been designed, built, and operated and is described in this section.

For now, assume that only the modulus of the 2-D transform is to be displayed. The rf signal from the SAW chirp transformer is detected incoherently, forming a signal proportional to the squared magnitude of the Fourier transform, which is then used to intensity-modulate a spot on a CRT display that is being scanned in a polar raster (Fig. 2). The polar angle of the raster is the same as the angle ϕ that specifies the orientation of the line of light in the flying-line scanner, while the radial variable on the raster corresponds to the frequency ρ. The time-averaged intensity on the screen represents the 2-D Fourier transform in a direct format and is equivalent to the intensity distribution in the Fourier plane of a coherent optical transformer with the same input function.

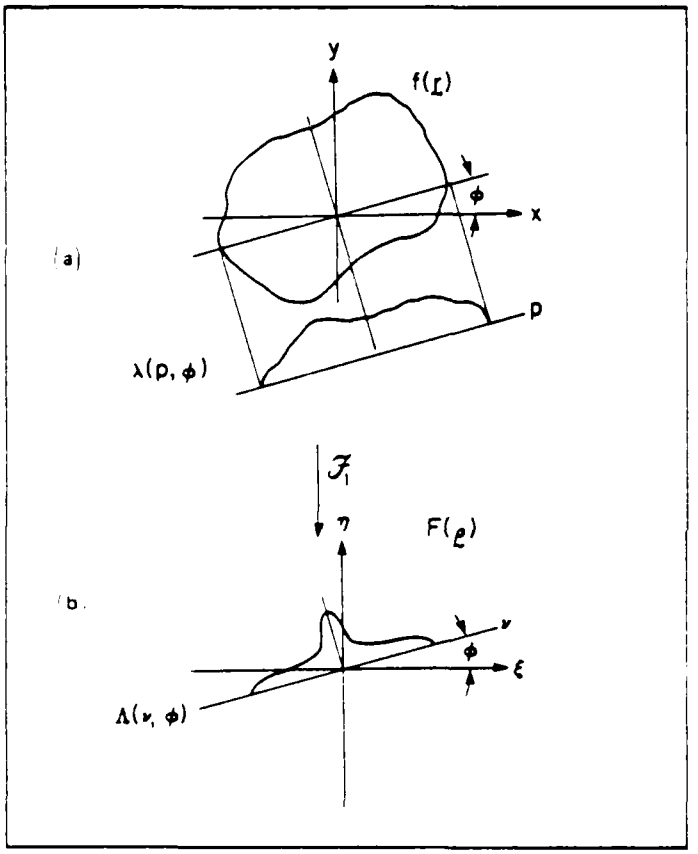

Fig. 1. (a) Geometry of the Radon transform and (b) illustration of the central-slice theorem.

To maintain synchronism between the polar raster and the flying-line scanner, a stepper motor is used to control the rotation of the prism in the scanner. Each step of the stepper motor changes the orientation of the scanning line by $\pi/100$ rad. A free-running circuit operates the stepper motor from about 1/2 to 1000 steps per second. Each time a step occurs, a short transistor-transistor logic (TTL) pulse is sent to a Commodore 64 computer. Upon receiving this pulse, the computer updates an index register to indicate the new angle, sends bytes representing the sine and cosine of the new angle to two digital-to-analog converters, and finally sends a short TTL pulse to a third output port to signal the rest of the system to generate a new line of data.

The start-of-line pulse from the computer starts a scan in the flying-line scanner, triggers the impulse generator for the premultiply chirp, and triggers a delay circuit whose output after the proper delay is a 30 μs pulse used to control the display. The delay is adjusted such that the Fourier transform data are centered within the 30 μs pulse. During this pulse, a bipolar ramp function is generated, passing through zero at the same time the zero-frequency component of the Fourier transform is available. This ramp function is multiplied by the sine and cosine values, and the results of these multiplications are used to control the x and y deflections of a spot on a CRT display. This causes the spot to travel across the screen at a constant speed at an angle equal to the scan angle ϕ, reaching the center of the screen at a time corresponding to the zero-frequency output time of the Fourier transformer.

If the signal coming out of the SAW transformer were simply detected and used to intensity-modulate the CRT, the screen would display the desired output except for one problem. As the entire output is built up, the radial scanning pattern fills the space near the center much more densely than near the edges. The resulting time-averaged intensty distribution would appear as $F(\rho)$ times $1/\rho$, where ρ is the 2-D frequency vector, ρ is its magnitude, and $F(\rho)$ is the 2-D Fourier transform of the input function $f(x, y)$. (Recall that ρ is also the magnitude of the 1-D frequency ν, but ν can be bipolar, while ρ is always nonnegative.) In order to eliminate the $1/\rho$ weighting, it is necessary to multiply the signal before detection by $|\nu|$. This is accomplished in the following manner. The ramp function driving the multipliers is used as the input to an absolute-value amplifier.

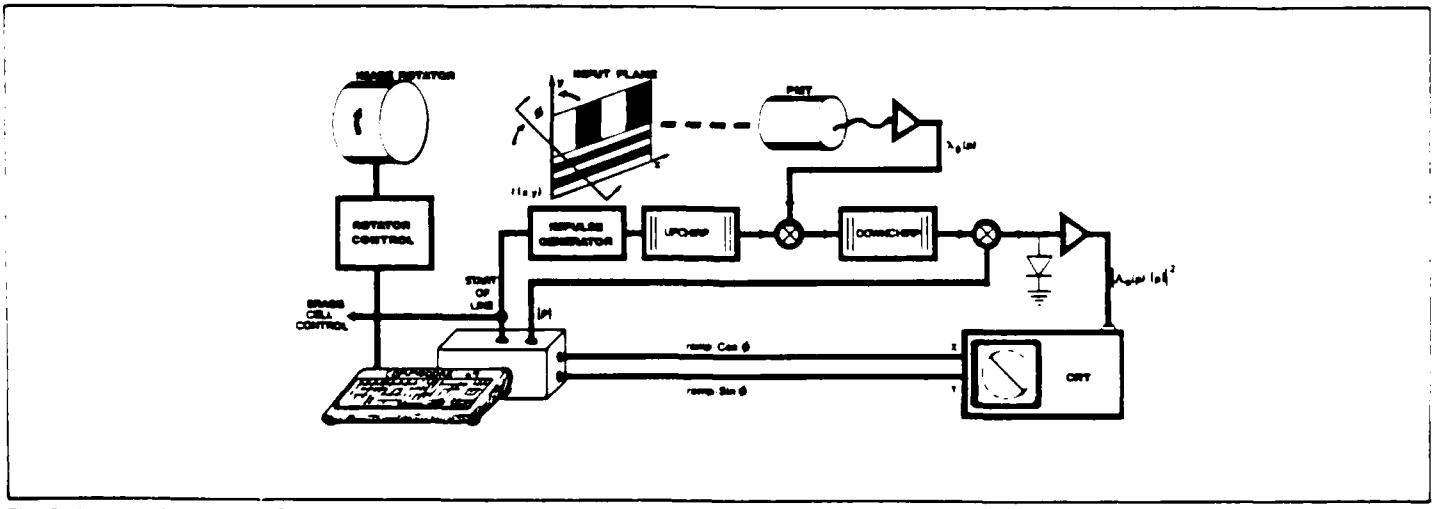

Fig. 2. Layout of the Radon-Fourier transformer. The acousto-optic deflector in the flying-line scanner is not shown but is to the left of the rotating prism.

Fig. 3. 2-D Fourier transform of a square-wave grating in a small circular aperture.

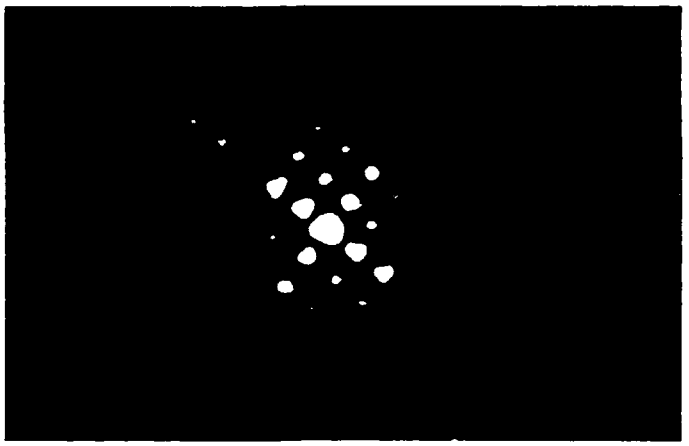

Fig. 4. 2-D Fourier transform of two crossed gratings making an angle of approximately 90°.

The output of this amplifier is a V-shaped function that is the desired multiplier.

Because the signal-to-noise ratio is generally decreasing with increasing frequency, it is also desirable to roll off or apodize the V function at higher frequencies. This is easily accomplished by current-limiting the output of the V generator. The signal resulting from multiplying the output of the convolving filter by the apodized V function is square-law detected and used to intensity-modulate the spot on the CRT. The resulting display from one scan is a line in 2-D Fourier space, filtered by ρ and the apodizing function. As all angles are traced out, an entire disk of Fourier space is built up on the screen.

It is straightforward to extend this system to a CRT display of complex Fourier transforms. The coherent detector in the chirp transformer provides bipolar signals proportional to the real and imaginary parts of the complex transform. These signals can be separated further into four nonnegative signals, namely, the positive-real, negative-real, positive-imaginary, and negative-imaginary components, each of which can be used to intensity-modulate a CRT display. Either four separate CRTs can be used, or a single display can be used sequentially for the four components. Alternatively, analog electronic modules are available to convert the real and imaginary parts to modulus and phase, which can be displayed with the system described above.

4. RESULTS

Several examples of 2-D Fourier transforms produced on the Radon-Fourier transformer are shown in Figs. 3 through 7.

Figure 3 shows the transform of a square-wave grating with a duty cycle of about 0.7; the ± 1 and ± 2 orders are seen. The aperture of the grating is a small circular iris, and the rings of the Airy disk are visible in the ± 1 orders. The effects of the angular sampling can be seen in the ± 2 orders since only four or five sweeps of the flying-line scanner intersect these orders

Figure 4 shows the transform of two overlapping orthogonal square-wave gratings. Again, the duty cycle of the gratings is about 0.7. The product orders resulting from the convolution of the two individual grating spectra are clearly seen. Figure 5 is similar except that the angle between the gratings is approximately 45°

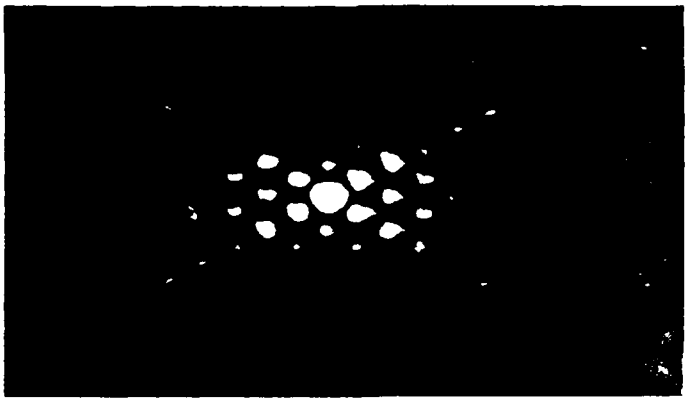

Fig. 5. 2-D Fourier transform of two crossed gratings making an angle of approximately 45°.

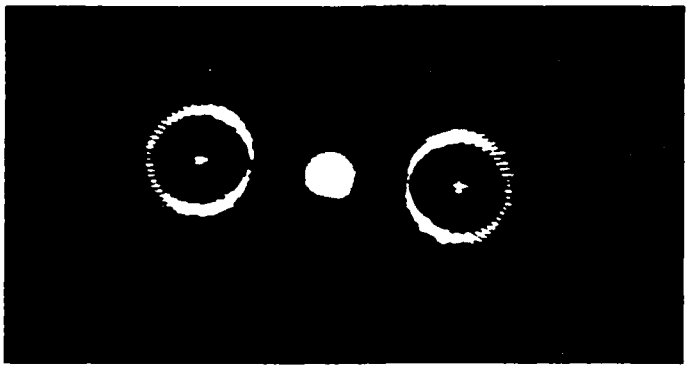

Fig. 6. 2-D Fourier transform of a computer-generated hologram with an annular impulse response.

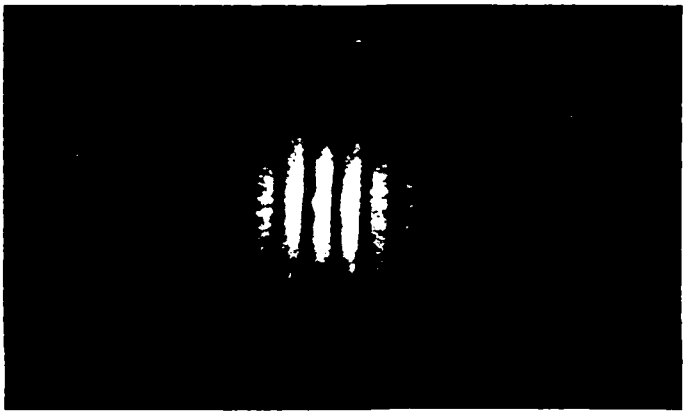

Fig. 7. 2-D Fourier transform of a double pinhole.

Figure 6 shows the transform of a computer-generated hologram that has an annular impulse response

Figure 7 is the transform of a double pinhole The two notches are due to limited dynamic range in the rf mixers, a problem that can be solved with better mixers.

With the SAW filters we actually used, the time-bandwidth product in the 1-D transforms was only about 50, so the results shown in these figures have relatively low resolution, containing roughly 2000 resolvable spots However, this is by no means a fundamental limitation; SAW filters are commercially available that will provide 6000

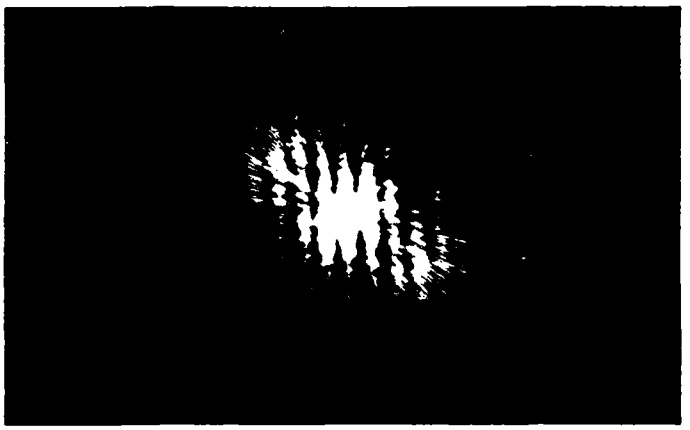

Fig. 8. Speckle interferogram of a simulated binary star. The original speckle patterns were produced on a computer, but this figure was produced by the Radon-Fourier transformer.

spots in a 1-D Fourier transform, or almost 30 million in a 2-D transform.

For our experiments, the time required to produce a complete 2-D Fourier transform was about 0.3 s, but again this is not a fundamental limitation; rather it is a limitation on how rapidly the prism in the flying-line scanner could be rotated. It is easily possible to rotate a prism at 450 rpm, which would yield 2-D transforms at video rates, and even 1 ms per transform appears feasible.

5. SPECKLE INTERFEROMETRY

Astronomical speckle interferometry is an ingenious technique invented by Labeyrie to obtain diffraction-limited resolution from a telescope in spite of phase perturbations by the atmosphere.[10] In this technique, a series of photographic exposures is made, with each exposure time being short compared to the scintillation time of the atmosphere. Each image is Fourier transformed, either digitally or optically, the sum of the squared moduli of the Fourier transforms is accumulated. One final Fourier transform then yields the autocorrelation of the object with diffraction-limited resolution.

Since this method involves a large number of Fourier transforms, it is natural to consider the use of the Radon transform to reduce the 2-D Fourier transforms to 1-D. Indeed, in some infrared applications, 1-D projections of speckle patterns are observed directly by use of a scanning slit in the image plane.[11,12]

To demonstrate the use of our Radon-Fourier transformer in speckle interferometry, we simulated a series of 20 speckle patterns on a digital computer. Each speckle pattern consisted of 50 pairs of ellipses of random size and ellipticity but with constant spacing between members of the same pair. The resulting configuration of ellipses was intended to represent the speckle pattern that would be produced by a binary star. The 20 speckle patterns were photographed on 35 mm transparency film, and after development the film strip was pulled through the input plane of the Radon-Fourier transformer. The modulus of the 2-D Fourier transform was displayed on a CRT as described above, and a camera with an open shutter was used to accumulate the sum of the Fourier moduli. The resulting image, Fig. 8, clearly shows the fringe pattern characteristic of a double star. One further 2-D Fourier transform, also carried out with the Radon-Fourier transformer, yielded the autocorrelation of the double star, as shown in Fig. 9.

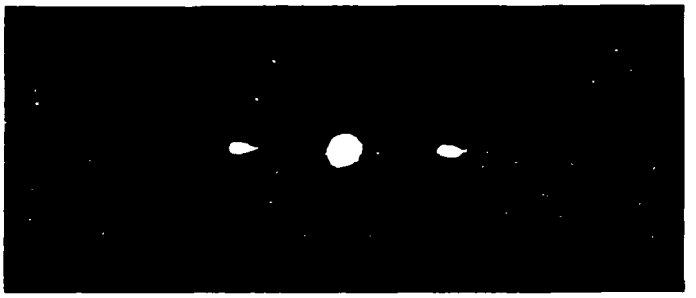

Fig. 9. Fourier transform of Fig. 8, which is the autocorrelation function of the simulated binary star.

6. CONCLUSIONS

We have shown that the Radon transform is a convenient and rapid vehicle for the calculation of 2-D Fourier transforms. The particular system described here, which is based on a flying-line scanner and a SAW chirp Fourier transformer, has a number of advantages over coherent optical Fourier transformers. It does not require that the function to be transformed be in the form of a transparency; it works also when the function is recorded as a photographic print or is a natural reflecting scene. Although it uses a laser as a convenient source, its operation does not depend on the coherence of the source. Furthermore, the full complex Fourier transform is available, something that is very difficult to obtain with coherent optical techniques. The system is also extremely fast. With presently available SAW filters, a system similar to the one described here could be built that would produce a 500×500 (500 points across the diameter of the Fourier plane and 500 angles in the range 0 to π) 2-D transform in 1 30 s and a 5000×5000 transform in a few seconds.

7. ACKNOWLEDGMENTS

The authors would like to thank Robert Shannon for the suggestion of applying the Radon transform to speckle interferometry. Helpful discussions with Adolf Lohmann, Stanley Deans, Keith Hege, and William Stoner are also appreciated.

This work was supported by the Air Force Office of Scientific Research under grant no. 82-0249.

8. REFERENCES

1. H. H. Barrett, Opt. Lett. 7, 248 (1982).
2. R. L. Easton, Jr., H. H. Barrett, and A. J. Ticknor, Proc. 1983 IEEE Ultrasonics Symposium, B. R. McAvoy, ed., p. 185 (1983).
3. R. L. Easton, Jr., A. J. Ticknor, and H. H. Barrett, Opt. Eng. 23(6), 738 (1984).
4. G. R. Gindi and A. F. Gmitro, Opt. Eng. 23(5), 499 (1984).
5. G. Eichmann and B. Z. Dong, Appl. Opt. 22, 830 (1983).
6. A. F. Gmitro, G. R. Gindi, H. H. Barrett, and R. L. Easton, Jr., in *Advances in Optical Information Processing*, G. Michael Morris, ed., Proc. SPIE 388, 132 (1983).
7. H. H. Barrett, in *Transformations in Optical Signal Processing*, William T. Rhodes, James F. Fienup, and Bahaa E. A. Saleh, eds., Proc. SPIE 373, 179 (1984).
8. W. E. Smith and H. H. Barrett, Opt. Lett. 8, 395 (1983).
9. M. A. Jack, P. M. Grant, and J. H. Collins, Proc. IEEE 68, 450 (1980).
10. A. Labeyrie, Astron. Astrophys. 6, 85 (1970).
11. F. Sibille, A. Chelli, and P. Lane, Astron. Astrophys. 79, 315 (1979).
12. C. Aime, S. Kadiri, G. Ricort, C. Roddier, and J. Vernin, Opt. Acta 26, 575 (1979).

Reprinted from Optics Letters, Vol. 8, page 395, July, 1983
Copyright © 1983 by the Optical Society of America and reprinted by permission of the copyright owner.

Radon transform and bandwidth compression

Warren E. Smith and Harrison H. Barrett

Optical Sciences Center, University of Arizona, Tucson, Arizona 85721

Received April 11, 1983

A bandwidth-compression scheme for two-dimensional data is presented that incorporates the Radon transform. There are three advantages to this approach: only one-dimensional operations are required, the dynamic range requirements of the compression are reduced by a filtering step associated with the inverse Radon transform, and the technique is readily adaptive to the data structure. A rectilinear object is compressed to demonstrate the algorithm.

Introduction

The Radon transform[1-3] is best known as the theoretical backbone of computed tomography, the technique that produces cross-sectional maps of x-ray attenuation. This transform entails projecting a two-dimensional slice of an object's x-ray attenuation coefficient along a given direction in the plane of the slice, forming a one-dimensional data set for each projection direction. Thus the two spatial dimensions of the slice are transformed into one spatial and one angular dimension in Radon space. This reduction of spatial dimension can be used to reduce two-dimensional operations on a two-dimensional object to a set of one-dimensional operations on one-dimensional objects, with each member of the set corresponding to a projection angle. In particular, as a consequence of the central-slice theorem, the Radon transform makes the two-dimensional Fourier transform of a two-dimensional function readily accessible without two-dimensional operations' actually having to be performed. Thus the motivation exists for exploring the use of the Radon transform in areas outside clinical tomography.[4,5] A particularly direct application is to bandwidth compression.[6]

Compressing the data necessary to represent an image (with minimum image degradation) is important for two reasons: storage requirements are reduced, and transmission bandwidth requirements are reduced. If we define the data set to be an image of $N \times N$ pixels with each pixel corresponding to M gray levels, compression can be imposed in the spatial domain or in a transform domain. Spatial compression consists of reducing (quantizing) the number of gray levels per pixel and/or reducing the number of pixels in the image (i.e., reducing the radiometric and spatial redundancy, respectively). Transform compression consists of transforming the image (e.g., Fourier, Hadamard, Haar) and then quantizing and/or eliminating the coefficients of the transformed image.[7] To reconstruct the image, the inverse transform of the compressed coefficients is taken.

The Radon transform lends itself to Fourier-transform compression for three reasons:

(1) The entire coding process can be performed with state-of-the-art one-dimensional devices.

(2) The large dynamic range typical of the components of the Fourier transform is significantly reduced by the filtering operation.

(3) One line through the center of the two-dimensional Fourier transform can be examined at a time and adaptively compressed.

Theory

Radon Transform

The Radon transform and its inverse[2,3] are central to the compression technique. Given a two-dimensional function $f(\mathbf{r})$, where $\mathbf{r}$ is the spatial-position vector (x, y), the set of one-dimensional projections of f along a given direction ϕ can be written as

$$\lambda_\phi(p) = \iint_{-\infty}^{\infty} f(\mathbf{r})\delta(p - \mathbf{r}\cdot\mathbf{n})\mathrm{d}^2r, \qquad (1)$$

where $\delta(p - \mathbf{r}\cdot\mathbf{n})$ is a one-dimensional Dirac delta function restricting the integration of f to a line (with normal $\mathbf{n}$) located a distance p from the origin. Thus, for each projection direction ϕ, a one-dimensional function $\lambda_\phi(p)$ is constructed. The set of all $\lambda_\phi(p)$ $(-\infty < p < \infty, 0 \le \phi \le \pi)$ constitutes the Radon transform of $f(x, y)$.

Performing the one-dimensional Fourier transform on Eq. (1) and using the sifting property of the delta function results in

$$\Lambda_\phi(\nu) = \iint_{-\infty}^{\infty} f(\mathbf{r})\exp(-2\pi i\nu\mathbf{r}\cdot\mathbf{n})\mathrm{d}^2r = F(\rho)|_{\rho=\nu\mathbf{n}}, \qquad (2)$$

where ν is the frequency-variable conjugate to p, ρ is the frequency-variable conjugate to $\mathbf{r}$, and $F(\rho)$ is the two-dimensional Fourier transform of $f(\mathbf{r})$, evaluated along the line $\rho = \mathbf{n}\nu$, where $\mathbf{n}$ in the frequency domain is parallel to $\mathbf{n}$ in the spatial domain. This is the central-slice theorem.

By writing $f(\mathbf{r})$ in terms of its inverse Fourier trans-

0146-9592/83/070395-03$1.00/0 © 1983, Optical Society of America

form in polar-coordinate form and using Eq. (2), we can write the inverse Radon transform as

$$f(\mathbf{r}) = \int_0^{\pi} d\phi \left[\int_{-\infty}^{\infty} d\nu \{ |\nu| \Lambda_\phi(\nu) \} \exp(2\pi i \nu p) \right]_{p=\mathbf{n}\cdot\mathbf{r}}. \tag{3}$$

If one looks at the bracketed term in Eq. (3), the following operations are evident: The one-dimensional Fourier transform of each Radon projection $\Lambda_\phi(\nu)$ is multiplied by the frequency filter $|\nu|$; then the inverse one-dimensional Fourier transform is applied to this product and evaluated at $p = \mathbf{n} \cdot \mathbf{r}$. This is the backprojection step. The integral over ϕ is the summation of the backprojections to produce $f(\mathbf{r})$.

Compression Scheme

From the central-slice theorem of Eq. (2), access to a line passing through the center of the two-dimensional Fourier transform is immediately available by the one-dimensional Fourier transform of a given Radon projection. This suggests that an adaptive transform-compression scheme can be applied to one line of the two-dimensional Fourier transform at a time. In fact, the compression step can be advantageously applied to the filtered line, i.e., $|\nu| \Lambda_\phi(\nu)$ of Eq. (3). The filtered and compressed line is then stored or transmitted. To reconstruct the image, the inverse Fourier transform is applied to each previously compressed line, the result is backprojected, and the backprojections are summed to produce the final image.

The compression is accomplished by thresholding and quantizing the components of each Fourier line. Because the projection $\lambda_\phi(p)$ is real, its Fourier transform $\Lambda_\phi(\nu)$ is hermitian (i.e., the real part is even; the imaginary part is odd), so that only the positive half ($\nu > 0$) of each Fourier line need be transmitted or stored. The thresholding that we apply is to truncate each line past some cutoff frequency C_ϕ, which is variable from line to line (i.e., depends on ϕ). The value of C_ϕ is found from

$$\int_0^{C_\phi} \left| |\nu| \Lambda_\phi(\nu) \right| d\nu = S_\phi \left(\frac{S_\phi}{S_{\phi\max}} \right)^T, \tag{4}$$

where

$$S_\phi \equiv \int_0^{\infty} \left| |\nu| \Lambda_\phi(\nu) \right| d\nu, \tag{5}$$

$S_{\phi\max}$ is the largest value of S_ϕ for $0 \le \phi \le \pi$, and T is a parameter that controls the degree of truncation. Note that the line corresponding to $S_{\phi\max}$ is never truncated and that, as $T \to 0$, $C_\phi \to \infty$ for all lines (limit of no truncation). This method of choosing C_ϕ is not, of course, fundamental; other algorithms may be derived.

After truncating the line, we quantize the components by dividing the full dynamic range (positive to negative) specific to the line into a series of uniform, discrete ranges. Actually, two dynamic ranges exist, one each for the real and imaginary parts. The component that falls within a particular range is assigned the constant value for that range.

The advantages of the Radon approach are now discussed.

From an implementation point of view, hardware devices for carrying out one-dimensional operations are well developed. The operations for each projection at the compression end involve a one-dimensional Fourier transform, multiplication by a linear filter, thresholding, quantizing, and coding for transmission or storage. At the receiving end, only a one-dimensional inverse Fourier transform is required, followed by the backprojection operation.

The dynamic range of a line through the center of a two-dimensional Fourier transform is large. To quantize such a range efficiently, a variable quantizer would be required. Multiplying by the $|\nu|$ filter, however, reduces the dynamic range of the line (near $|\nu| = 0$, where the components are usually largest), simplifying the requirements of the quantizer.

The third advantage is related to the image-dependent adaptability of the compression scheme. An image with relatively sharp, straight edges, oriented in particular directions, will exhibit a transform with the energy distributed along conjugate directions, depending on the symmetry of the original image. Because the Radon transform handles one Fourier-transform line at a time, each filtered line can be adaptively compressed to take advantage of the structure in the two-dimensional Fourier-transform plane.

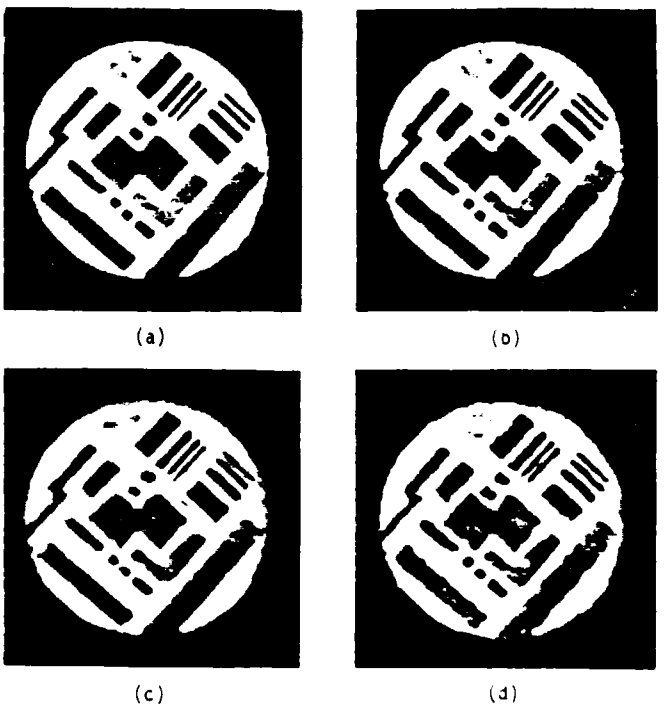

Fig. 1. (a) Reconstruction from Radon projections without thresholding and nominal 8-bit quantization (8 bits/pixel), (b) truncation of 48% of components with 3-bit quantization (1.6 bits/pixel), (c) truncation of 66% of components with 3-bit quantization (1.1 bits/pixel), (d) truncation of 48% of components with two-bit quantization (1.1 bits/pixel).

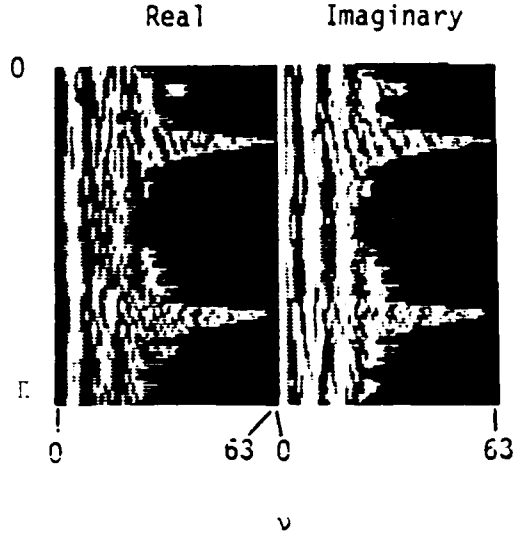

Fig. 2. Truncated and quantized Fourier components of Fig. 1(d).

Illustrative Example

To demonstrate the method, the object illustrated in Fig. 1(a) is compressed. The region to be compressed is a circle with a radius of 64 pixels, yielding an area of 12,868 pixels. The rectilinear nature of the figure is useful in demonstrating the variable compression with projection angle.

The object is viewed by a TV camera through an image rotator. The one-dimensional Radon projection $\lambda_\phi(p)$ of the object is obtained (at the angle ϕ defined by the image rotator) by summing the camera output along a horizontal raster line, giving the digital equivalent of the line integral of the object along the line. This summation is performed for each of 128 raster lines to yield a 128-element projection. We then rotate the image rotator through a small angle (1.8 deg) and find the next projection, until a total of 100 projections, each with 128 elements, has been taken.

Each projection is Fourier transformed, yielding a line through the center of the two-dimensional transform of the original object. This line is then filtered [multiplied by $|\nu|$; see Eq. (3)] and compressed by thresholding and uniformly quantizing the components, as described above. The object is reconstructed by taking the one-dimensional inverse Fourier transform of the filtered and compressed line, backprojecting, and summing over all projection angles. Figure 1(a) illustrates the reconstruction from the Radon-transformed original object without thresholding or quantizing to provide a control case.

The measure of the compression in bits per pixel (the bit rate) is determined by counting the total number of bits required to store or transmit the image (including any overhead) divided by the number of pixels in the image. Figure 1(a) has approximately 8.0 bits/pixel because there are 100 angles times 128 Fourier components per angle, times 8 bits per Fourier component, divided by 12,868 pixels.

Three different compressions of Fig. 1(a) are now demonstrated. Figure 1(b) represents thresholding with $T = 0.3$ and quantization of the Fourier component's full range to eight gray levels (3 bits). The thresholding eliminates 48% of the Fourier components. The overall bit rate is 1.6 bits/pixel. Figure 1(c) has $T = 0.6$, eliminating 66% of the components, again with eight gray levels per component, giving a bit rate of 1.1 bits/pixel. To investigate a coarser quantization, Fig. 1(d) represents the same thresholding as in Fig. 1(b) but with four gray levels per component, giving a bit rate of 1.1 bits/pixel. Figure 2 is a representation of the truncated and quantized components that produce Fig. 1(d). The adaptive nature of the compression is evident for this type of object. Note that an overhead of approximately 0.1 bit/pixel is incurred independently of the amount of compression, to keep track of the number of components truncated per line and the scale factors relating the dynamic range (both real and imaginary) of each line to the maximum dynamic range. This overhead is included in the results.

Summary

We have shown that the Radon transform can be used to advantage in bandwidth compression for several reasons. First, a line passing through the center of the two-dimensional Fourier transform of the object is attainable by a one-dimensional operation that can be carried out by existing fast devices. Second, the dynamic range of this line is reduced in a filtering operation required by the inverse Radon transform. This reduction enhances compression performance (i.e., quantization error is reduced). Finally, each line in Fourier space is obtained independently, so the compression can be adapted to the amount of structure in that line. The technique was demonstrated on a rectilinear object, and a bit rate of 1.6 bits/pixel was achieved with good fidelity.

This research was sponsored by the U.S. Air Force Office of Scientific Research under grant AFOSR-82-0249.

References

1. J. Radon, "Über die Bestimmung von Funktionen durch ihre Integralwerte längs gewisser Mannigfaltigkeiten," Ber. Saechs. Akad. Wiss. (Leipzig) 69, 262–278 (1917).
2. H. H. Barrett and W. Swindell, *Radiological Imaging: Theory of Image Formation, Detection, and Processing* (Academic, New York, 1981), Vols. I and II.
3. H. H. Barrett, "The Radon transform and its applications," in *Progress in Optics*, E. Wolf, ed. (to be published).
4. H. H. Barrett, "Optical processing in Radon space," Opt. Lett. 7, 248–250, (1982).
5. G. Eichmann and P. Z. Dong, "Coherent optical production of the Hough transform," presented at the Conference on Optics, Los Alamos, New Mexico, April 11–15, 1983.
6. W. G. Wee, "Application of projection techniques to image transmission," presented at the Techniques of Three-Dimensional Reconstruction International Workshop, Upton, New York, July 16–19, 1974.
7. W. K. Pratt, *Digital Image Processing* (Wiley, New York, 1978).

END

DTIC

8-86

END

DTIC

8-86